MATHEMATICAL TECHNIQUES FOR SCATTERING OF WATER WAVES BY HORIZONTAL/VERTICAL BARRIER(S) OVER DIFFERENT BOTTOM TOPOGRAPHIES

DOCTORAL THESIS

by

Naveen Kumar

(2016MAZ0007)

DEPARTMENT OF MATHEMATICS

INDIAN INSTITUTE OF TECHNOLOGY ROPAR

JUNE, 2023

MATHEMATICAL TECHNIQUES FOR SCATTERING OF WATER WAVES BY HORIZONTAL/VERTICAL BARRIER(S) OVER DIFFERENT BOTTOM TOPOGRAPHIES
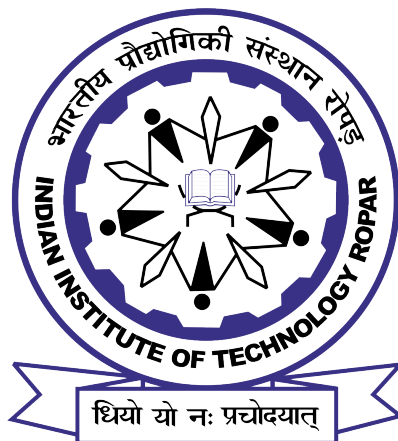
A Thesis Submitted

in Partial Fulfilment of the Requirements

for the Degree of

DOCTOR OF PHILOSOPHY

by

Naveen Kumar

(2016MAZ0007)

DEPARTMENT OF MATHEMATICS

INDIAN INSTITUTE OF TECHNOLOGY ROPAR

JUNE, 2023

Dedicated to
My Father **Mr. Sher Singh Yadav**
and
My Mother **Mrs. Sumitra Yadav**

Declaration of Originality

I hereby declare that the work which is being presented in the thesis entitled **"Mathematical Techniques for Scattering of Water Waves by Horizontal/Vertical Barrier(s) Over Different Bottom Topographies"** has been solely au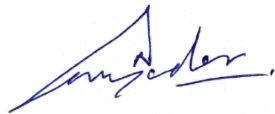thored by me. It presents the result of my own independent investigation/research conducted during the time period from January 2017 to June 2023 under the supervision of Dr. S. C. Martha, Associate Professor, Department of Mathematics, IIT Ropar. To the best of my knowledge, it is an original work, both in terms of research content and narrative, and has not been submitted or accepted elsewhere, in part or in full, for the award of any degree, diploma, fellowship, associateship, or similar title of any university or institution. Further, due credit has been attributed to the relevant state-of-the-art and collaborations (if any) with appropriate citations and acknowledgments, in line with established ethical norms and practices. I also declare that any idea/data/fact/source stated in my thesis has not been fabricated/ falsified/ misrepresented. All the principles of academic honesty and integrity have been followed. I fully understand that if the thesis is found to be unoriginal, fabricated, or plagiarized, the Institute reserves the right to withdraw the thesis from its archive and revoke the associated Degree conferred. Additionally, the Institute also reserves the right to appraise all concerned sections of society of the matter for their information and necessary action (if any). If accepted, I hereby consent for my thesis to be available online in the Institute's Open Access repository, inter-library loan, and the title & abstract to be made available to outside organizations.

Signature

Name: Naveen Kumar

Entry Number: 2016MAZ0007

Program: PhD

Department: Mathematics

Indian Institute of Technology Ropar

Rupnagar, Punjab 140001

Date: 20/06/2023

Acknowledgement

It is a great pleasure and privilege to express my deepest sense of gratitude to lots of wonderful people who all have helped me in various ways during my doctoral study. First, I would like to express my everlasting indebtedness to my thesis supervisor Dr. Subash Chandra Martha, who has introduced me to the areas of research in water wave theory, an interesting area of applied mathematics. I am immensely grateful to him for his enthusiasm, continuous encouragement and guidance which have been the main source of inspiration during my doctoral study. I am highly indebted to his valuable suggestions and feedback on the minutest of detail on my research right from the inception of the problem to the final preparation of the manuscript.

I must take this opportunity to express my gratitude to all members of Doctoral Committee viz. Dr. Arvind Kumar Gupta (Chairperson), Dr. Partha Sharathi Dutta, Dr. Bidhan Chandra Sardar and Dr. Srikant Sekhar Padhee (Department of Mechanical Engineering) for their valuable suggestions and meaningful comments during the progress of my research work. My special thanks to them for their valuable discussions regarding some of my research works. I sincerely acknowledge Dr. Chittaranjan Mishra, former member of Doctoral Committee, for providing excellent suggestions and meaningful comments during the research work. I am very thankful to Dr. Manoranjan Mishra for not only his suggestions and useful comments during the progress of my research work but also his friendly interactions that create an enjoyable working style in me. I also take this opportunity to express my gratitude to other faculty members of the department Prof. Jitendra Kumar (HOD), Dr. G Sankara Raju Kosuru, Dr. Manju Khan, Dr. M. Prabhakar, Dr. Tapas Chatterjee, Dr. Arun Kumar, Dr. Arti Pandey, Dr. Balesh Kumar, Dr. Kaushik Mondal, Dr. A. Sairam Kaliraj and Dr. Santanu Sarkar for their kind assistant on various occasions. I would also like to thank the department's office staff Mr. Neeraj, Ms. Jaspreet and other staff members from IT department, administrative and library for their help. I am thankful to Dr. Santanu Koley, Birla Institute of Technology and Science, Pilani - Hyderabad Campus for his suggestions during the preparation of the manuscript. I gratefully acknowledge my lab mates Dr. Arun Choudhary, Dr. Amandeep Kaur, Dr. Sofia Singla, Gagan Sahoo, Sunita Choudhary, Deepali Goyal, Akashita Aggarwal and Nidhi for their kind support, discussions and also for being there to listen when I needed an ear. I also acknowledge the support and care from my dear friends in department of Mathematics. A special and heartfelt thanks to my friend Dr. Anoop Kumar, Dr. Sadanand and Mr. Sandeep Kumar who has always stood with me in all happy and sad times. The time spent with them has always been full of fruitful discussion along with excitement and fun. I would also like to thank my department colleagues Dr. Amrendra Singh Gill, Dr. Subhajit Saha, Dr. Sukanta Sarkar, Dr. Sonika, Dr. Kirandeep Kaur, Dr. Yogita, Dr. Tripti Midha, Dr. Suraj Singh Khurana, Dr. Atul Kumar Verma and Dr. Abhik Digar for their friendship and assistance in various academic and non-academic matters. I am also thankful to Surya Narayan, Vikash Tripathi and Neha Gupta for their help and encouragement. I would also like to thank my

June, 2023   **Naveen Kumar**

Certificate

This is to certify that the thesis entitled **"Mathematical Techniques for Scattering of Water Waves by Horizontal/Vertical Barrier(s) Over Different Bottom Topographies"** submitted by **Mr. Naveen Kumar (2016MAZ0007)** for the award of the degree of **Doctor of Philosophy** of Indian Institute of Technology Ropar, is a record of bonafide research work carried out under my guidance and supervision. To the best of my knowledge and belief, the work presented in this thesis is original and has not been submitted, either in part or full, for the award of any other degree, diploma, fellowship, associateship or similar title of any university or institution.

In my opinion, the thesis has reached the standard fulfilling the requirements of the regulations relating to the Degree.

Signature of the Supervisor
Dr. S. C. Martha
Associate Professor
Department of Mathematics
Indian Institute of Technology Ropar
Rupnagar, Punjab 140001
Date: 20/06/2023

Lay Summary

The thesis provides a detailed analysis for finding the approximate solutions to boundary value problems arising in the study of interaction of water waves with barrier(s) over different bottom profiles. Under suitable assumptions, the physical problems of water wave interaction are modelled mathematically. The boundary value problems obtained in mathematical formulation are linearized using small amplitude wave theory. The cases of horizontal and vertical barriers over different bottom profiles are discussed in this thesis. Depending on the bottom boundary conditions, the boundary value problems are solved either by the eigenfunction expansions in conjunction with the orthogonality of eigenfunctions or the eigenfunction expansions in conjunction with least-square method or the finite element based technique. The physical quantities, namely, reflection and transmission coefficients, force on the barrier(s), and free surface elevation, are calculated. These physical quantities have significant importance in the area of Ocean and Marine Engineering to construct coastal structures such as sea walls, barriers, bottom mattress, dike etc. The coastal structures are required for the protection of ports, harbours, floating bridges, floating storage bases, floating buildings, tourism points etc. from natural calamities such as tsunamis, cyclones, red tides, harmful algal blooms and increased sea level. These coastal structures are constructed offshore parallel to the coastal line to reduce the impact of incident wave loads. Thus, they lessen coastal erosion and provide safety to various coastal infrastructures and facilities near the shoreline. It is apparent from the above description that the study of water wave problems is of immense importance in the field of ocean engineering for various applications.

Abstract

In this thesis, a detailed analysis of a class of water wave problems arising in Ocean and Marine Engineering due to water waves interaction with the barrier(s) over different type of bottom topographies is carried out. The physical problems associated with water wave propagation are modelled mathematically by utilizing the assumptions that the fluid under consideration is homogeneous, inviscid, incompressible, and the motion of the fluid is irrotational and harmonic in time. Further, the motion of the fluid which is under gravity and the free surface deviation from its horizontal position are assumed to be small in the sense that the linearized theory of water waves can be utilized.

The objective of the thesis is to give emphasis for a class of wave-structure interaction problems with significance being given for i) developing various numerical techniques for a class of physical problems associated with surface wave interaction with rigid barriers in presence of uneven bottom topography, and ii) investigating the influence of various system parameters associated with the physical problems. Both the cases of horizontal and vertical barriers are considered in this thesis. On formulating the physical problems, the governing partial differential equation comes about Laplace equation for the case of normal incidence of surface waves while it is Helmholtz equation for the case of oblique incidence of water waves. The boundary condition at the free surface i.e. at the air-water interface is of the Robin type and the impermeable boundary condition at the bottom is of Neumann type. In addition to this, far-field conditions are imposed at infinite fluid boundaries to ensure the uniqueness of the solution. The boundary value problem involving the scattering of water waves by finite dock over stepped-type bottom profile is solved by using eigenfunction expansions in conjunction with orthogonality of eigenfunctions. The problems of vertical barrier(s) over step type or shelf type bottom are solved by utilizing the eigenfunction expansions in conjunction with least-square method. The physical quantities, namely, reflection and transmission coefficients, force on the barriers and free surface elevation are calculated. The variation of these physical quantities against the various system parameters is presented and depicted through different graphs and tabular data. In the last part of the thesis, a different approach namely, the finite element based technique is used to solve the boundary value problem involving arbitrary topography at the bottom. The finite domain is constructed by truncating the radiation boundary conditions at some finite distance. The finite element formulation is done using weighted residual method. The solution of boundary value problem, the scattered velocity potential, is further utilized to determine the various physical quantities, namely, reflection and transmission coefficients, the force on the barriers. For each of the above physical problems, the energy balance relation is derived with the aid of Green's integral theorem and the verification of this identity ensures the accuracy of the present numerical results carried out for the physical quantities. In addition, the convergence of number of evanescent modes in the series expansions is performed numerically. Also, the convergence of the finite element analysis is computationally carried out. The present numerical results are also compared with the results available in the literature for validating the

model. The present study is of immense importance in the field of ocean and marine engineering towards the application of breakwaters.

List of Publications

Papers Published/Under Review:

1. A. Choudhary, **Naveen Kumar** and S. C. Martha (2022),"Interaction of surface water waves with a finite dock over two-stepped bottom profile", Marine Systems & Ocean Technology - Springer, 17, 39-52.

2. **Naveen Kumar**, D. Goyal and S. C. Martha (2022),"Algebraic method for approximate solution of scattering of surface waves by thin vertical barrier over a stepped bottom topography", Contemporary Mathematics - Universal Wisher, 3(4), 500-513.

3. **Naveen Kumar**, A. Kaur and S. C. Martha (2023),"Scattering of water waves by two thin vertical barriers over shelf bottom topography", Geophysical and Astrophysical Fluid Dynamics - Taylor & Francis, 117(1), 1-25.

4. **Naveen Kumar** and S. C. Martha,"Mathematical study of interaction of surface waves with two vertical barriers over arbitrary bottom topography" (Under Review).

Contents

List of Figures

List of Tables

Chapter 1

Introduction

1.1   Preamble

There are many types of coastal infrastructures and facilities near the seashore due to increased human activities such as ports, harbours, floating buildings, tourism points, floating bridges, navigation channels, embankments, movement of armies etc. The pressure on land-scarce island countries is drastically increasing day by day. They are trying to find alternatives to this scarcity of land by constructing artificial floating structures near the shoreline, that is, also known as land reclamation. But, this land reclamation and coastal infrastructures have its limitations due to natural calamities such as tsunamis, cyclones, red tides, harmful algal blooms and increased sea level, and also the burden on these. So, it has become a challenge for the engineers to protect these coastal infrastructures and facilities. Due to this, the renewal and innovation of coastal structures such as sea walls, barriers, bottom mattress, groins, dike etc. have become an important topic to protect these coastal infrastructures and facilities. Among these coastal structures for the protection of coastal developments, design and construction of breakwaters have taken a leading role. There are essentially three types of breakwaters which are in use worldwide such as rubble-mound breakwaters, vertical breakwaters, and horizontal breakwaters (docks). These breakwaters are the structures which are constructed offshore parallel to the coast to protect shoreline from the incident waves by reducing the impact of waves on the shore, much like a natural reef. Thus, they lessen coastal erosion and provide safety for various constructions near the seashore including harbors and inlets. It is apparent from the above description that the study of water waves problems is of immense importance in the fields of ocean engineering for various applications. To study water waves interactions with barriers, the interdisciplinary subject "Fluid Dynamics" has significant importance. In fluid dynamics, we study the motion state of fluid and here in our study we deals with wave propagation. These waves are produced in ocean due to various types of forces such as meteorological forces (wind pressure), astronomical forces, and earthquake. The water waves are waves propagating on the free surface i.e. at the air-water interface under the restoring forces, gravity and surface tension. The water waves propagating towards the shoreline are both longitudinal and transverse in nature and through these surface deformation waves energy propagate towards the shore. On the basis of the ratio of the water depth and wavelength, water waves are of two types, shallow-water waves and deep-water waves. In case of shallow water wave propagation, water molecules travel in an elliptic orbit while in deep water wave propagation, water

molecules travel in a circular orbit. During extreme events like tsunamis, cyclones, red tides shallow water waves generate even in deep sea because it has a very long wavelength while deep-water waves generated by local winds or distant winds (swell).

To examine the water wave problems mathematically various assumptions are imposed on the seabed, barriers and the nature of fluids. Under suitable assumptions, these problems can be solved by utilizing two different theories, namely 1) Linearized wave theory 2) Non-linear wave theory. In the linearized theory of water waves, the motion of water waves which is under the action of gravity and the free surface deviation from its horizontal position are assumed to be small. These assumptions of smallness constitute the basis for the linearized theory of water waves. This mean, the velocity components together with their derivatives (assumed to be exist) are quantities of first order of smallness so that their squares, products and higher powers can be neglected. Thus, the free surface boundary conditions can be linearized. However, in many engineering applications, the water wave problems are non-linear. For example, in design of offshore structures, the wave heights of interest are such that the non-linearities must be considered. But, many researchers are restricting their study to linearized wave theory in many of water wave problems because linear theory is enough, upto some extent, to handle most of the problems in the area of coastal and marine engineering and also this theory probably provides the sufficient information to the engineers for their use. Due to this reason, in recent decades, many researchers are using linearized theory of water waves in mathematical modelling of problems arising in the area of coastal and marine engineering. The basic equations in the formulation of water waves problems are derived from the equation of continuity (equation conservation of mass) and Euler's equation of motion (equation of conservation of momentum). In our study, we lead to a class of problems consisting of two-dimensional Laplace/Helmholtz equation along with mixed type boundary conditions. It may be argued that a Laplace/Helmholtz partial differential equation along with specified boundary condition may not lead to non-trivial mathematical difficulties and may be solved semi-analytically or numerically. But, in reality, things are not much easy due to the fact that in water waves problems the boundary conditions at infinity are not completely known and therefore, methods will have to be developed to determine the solution of Laplace/Helmholtz equation along with unknown boundary conditions at infinity. Further, in the context of the problems consisting in the present thesis, when the surface wave train coming from the infinity large distance strikes the coastal structure(s) i.e. barrier(s), then the scattering of incident water waves occurs in two parts, namely reflected wave and transmitted wave. The part of incident water wave reflected back by the barrier(s) is known as reflected wave and the ratio of amplitude of reflected wave to the amplitude of incident wave is called "reflection coefficient". The other part of incident water wave which is transmitted forward is known as transmitted wave and the ratio of amplitude of transmitted wave to the amplitude of incident wave is called "transmission coefficient". In the mathematical study of water wave scattering problems, these two coefficients have vital role since they provide a measure for the amount of

reflected and transmitted waves. This information is highly important in the areas of marine and coastal engineering for constructing the offshore structures. The analysis of the problems involving scattering of water waves has practical importance in various applications e.g. design and construction of breakwaters for the protection from open sea and wavemakers etc. The impact of the surface water waves on the barriers is also necessary to analyse in terms of the forces as their durability depend on the forces acting on them. Due to these significant applications, the scattering problems are being studied by the scientists and ocean technologists with interest. The mathematical analysis of such problems consists of mixed boundary value problem having Laplace/Helmholtz equation as the governing equation, the Robin type boundary condition at the free surface, the Neumann type boundary conditions at the bottom, the radiation boundary conditions and the boundary conditions (Robin/Neumann-type) on the structure(s). The researchers are drawing their attention in developing various analytical, semi-analytical and numerical methods to determine their complete solutions. In some of the problems, due to their complexity, the researchers have emphasized to determine the physical quantities directly instead of going into detailed solution for unknown velocity potential. After, this preamble, a brief history of the investigations done by many researchers for various types of water wave problems over the last decades, which are relevant to this thesis are described in the next section.

1.2 Brief History and Motivation

The theory of water waves has been a subject of great significance for scientific researches since the days of Airy. In 1845, Airy made substantial contribution to this field by producing linear water wave theory. In 1872, Boussinesq developed the long wave theory for the water waves problems. The limiting wave heights theory was developed by Michell in 1893 and McCowan in 1894. But, at first, the theory of water waves was initiated by Sir Isaac Newton in Book II: Prop. XLV of Principia in 1687. Later on, the theoretical studies pioneers namely, Euler, Laplace, Gerstner, Poissson, Cauchy etc. developed some theories on water waves. In 1850, the effect of wind on surface waves was studied by Stevenson and derived empirical relationship relating the rate of wave growth to the wind. The higher order wave theories was developed by Stokes in 1947. To observe physical insight of the behaviour of oceanic and tidal surface waves, scientists and researchers have great practical importance from the theory of water waves.

1.2.1 Water wave scattering by rigid vertical barrier(s)

The study of scattering of surface water waves by fixed obstacles became significant to ensure the safety of coastal structures like bays, ports, and harbours. Many researchers are drawing great attention to the study of scattering of water waves to create a transquility zone by dissipating maximum incident wave energy or by reflecting maximum incident wave energy. A suitable option to reduce the transmission of incident wave energy is by

the help of rigid vertical barriers. The scattering of water waves by vertical barrier(s)
over different type of sea bottom topography is governed by the Laplace/Helmholtz
equation along with appropriate boundary conditions for the free surface, barriers, bottom
and the radiation conditions. Both linear and non-linear theories can be used to solve
these water waves boundary value problems mathematically to determine the physical
quantities, namely, the reflection and transmission coefficients, forces on the barriers, free
surface elevation etc. The problems involving the scattering of surface waves by rigid
vertical barrier(s) were investigated by many authors in the literature. For example,
among theoretical studies of single vertical barrier, Ursell [137] considered the problem of
interaction of surface waves with a thin vertical barrier and found out the expressions for
reflection and transmission coefficients with the aid of modified Bessel functions. Dean
[34] constructed the solution of the problem by utilizing the complex variable technique
in infinite depth of water. Evans [37] also utilized the complex variable technique to solve
Ursell's [137] problem with incorporating the effect of surface tension and investigated
the reflection and transmission coefficients. Evans [38] introduced the reduced velocity
potential and derived the expressions for velocity potential in closed form everywhere
within the fluid and on the plate. They derived first and second order forces, moments
on the plate, and the reflection and transmission coefficients. Faulkner [41] studied
the interaction of obliquely incident surface waves with a completely submerged vertical
barrier in deep water based on the Wiener-Hopf technique and derived the reflection and
transmission coefficients. Porter and Evans [106] and Mandal and Das [83] employed
one-term and multi-term Galerkin approximation methods to calculate very accurate
upper and lower bounds for the reflection and transmission coefficients by vertical barrier
for finite and deep depths respectively. Losada et al. [78] examined the reflection and
transmission coefficients of monochromatic surface waves over uniform water depth using
an eigenfunction expansion method. Reddy and Neelamani [112] used a wave flume for
the experimental analysis of water wave scattering by a partially immersed rigid vertical
barrier to investigate the reflection and transmission characteristics of waves. Mandal and
Gayen [87] employed the simplified perturbation analysis to study surface wave scattering
problem over bottom undulations in the presence of a partially immersed thin vertical
barrier. Koley et al. [63] investigated the oblique wave trapping by bottom standing
and surface-piercing porous structures of finite width placed at a finite distance from
a vertical rigid wall using the Sollitt and Cross Model. Choudhary and Martha [21]
studied diffraction of surface waves by an undulating bed topography in the presence of
vertical barrier. Many researchers like Chakrabarti [11] and Mandal and Kundu [88] etc.
developed different mathematical techniques to obtain the reflection and transmission
coefficients instead of determining the velocity potential. Thorne [131] employed a
multi-pole expansion method to obtain a necessary form of the Green's function for the
boundary value problem arising from the physical problem. Levine and Rodemich [74]
reduced the problem of partially immersed barrier into a problem of singular integral
equation and obtained the solution in known form by using an appropriate Green's

function. They also investigated the problem of scattering of water waves by two vertical parallel barriers. Evans [40] studied the small oscillation of partially immersed plate by a suitable application of the Green's integral theorem and obtained the results of Ursell [137]. Porter [105] examined the solution for the interaction of surface waves involving by vertical barrier having a gap in infinite depth of water by employing the complex variable technique as well as Green's integral theorem. Venkateswarlu and Karmakar [138] analyzed the effect of vertical porous structure over flat and elevated bottom profiles. The impact of a porous rectangular barrier placed over the seabed with the dynamic characteristics of gravity waves was analysed by Meng and Lu [95] by employing the method of matched eigenfunction expansions. Mandal and Dolai [86] employed the Galerkin approximation method to derive the solution for water wave interaction problem due to vertical barrier. Chakrabarti et al. [13] employed special logarithmic singular integral equation technique to study the scattering of water waves by a vertical barrier with a gap. Banerjea et al. [3] utilized the one-term and multi-term Galerkin approximation to evaluate the reflection coefficient for the problem handled by Porter [105]. Mandal and Chakrabarti [84] obtained the approximate solutions of a number of water wave scattering problems involving thin vertical barriers by utilizing the Galerkin's method. Ray et al. [110] investigated water wave scattering by thin vertical barriers for four different geometrical configurations in deep water with the aid of Galerkin approximation. Gayen and Mondal [44] studied wave scattering by a thin inclined porous plate by using hypersingular integral equation approach. Mondal and Banerjea [98] studied scattering of water waves by an submerged inclined porous plate beneath an ice cover with the aid of hypersingular integral equation approach and using collocation method to represent the unknown function using Chebychev polynomials. The scattering of water waves by thick vertical barrier was studied by Choudhary et al. [22] over an arbitrary bottom using a coupled eigenfunction expansion-boundary element method. Kanoria et al. [59] examined the problem involving scattering of water waves by different kinds of thick vertical barriers. Bhatta and Rahman [7] studied scattering as well as radiation problems for a floating vertical circular cylinder in a finite depth of water. Das and Bora [29] considered the problem of water wave diffraction by a vertical porous structures placed over stepped bottom topography. Chakrabarti et al. [12] examined the interaction of surface waves with vertical barrier in the presence of ice-cover. Bhatta [5] also examined the problem involving the diffraction of water waves by the elliptical and circular cylinders in water of finite depth. The interaction of laminar wakes with free-surface waves generated by a moving body beneath the surface of an incompressible viscous fluid of infinite depth was investigated analytically by Lu [79] using the method of integral transforms. Manam et al. [81] derived the mode-coupling relations by utilizing Fourier integral theorem for the fluid structure interaction problems in semi-infinite strip and semi-infinite domain. The problem of diffraction of oblique water waves incident upon an infinite cylinder floating on the free surface was studied by Bai [2] using finite element technique and calculated the reflection and transmission characteristics and also diffraction forces and moment. Ni and Teng [102] studied the

reflection of incident surface waves by a breakwater with permeable trapezoidal bars on a sloping porous seabed using modified mild-slope equations.

For improved performance, twin vertical barriers were investigated by several researchers. Newman [101] studied the diffraction of surface waves in deep water by two thin vertical barriers and derived the expressions for reflection and transmission coefficients with the aid of modified Bessel functions. McIver [91] studied the same problem in uniform depth of water using the eigenfunction expansion method and investigated the zeros of reflection and transmission coefficients. Isaacson et al. [56] constructed a physical model in support of theoretical results carried out by the eigenfunction method for a diffraction problem involving a pair of thin vertical permeable barriers. The experimental investigation was also carried out by Neelamani and Vedagiri [99] for the wave reflection, transmission, free surface fluctuations in between barriers, and energy dissipation characteristics for the problem of twin vertical barriers. Das et al. [27] studied the diffraction of oblique surface wave in uniform water depth by twin thin vertical barriers using one-term Galerkin approximation and the expressions of upper and lower bounds for reflection and transmission characteristics were derived. Rezanejad et al. [114] analysed the efficiency of the device of executing a double-chamber oscillating water column over stepped bottom by using both analytical and numerical methods such as the eigenfunction expansion method (EEM) and boundary integral equation method (BIEM). Roy et al. [116] studied oblique incident wave scattering by twin non-identical thin vertical barriers in infinity depth of water by employing Havelock's expansion of velocity potential and reduced the problem finally to the solution of a pair of integral equations of the first kind. Evans and Morris [39] discussed the problem of surface waves interaction by two parallel vertical barriers in deep water depths. They calculated the upper and lower bounds to the reflection coefficient by assuming an appropriate solution to the integral equation generated by using Havelock's inversion. Wang et al. [141] solved the scattering problem by two thin non-identical surface piercing vertical barriers over stepped-type bottom topography using the eigenfunction expansion method and least square approach. The reflection coefficient, the horizontal forces acting on the two barriers, and the free surface elevation between them were numerically calculated for various system parameters. Sarkar and De [122] investigated the scattering of water waves by a pair of partially immersed barriers over a shelf-type bottom topography using multi-term Galerkin approach, where the half-singularities at the edges of the barriers are handled using Chebyshev polynomials and the one-third singularities at the sharp edges of the shelf are handled using ultra-spherical Gegenbauer polynomials with suitable weight functions. Gupta and Gayen [46] studied the influence of two submerged non-identical permeable plates using a multi-term Galerkin approximation method. Chanda and Bora ([18], [19]) investigated the influence of a permeable sea-bed on water waves scattering by twin thin vertical submerged porous barriers employing eigenfunction expansion and least square method. Sannasiraj et al. ([119], [120]) carried out research on diffraction due to floating rectangular structure over the flat seabed and examined the hydrodynamic responses using sway, heave and roll modes. In the former, the

behaviour of pontoon type floating breakwaters in the beam waves using finite element method which was further supported by experimental investigations while in the latter paper the dynamics of multiple floating structures was discussed.

In addition to this, the interaction of surface waves with a long linear array of offshore breakwaters with arbitrary gaps was studied by Lewin [75], Mei [93] and Dalrymple [26]. Dalrymple [26] used eigenfunction expansion method while Lewin [75] and Mei [93] used the theory of Riemann-Hilbert problems to examine their respective problems. Leonard et al. [71] investigated the diffraction arising due to the interaction of obliquely incident water waves and multiple two-dimensional horizontal cylinders by using FEM. Parsons and Martin [104] studied the scattering of linear monochromatic surface waves by thin arbitrary oriented straight barriers and curved barriers using hypersingular integral equations. Roy et al. [117] analysed water waves scattering by multiple thin vertical barriers utilizing a multi-term Galerkin method. Liu et al. [77] constructed an analytical solution in terms of Taylor series to the modified mild-slope equation for surface waves propagating over a finite array of trapezoidal artificial bars from deep water to shallow water. Tseng et al. [136] studied the scattering problem due the presence of periodic arrangement breakwaters for surface piercing and submerged configurations. Panduranga et al. [103] investigated the effectiveness of multiple slatted screens placed in front of a caissons porous breakwater in the presence of seabed undulation to dissipate the incident wave energy using an iterative multi-domain boundary element method. Tran et al. [132] investigated oblique water waves scattering by multiple thin vertical barriers over undulating bottom using the eigenfunction matching method by slicing the bottom topographies into shelves separated by steps.

1.2.2 Water wave scattering by rigid horizontal floating barrier(s)

In case, some part of the free surface of water is covered by some floating structures of different shape, size and nature e.g. floating rigid or flexible dock, floating bridges, floating oil storage base etc., then in the mathematical formulation of such physical problems discontinuities occur in the free surface boundary conditions where the edges of the obstacles meet with the free water surface. This kind of discontinuities at the free surface provide hinderance to the incoming surface waves as the phenomenon of reflection and transmission of the incident waves occurs. Many researchers are drawing a great attention to this kind of problems because of their significant importance in the field of costal and marine engineering. Heins [52] examined the interaction of surface waves with a semi-infinite rigid floating dock in uniform depth of water by employing the Weiner-Hopf technique. The same problem in deep water depth was investigated by Friedrichs and Lewy [43] by employing the complex variable technique. Then, Rubin [118] investigated the finite dock problem in an ocean of infinite depth using variational method. Later, Chakrabarti et al. [14] recovered the results for the same problem as Friedrichs and Lewy [43] by solving Carleman-type singular integral equations. Haskind [48] studied the problem of diffraction of surface water waves with a finite dock by utilizing the complex variable

technique. However, Holford ([54], [55]) utilized the Green's function technique to solve the problem of interaction of surface waves by a finite dock. Mei and Black [94] investigated the scattering of water waves by floating as well as submerged configuration of rectangular obstacle in uniform finite depth of the water. The scattering of normal incident of surface waves by a finite dock using the Laplace transform was examined by Leppington [72]. Later on, Leppington [73] utilized the integral equation technique to study the problem of radiation of short water waves by a finite dock and analyzed the amplitude of reflected and transmitted waves. Linton [76] utilized the modified residue calculus technique to determine the solution of the finite dock problem. Hermans [53] proposed an integral equation method based on Green's theorem to derive a solution for the problem on the wave interaction with rigid or flexible dock of zero draught. Karmakar and Sahoo [60] analyzed the problem of scattering of surface water waves by a semi-infinite floating membrane due to abrupt change in bottom topography by using expansion formulae for finite and infinite steps. Choudhary et al. [24] studied the scattering and radiation of surface waves by a finite dock over an asymmetric rectangular-trench type bottom topography using matched eigenfunction expansion method and boundary element method. Tsai et al. [134] studied the scattering of water waves induced by tension leg structures over the uneven bottom topography, where the uneven bottom was sliced into a number of shelves separated by abrupt steps and then they applied the matched eigenfunction method over each shelf region to solve the problem. Chakrabarti and Martha [15] studied interaction due to floating elastic plate and derived the energy balance relations. Bhattacharjee and Soares [8] employed the matched eigenfunction expansion method to find the solution of scattering of water waves by a floating structure near a wall over stepped bottom topography. Dhillon et al. [36] studied the problem of scattering of surface waves by a rigid dock over a step-type bottom topography by applying matched eigenfunction expansion method. Singla et al. [126] examined the scattering of obliquely incident surface waves by a surface-piercing porous box using matched eigenfunction expansion method. Further, Singla et al. [127] investigated the interaction of surface waves with a thin elastic plate in the presence of a porous box with the aid of matched eigenfunction expansion method. Choudhary and Martha [25] studied the interaction of oblique water waves by two non-uniform submerged horizontal porous plates in the presence of a pair of trenches using Havelock's expansions. Guo et al. [47] examined oblique wave scattering by a semi infinite elastic dock with finite draft floating over a step topography. The scattering of water waves by a floating flexible porous plate was studied using integro-differential equation approach by Koley and Sahoo [64]. Kaligatla et al. [58] studied oblique wave interaction due to a partially submerged rectangular breakwater where as the problem of a rectangular submarine trench in the presence of a thin vertical partially immersed barrier was investigated using Galerkin approximation method by Ray et al. [111]. Manisha et al. [89] studied the influence of undulating bottom for reducing wave-induced forces on a floating bridge with the aid of modified mild-slope and eigenfunction expansion method. Recently, Jain and Bora [57] studied the scattering of obliquely incident water

waves by a floating bridge with rectangular porous wall using matched eigenfunction method. Maiti and Mandal [80] studied surface wave interaction by an elastic floating plate over a porous sea-bed using the matched eigenfunction expansion method. Selvan et al. [123] investigated the reduction of hydro-elastic response of a flexible floating structure by an annular flexible permeable membrane using the matched eigenfunction expansion method along with the orthogonality of the eigenfunction in the open water region. Das et al. [30] studied gravity waves interaction with an elliptic disc submerged in a two-layer fluid with the aid of matched eigenfunction expansion method along with the orthogonal properties of eigenfunctions. Borah and Hassan [10] studied the problem of diffraction of water waves by partially submerged floating hollow cylinder placed over a fixed coaxial bottom-mounted obstacle with the aid of matched eigenfunction expansion and obtained the analytical expressions of potentials. Recently, Hassan et al. [49] examined the radiation problem due to two coaxial cylinders using the method of separation of variables along with eigenfunction expansion matching method. Sarkar and Bora [121] used the same approach as in Hassan et al. [49] to obtain the solution of the water wave radiation problem involving a floating semi-porous compound cylinder. Singh et al. [124, 125] studied the reflection of plane waves at the stress-free/rigid surface of a micro-mechanically modelled piezo-electro-magnetic fiber-reinforced composite half-space. A study on the head-on collision between two solitary waves in a thin elastic plate floating on an inviscid fluid of finite depth was examined analytically by means of a singular perturbation method by Bhatti and Lu [6]. Praveen et al. [108] investigated wave transformation due to finite elastic dock over abrupt change in bottom topography. Vijay et al. [139] studied Bragg scattering of surface wave train by an array of submerged breakwater and a floating dock. Guha and Singh [45] studied reflection/transmission of plane waves in an initially stressed rotating piezo-electro-magnetic fiber-reinforced composite half-space.

1.2.3   Water wave scattering due to bottom undulations

Often the ocean floor is uneven rather than flat-type. This makes, it is significant to consider the problems of propagation of water wave over an uneven sea bed, which are also interesting due to their importance in coastal and marine engineering. Mei and Mehaute [92] gave a note on the equations of long waves over an undulating bottom. The problems of scattering of surface waves by a small undulation present in the bottom have been considered by many researchers (see Miles [96], Davies [31], Davies and Heathershaw [33], Martha and Bora [90] etc.). Newman [100] investigated the problem of propagation of water waves over a step region between the regions of finite and infinite depth. He presented the experimental results in support of theoretical calculated results for reflection and transmission coefficients. Fitz-Gerald [42] studied the reflection of incident surface gravity waves traveling over varying depth. He employed the Fourier transform method to convert the boundary value problem to a pair of integro-differential equation. Miles [96] derived the first order reflection and transmission coefficients in terms of integrals by using perturbation theory along with the Finite cosine transformation technique when

oblique waves strike to the cylindrical obstacle. Davies [31] examined the interaction of progressive waves with small sinusoidal undulations of infinite horizontal extent and then showed that this interaction gave rise to two new waves with wave numbers which were the sum and difference of those of the surface waves and undulations. Davies [32] used a somewhat elaborate method to handle the problem of water wave scattering by a sinusoidal undulating bottom for normal incidence. Heathershaw [51] gave a experimental proof to the theoretical results of reflection of wave energy due to the resonant interactions between surface water waves and undulating bottom topography. Davies and Heathershaw [33] discussed the problem of the reflection of the incident waves by irregular bottom using Fourier transform technique. Mandal and Basu [82] generalized the Miles [96] problem with the inclusion of surface tension at the free surface. Porter and Porter [107] examined the interaction of linearized surface gravity water waves with three dimensional periodic topography. They studied the trapping and scattering of water waves by three dimensional submerged topography, infinite and periodic in one horizontal coordinate and of finite extent in the other. Martha and Bora [90] and Bora and Martha [9] considered the problem of water wave scattering by different types of undulating topography by making use of perturbation theory. Mandal and De [85] analysed surface wave scattering over small undulations with surface discontinuity by employing simplified perturbation analysis. Tsai et al. [135] examined oblique surface wave scattering and breaking by variable porous breakwater placed at the uneven bottom using matched eigenfunction expansion method. In case of bottom profile for undulating bottom, one may also look at step-type bottom topography in which an abrupt change occur in the depth of ocean. Wave propagation over an abrupt change in bottom topography give rise to wave reflection, shoaling and refraction, which have important effects on the constructions and design of offshore platforms. Bartholomeusz [4] utilized long wave theory to study the problem of scattering of surface water waves by sudden change of the depth. He presented the theoretical as well as experimental results for reflection and transmission coefficients. Tsai et al. [133] developed an eigenfunction matching method to provide different kinds of step approximations for water wave problems. Chakraborty and Mandal ([16],[17]) studied oblique wave scattering by a rectangular submarine trench. Kaur et al. [61] studied the propagation of obliquely incident surface water waves over a pair of asymmetrical rectangular trenches by incorporating the edge conditions at the sharp edges of the trenches with the aid of a system of singular integral equations of first kind, where the one-third singularity at each edge of trench is handled using suitably designed polynomial as a basis function having collocation points as the zeros of the Chebyshev polynomial. Rezanejad et al. [113] analyzed the role of stepped bottom topography by increasing the efficiency of a nearshore oscillating water column device. They employed methods namely, the matched eigenfunction expansion method and boundary integral equation method to find the solution of the problem. Cho et al. [20] developed finite element formulation for the diffraction of waves caused by depth changes. The model developed was applied to calculate reflection and transmission coefficients. Kreisel [65] studied the problem of

propagation of normal incident waves over a variable-depth geometries which involves the conformal mapping of a fluid domain into a rectangular strip through which the problem for the velocity function is reduced to an integral equation. Lassiter [69] investigated the problem of scattering of water waves by a rectangular trench where the water depths on the both sides of the trench are constant and may be different (an asymmetric trench). He formulated the problem in terms of complementary variational integrals and determined the reflection and transmission coefficients by utilizing the conditions that velocity and pressure is continuous across the vertical lines before and after trench. Lee and Ayer [70] employed the transform method to the symmetric infinite trench problem by conveying solutions in two regions, one with infinitely uniform finite depth region and the other with a rectangular region representing the trench below the uniform seabed level. They performed a number of laboratory experiments in a wave tank and compared their results with the theoretical results. Miles [97] utilized a conformal mapping algorithm to the rectangular trench problem for normal incidence. He also obtained the solution for the case of oblique incidence through a variational formulation of Mei and Black [94]. Kirby and Dalrymple [62] investigated the problem of diffraction of surface water waves by an asymmetric rectangular trench with the aid of matched eigenfunction expansion method and compared their results with the data received from a small-scale wave tank experiment. Au and Brebbia [1] considered a problem in which wave forces are calculated on floating and submerged bodies of different geometries using the boundary element method.

The problems involving scattering of water waves by the structures horizontal/vertical along with some bottom topography will serve as an effective wave barrier to protect various coastal facilities from wave loads. To the best of our knowledge, this type of work involving different structures and different bottom topographies are very less. Thus, this motivate us to study such kind of problems for different configurations of the structures over an uneven bottom with application of suitable mathematical methods.

In the following section, the aims and objectives of the thesis are presented concisely.

1.3 Aims and Objectives

This thesis mainly focuses on the solution of class of problems involving surface water waves interaction with horizontal/vertical barrier(s) over different type of bottom topographies with the aid of different mathematical techniques. The emphasis is given to

(i) analyzing reflection and transmission of incident water waves by barriers (floating dock, vertical rigid barrier, a pair of partial and submerged barriers, multiple rigid vertical barriers) over bottom topographies with respect to various system parameters

(ii) analyzing force, moments on the the barriers and free surface elevation

(iii) development of different mathematical techniques depending on the complexity (arising due to different boundary conditions) of the problem.

The basic equations associated under the assumption of linearized theory of water waves in single layered fluid can be found in Lamb [68], Dean and Dalrymple [35], Rahman [109] and Stoker [130]. In the next section, the relevant basic equations of the linearized theory of water waves are presented in details.

1.4   Basic Equations

The mathematical modelling of the real life physical problems are always made under certain physical assumptions. There is a class of physical problems in ocean/marine engineering which are analyzed with the aid of the linear theory of water waves. In the linear wave theory, the motion of water waves which is under the action of gravity and the free surface deviation from its horizontal position are assumed to be very small such that the velocity components together with their derivatives (assumed to be exist) are quantities of first order of smallness so that their squares, products and higher powers can be neglected. Thus, the boundary conditions can be linearized. In this section, the basic equations are derived which are used frequently in the Chapters 2-5 of this thesis.

1.4.1   Governing equations and boundary conditions of water waves in the context of homogeneous fluid

The rectangular Cartesian co-ordinate system has been chosen in which the positive direction of y-axis is taken vertically downwards and the xz-plane is taken along the undisturbed free surface of the fluid. The fluid under consideration occupies the region $-\infty < x, z < \infty, 0 \leq y \leq h$. The flat bottom surface is represented by $y = h$. It is assumed that the fluid is incompressible, inviscid and the motion of the fluid is irrotational and simple harmonic in time.

(i) Governing equation:

Since, the motion is irrotational, there exists a velocity potential $\Phi(x, y, z, t)$ such that velocity $\vec{q}$ of fluid can be expressed as

$$\vec{q} = (u, v, w) = \nabla\Phi \tag{1.1}$$

The equation of continuity for incompressible and inviscid is

$$\nabla.\vec{q} = 0 \tag{1.2}$$

From the equation (1.1) and (1.2), we have the governing equation as Laplace's equation

$$\frac{\partial^2\Phi}{\partial x^2} + \frac{\partial^2\Phi}{\partial y^2} + \frac{\partial^2\Phi}{\partial z^2} = 0, \quad \text{in the fluid region.} \tag{1.3}$$

(ii) Dynamic free surface boundary conditions:

The Euler's equation of motion is

$$\frac{\partial \vec{q}}{\partial t} + (\vec{q}.\nabla)\vec{q} = g - \frac{1}{\rho}\nabla p \qquad (1.4)$$

where p is the pressure at the fluid, ρ is the density of the fluid and g is the acceleration due to gravity.

On simplifying the relation (1.4), the Euler's equation of motion gives

$$\frac{\partial \Phi}{\partial t} + \frac{1}{2}\left[\left(\frac{\partial \Phi}{\partial x}\right)^2 + \left(\frac{\partial \Phi}{\partial y}\right)^2 + \left(\frac{\partial \Phi}{\partial z}\right)^2\right] + \frac{p}{\rho} - gy = 0, \qquad (1.5)$$

which is known as Bernoulli's equation of motion. The pressure at the free surface $y = \eta(x, z, t)$ is equal to the atmospheric pressure which is constant, taken zero here without lose of generality. Thus, the relation (1.5) reduces to

$$\frac{\partial \Phi}{\partial t} + \frac{1}{2}\left[\left(\frac{\partial \Phi}{\partial x}\right)^2 + \left(\frac{\partial \Phi}{\partial y}\right)^2 + \left(\frac{\partial \Phi}{\partial z}\right)^2\right] - g\eta = 0, \text{on } y = \eta(x, z, t), \qquad (1.6)$$

which is known as dynamic free surface boundary condition.

(iii) Kinematic free surface boundary condition:

The vertical velocity component of the fluid over the free surface is equal to the rate of rise/fall of the surface at any point which gives the condition as given by

$$\frac{\partial \Phi}{\partial y} = \frac{\partial \eta}{\partial t} + \frac{\partial \eta}{\partial x}\frac{\partial \Phi}{\partial x} + \frac{\partial \eta}{\partial z}\frac{\partial \Phi}{\partial z}, \qquad \text{on } y = \eta(x, z, t), \qquad (1.7)$$

(iv) Linearized free surface boundary condition:

Under the assumption of linear water wave theory, the velocity components and the free surface elevation/depression together with their partial derivatives are small quantities, so their squares, higher powers and the product may be neglected so that the conditions (1.6) and (1.7) respectively become

$$\frac{\partial \Phi}{\partial t} - g\eta = 0, \quad \text{on } y = \eta(x, z, t), \qquad (1.8)$$

and

$$\frac{\partial \Phi}{\partial y} = \frac{\partial \eta}{\partial t}, \quad \text{on } y = \eta(x, z, t). \qquad (1.9)$$

By using Taylor's series expansion and neglecting the second and higher orders of smallness, the relations (1.8) and (1.9) reduce to the linearized boundary conditions:

$$\frac{\partial \Phi}{\partial t} - g\eta = 0, \quad \text{on } y = 0, \qquad (1.10)$$

and

$$\frac{\partial \Phi}{\partial y} = \frac{\partial \eta}{\partial t}, \quad \text{on } y = 0. \qquad (1.11)$$

Now, eliminating η between the relation (1.10) and (1.11), we have

$$\frac{\partial^2 \Phi}{\partial t^2} = g\frac{\partial \Phi}{\partial y}, \quad \text{on } y = 0, \tag{1.12}$$

which is the combined linearized free surface condition.

(v) Bottom boundary condition:

In this thesis, a flat rigid bottom is considered, thus, no flux boundary condition on the bottom bed at $y = h$, is given by

$$\frac{\partial \Phi}{\partial y} = 0, \quad \text{on } y = h, \tag{1.13}$$

The equations (1.3), (1.12) and (1.13) are the basic equations of the linearized water wave theory.

In case, the surface water waves incident at an angle, α with the positive direction of $x-$axis, the characteristic behaviour of the motion of the fluid remains the same along the $z-$direction and as the motion of fluid is taken to be simple harmonic in time with angular frequency ω, the velocity potential $\Phi(x, y, z, t)$ may be expressed as

$$\Phi(x, y, z, t) = \Re[\phi(x, y)e^{i(\mu z - \omega t)}], \tag{1.14}$$

where $\Re$ represents the rear part and μ is the component of the incident wavenumber k_0 along $z-$direction which is given by $\mu = k_0 \sin \alpha$ and k_0 is the unique real positive root of the transcendental equation $K - k \tanh kh = 0$.

Substituting the relation (1.14) in relations (1.3), (1.12) and (1.13), the governing equation, the free surface and bottom boundary conditions become

$$\frac{\partial^2 \phi}{\partial x^2} + \frac{\partial^2 \phi}{\partial y^2} - \mu^2 \phi = 0, \quad \text{in the fluid region.} \tag{1.15}$$

$$K\phi + \frac{\partial \phi}{\partial y} = 0, \quad \text{on } y = 0, \tag{1.16}$$

$$\frac{\partial \phi}{\partial y} = 0, \quad \text{on } y = h, \tag{1.17}$$

where $K = \omega^2/g$. In case of the normal incidence ($\alpha = 0$) of surface water waves, the equations (1.16) and (1.17) remain the same while the equation (1.15) becomes

$$\frac{\partial^2 \phi}{\partial x^2} + \frac{\partial^2 \phi}{\partial y^2} = 0, \quad \text{in the fluid region.} \tag{1.18}$$

The governing Helmholtz equation (1.15) along with boundary conditions (1.16) and (1.17) has two types solutions: the wave like solution and the non-wave like solution which are described as follows:

Solution for the velocity potential:

The progressive wave solution (wave like solution) of the Helmholtz equation is given by

$$\phi(x, y) = \frac{\cosh k_0(h - y)}{\cosh k_0 h} e^{\pm i(k_0 \cos \alpha)x}, \tag{1.19}$$

where k_0 is the unique real positive root of the dispersion relation in k which is given by

$$K - k \tanh kh = 0. \tag{1.20}$$

The local solutions (non-wave like solution) are given by

$$\phi(x, y) = \cos k_n(h - y) e^{\pm (k_n cos\alpha)|x|}, \tag{1.21}$$

where $k_n (n = 1, 2, 3, ...)$ are purely imaginary roots of the dispersion relation (1.20).

1.5   Outline of the thesis

In the thesis, there are six chapters: Chapters 2-5 describe different research problems where as Chapter 1 represents the introduction and Chapter 6 summarizes the whole research work done in the thesis and highlights the future directions of the work.

In **Chapter 1**, a basic introduction, relevant literature, aims and objectives behind the current work are presented. In addition, the basis equations for the linearized theory of surface water waves followed by the summary of each chapter are presented.

In **Chapter 2**, a study on the scattering of surface water waves by a finite dock over a two stepped bottom topography is examined under the assumptions of the linearized water wave theory using eigenfunction expansion method followed by suitable application of orthogonality of eigenfunctions for normal incident of surface water waves. The effect of abrupt change in bottom topography on the wave propagation from lower depth region as well as from higher depth region is analyzed. It is observed that the reflection coefficient is decreasing slightly and transmission coefficient is increasing with increasing the depth ratios for wave propagation from lower depth region. On the other hand, for wave propagation from higher depth region, the reflection coefficient is increasing as the values of the depth ratios are increasing while the transmission coefficient is decreasing. The reflection coefficient is also increasing by increasing the wavenumber, dock length and width of the step whereas the transmission coefficient is decreasing for the same. Furthermore, this problem is generalized for multi-steps and it is found that the transmission coefficient is increasing but the reflection coefficient is slightly decreasing by increasing the number of steps. The energy balance relation is also derived and verified, where it is observed that the numerical results obtained for reflection and transmission coefficients satisfy the energy balance relation almost accurately. The present results are also validated through the results available in the literature. This study concludes that the horizontal breakwater over multi-stepped bottom is important and may be helpful for designing the structures for protection of seashore.

Chapter 3 deals with the scattering of oblique incident surface gravity waves by a thin vertical rigid barrier over a stepped bottom topography with the aid of matched eigenfunction expansion method using algebraic least squares method. The energy balance relation for the present problem is derived and verified numerically. Also, the present problem validated through the available results in the literature. The effect of different parameters are studied by plotting the graphs for reflection and transmission coefficients, non-dimensional horizontal force. The reflection coefficient increases as the length of the barrier and the step height increase while it decreases as the angle of incidence increases. It is observed that the maximum reflection occurs for normal incidence of the incident waves in comparison to oblique incidence. The analysis of non-dimensional horizontal force per unit width of the barrier is also examined. As the length of the barrier over the step increases, the absolute maximum of force curves goes on increasing. The non-dimensional horizontal force on the barrier decreases as the reflection coefficient due to the presence of the barrier decreases. Also, it is noticed that the force on the barrier is less for oblique incident waves in comparison to normal incident waves. Therefore, the barrier over stepped bottom may be utilized to effectively reflect the incident waves and create a calm zone along lee side, yielding less impact on seashore.

In **Chapter 4**, the problem of scattering of water waves by two thin vertical barriers over a shelf-type bottom topography is examined for its solution using the eigenfunction expansion method and the algebraic least square approach. The energy balance relation for the given problem is derived and checked. Also, the present results are validated with the available results in literature. The numerical values of the reflection and transmission coefficients are plotted through different graphs to demonstrate the influence of various system parameters. For identical length of the barriers over symmetric shelf bottom, the zeros in the reflection curve occur. These zeros in the reflection curve may be avoided by using non-identical length of the barriers or asymmetric shelf bottom topography. It is also observed that more energy is reflected by a pair of barriers in comparison to single barrier. On increasing the length of the barriers, more reflection and consequently less transmission occurs to the lee side. As the gap between the barriers increases, it causes more number of oscillations on both the reflection and transmission coefficients curves. The local maxima in reflection curve decreases as the angle of incidence increases. Also, the reflection coefficient decreases as the depth of submergence of the barriers increases. Furthermore, the problem is generalized for an array of surface piercing barriers over shelf bottom topography. It is noticed that local maxima in reflection curve increases as additional pairs of surface piercing barriers are considered between the barriers. It is also observed that the wave amplitude after the barriers can be decreased with the increased length of the barriers. The analysis of non-dimensional horizontal force per unit width of the front and rear barriers is also observed. It is shown that the front barrier experience more force as compared to the rear barrier.

The **Chapter 5** deals with the scattering of obliquely incident surface waves by two vertical barriers over an arbitrary bottom topography. To handle the problem with

arbitrary bottom topography, the finite element method is employed to solve the problem. The results are analyzed for parabolic and rectangular type hump bottom profiles. The radiation boundary conditions are kept at a finite distance from the vertical barriers as the local disturbances decay sufficiently within a distance. The scattered potential is determined computationally and is further used to obtain the numerical values of the reflection and transmission coefficients and the force on the barriers. It is observed that the zeros on the reflection and transmission curves exist for identical length of the barriers and these zeros increases as the gap between the barriers increases. Also, the lower frequency zeros of the transmission curve coalesce in pairs as the gap between the barriers increases. The study reveals that the reflection coefficient increases due to the height of bottom topography for smaller wave numbers while it has a negligible effect for larger wavenumbers. This means for larger wavenumbers the water depth throughout the region can be seen as deep enough. It is noticed that the reflection coefficient increases with the drafts and thickness of the barriers. Also, the influence of the angle of incidence on the reflection coefficient has been observed. In addition to this, the effect of the hump height and the drafts of the barriers on the non-dimensional horizontal force on the front and rear barriers is studied. The energy balance relation is derived from Green's identity which ensures the correctness of the present numerical results. The obtained results are compared with the results available in the literature for validation purpose.

Chapter 6 presents the summary of the work done in the thesis followed by the future scope of research. In this chapter, we have highlighted the major contributions.

Chapter 2

Scattering of surface water waves by a finite dock over two-stepped bottom profile

2.1 Introduction

In this chapter, the scattering of surface waves by the edges of a finite dock over a $2-$step bottom topography is investigated for normal incidence under the assumption of linear water wave theory. Here, the incidence of water waves is considered in two different manners (i) from lower depth region, and (ii) from higher depth region. Further, a generalization of the problem is made for multiple steps at the bottom profile. The problem under consideration give rise to a mixed boundary value problem which is solved with the aid of an eigenfunction expansion method in conjunction with the matching technique. The main idea behind this method is to apply appropriate matching conditions along with associated orthogonal relations of eigenfunctions which give rise to a determined system of linear algebraic equations involving the unknowns. The values of the physical quantities, namely, the reflection and transmission coefficients can be obtained by solving the system with any standard method as the determinant of coefficient matrix is non zero. The numerical values of these coefficients are compared with the known results of Linton [76] using graphical as well as tabular results. The energy identity relation, an important relation in the study involving scattering of surface water waves, is deducted for the present problem with the help of Green's integral theorem. The identity provides the correctness of numerical results obtained in this chapter. The force and moments of surface waves on the dock are also analyzed. A major part of the work presented in this chapter has been published in (Choudhary et al. [23]).

2.2 Mathematical Formulation and Method of Solution

2.2.1 Case-I: When waves incident from lower depth region

Here, the problem of scattering of surface water waves by the edges of a finite floating dock over a 2-step bottom topography is considered where the waves incident on the dock from the lower depth water region (see Fig. 2.1). Consider a two dimensional Cartesian co-ordinate system in which the x-axis represents the mean horizontal position of the free

surface of the fluid and the positive direction of the y-axis is taken vertically downward in the fluid region. We assume that a finite floating dock occupies the region $-a < x < a$, $y = 0$, whereas the region $(-\infty < x < -a) \bigcup (a < x < \infty)$, $y = 0$ is free to the upper atmosphere. The region $(x \leq 0, 0 \leq y \leq h_1)$ denotes the lower depth water region whereas the region $(x \geq b, 0 \leq y \leq h_3)$ represents the higher depth water region. The entire fluid
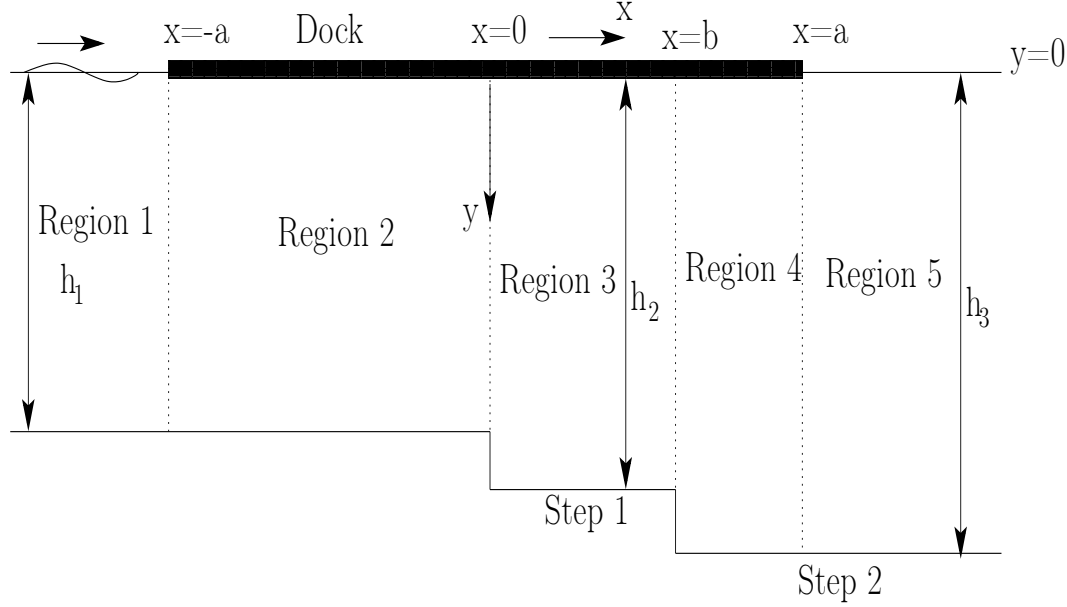
Figure 2.1: Definition sketch for case-I

domain is divided into five regions:

(i) The open region 1: $-\infty < x < -a, 0 < y < h_1$

(ii) The covered region 2: $-a < x < 0, 0 < y < h_1$

(iii) The covered region 3: $0 < x < b, 0 < y < h_2$

(iv) The covered region 4: $b < x < a, 0 < y < h_3$

(v) The open region 5: $a < x < \infty, 0 < y < h_3$.

Assuming the motion of the fluid is simple harmonic in time, the velocity potential can be written as $Re\{\phi(x,y)e^{-i\sigma t}\}$, where σ is the angular frequency. For the inviscid, incompressible and irrotational fluid, the complex velocity potential $\phi(x, y)$ satisfies the Laplace's equation:

$$\frac{\partial^2 \phi_j}{\partial x^2} + \frac{\partial^2 \phi_j}{\partial y^2} = 0, \quad j = 1, 2, 3, 4, 5, \quad \text{in the corresponding fluid region } j, \qquad (2.1)$$

along with the following boundary conditions in different regions.
In region 1, ϕ_1 satisfies the free surface condition

$$\frac{\partial \phi_1}{\partial y} + K\phi_1 = 0, \quad \text{on } y = 0, -\infty < x < -a, \qquad (2.2)$$

along with the bottom condition

$$\frac{\partial \phi_1}{\partial y} = 0, \quad \text{on } y = h_1, \tag{2.3}$$

where $K = \sigma^2/g$ with g is the acceleration due to gravity.

In region 2, ϕ_2 satisfies the condition on the rigid dock

$$\frac{\partial \phi_2}{\partial y} = 0, \quad \text{on } y = 0, -a < x < 0, \tag{2.4}$$

with the bottom condition

$$\frac{\partial \phi_2}{\partial y} = 0, \quad \text{on } y = h_1. \tag{2.5}$$

In region 3, ϕ_3 satisfies the dock condition and the vertical wall condition respectively as

$$\frac{\partial \phi_3}{\partial y} = 0, \quad \text{on } y = 0, 0 < x < b, \tag{2.6}$$

$$\frac{\partial \phi_3}{\partial x} = 0, \quad \text{on } x = 0, h_1 < y < h_2, \tag{2.7}$$

with the bottom condition

$$\frac{\partial \phi_3}{\partial y} = 0, \quad \text{on } y = h_2. \tag{2.8}$$

In region 4, ϕ_4 satisfies the conditions on the dock and vertical wall respectively as given by

$$\frac{\partial \phi_4}{\partial y} = 0, \quad \text{on } y = 0, b < x < a, \tag{2.9}$$

$$\frac{\partial \phi_4}{\partial x} = 0, \quad \text{on } x = b, h_2 < y < h_3, \tag{2.10}$$

with the bottom condition

$$\frac{\partial \phi_4}{\partial y} = 0, \quad \text{on } y = h_3. \tag{2.11}$$

In region 5, ϕ_5 satisfies the free surface condition

$$\frac{\partial \phi_5}{\partial y} + K\phi_5 = 0, \quad \text{on } y = 0, a < x < \infty, \tag{2.12}$$

with the bottom condition

$$\frac{\partial \phi_5}{\partial y} = 0, \quad \text{on } y = h_3. \tag{2.13}$$

The edge conditions at the two ends of the dock is given by the relation

$$\frac{\partial \phi_j}{\partial y} \sim \widehat{A} \ln r \text{ as } r \to 0 \tag{2.14}$$

where $\widehat{A}$ is a constant with $r^2 = [(x + a)^2 + y^2]$ for $j = 1, 2$ and $r^2 = [(x - a)^2 + y^2]$ for $j = 4, 5$.

The velocity potentials ϕ_1 and ϕ_5 satisfy the far filed conditions as given by

$$\phi_1(x,y) \sim (e^{ik_0(x+a)} + Re^{-ik_0(x+a)})\frac{\cosh k_0(h_1 - y)}{\cosh k_0 h_1}, \quad \text{as } x \to -\infty, \qquad (2.15)$$

$$\phi_5(x,y) \sim Te^{ip_0(x-a)}\frac{\cosh p_0(h_3 - y)}{\cosh p_0 h_3}, \qquad\qquad \text{as } x \to \infty. \qquad (2.16)$$

where $k = k_0$ and $k = p_0$ are, respectively, the positive real roots of the transcendental equations

$$K - k\tanh kh_1 = 0, \qquad (2.17)$$

$$K - k\tanh kh_3 = 0, \qquad (2.18)$$

and R and T represent, respectively, the reflection and transmission coefficients to be determined here. The other conditions that will be necessary to be applied to obtain the solution of the above problem are that the pressure and velocity are continuous across the interfaces $x = -a, x = 0, x = b$ and $x = a$. So we can write

$$\left.\begin{aligned}
\phi_1(-a_-,y) &= \phi_2(-a_+,y) \\
\frac{\partial\phi_1(-a_-,y)}{\partial x} &= \frac{\partial\phi_2(-a_+,y)}{\partial x}
\end{aligned}\right\} \; 0 < y < h_1, \qquad (2.19)$$

$$\left.\begin{aligned}
\phi_2(0_-,y) &= \phi_3(0_+,y) \\
\frac{\partial\phi_2(0_-,y)}{\partial x} &= \frac{\partial\phi_3(0_+,y)}{\partial x}
\end{aligned}\right\} \; 0 < y < h_1, \qquad (2.20)$$

$$\left.\begin{aligned}
\phi_3(b_-,y) &= \phi_4(b_+,y) \\
\frac{\partial\phi_3(b_-,y)}{\partial x} &= \frac{\partial\phi_4(b_+,y)}{\partial x}
\end{aligned}\right\} \; 0 < y < h_2, \qquad (2.21)$$

$$\left.\begin{aligned}
\phi_4(a_-,y) &= \phi_5(a_+,y) \\
\frac{\partial\phi_4(a_-,y)}{\partial x} &= \frac{\partial\phi_5(a_+,y)}{\partial x}
\end{aligned}\right\} \; 0 < y < h_3, \qquad (2.22)$$

Expansion method

The Havelock's expansion [50] of the velocity potential $\phi_j(j = 1, 2, 3, 4, 5)$ in terms of appropriate eigenfunctions can be expressed as

$$\phi_1(x,y) = \left(e^{ik_0(x+a)} + Re^{-ik_0(x+a)}\right)\frac{\cosh k_0(h_1 - y)}{\cosh k_0 h_1} + \sum_{n=1}^{\infty} A_n e^{k_n(x+a)}\frac{\cos k_n(h_1 - y)}{\cos k_n h_1},$$

$$(-\infty < x < -a, \; 0 < y < h_1), \quad (2.23)$$

$$\phi_2(x,y) = B_0 + B_1\frac{x}{a} + \sum_{n=1}^{\infty}\left(\hat{B}_n e^{\frac{n\pi x}{h_1}} + \tilde{B}_n e^{\frac{-n\pi x}{h_1}}\right)\cos\left(\frac{n\pi}{h_1}y\right),$$

$$(-a < x < 0, \; 0 < y < h_1), \quad (2.24)$$

$$\phi_3(x,y) = C_0 + C_1\frac{x}{a} + \sum_{n=1}^{\infty}\left(\hat{C}_n e^{\frac{n\pi x}{h_2}} + \tilde{C}_n e^{\frac{-n\pi x}{h_2}}\right)\cos\left(\frac{n\pi}{h_2}y\right),$$

$$(0 < x < b, \; 0 < y < h_2), \quad (2.25)$$

$$\phi_4(x,y) = D_0 + D_1\frac{x}{a} + \sum_{n=1}^{\infty}\left(\hat{D}_n e^{\frac{n\pi x}{h_3}} + \tilde{D}_n e^{\frac{-n\pi x}{h_3}}\right)\cos\left(\frac{n\pi}{h_3}y\right),$$

$$(b < x < a, \ 0 < y < h_3), \qquad (2.26)$$

$$\phi_5(x,y) = Te^{ip_0(x-a)}\frac{\cosh p_0(h_3 - y)}{\cosh p_0 h_3} + \sum_{n=1}^{\infty}E_n e^{-p_n(x-a)}\frac{\cos p_n(h_3 - y)}{\cos p_n h_3},$$

$$(a < x < \infty, \ 0 < y < h_3), \qquad (2.27)$$

where k_n and $p_n(n = 1, 2, \ldots)$ are the real positive roots of the transcendental equations $K + k\tan kh_1 = 0$ and $K + k\tan kh_3 = 0$, respectively and $R, A_n, B_0, B_1, \hat{B}_n, \tilde{B}_n, C_0, C_1, \hat{C}_n, \tilde{C}_n, \ D_0, D_1, \hat{D}_n, \tilde{D}_n, \ T, \ E_n, (n = 1, 2, 3, \ldots)$ are the unknown constants to be determined. On truncating the series given in relations (2.23)-(2.27) to a finite number N (say), we have $(8N + 8)$ unknowns. Now, multiplying both sides of the matching conditions (2.19)-(2.22) by $\cos(m\pi y/h_i)$, $(i = 1, 2, 3; m = 0, 1, 2, \ldots, N)$ appropriately, we have

$$\left.\begin{array}{rcl}\phi_1(-a_-, y)\cos\left(\dfrac{m\pi}{h_1}y\right) & = & \phi_2(-a_+, y)\cos\left(\frac{m\pi}{h_1}y\right) \\[2mm] \dfrac{\partial\phi_1(-a_-, y)}{\partial x}\cos\left(\dfrac{m\pi}{h_1}y\right) & = & \dfrac{\partial\phi_2(-a_+, y)}{\partial x}\cos\left(\dfrac{m\pi}{h_1}y\right)\end{array}\right\}, \qquad (2.28)$$

$$\left.\begin{array}{rcl}\phi_2(0_-, y)\cos\left(\dfrac{m\pi}{h_1}y\right) & = & \phi_3(0_+, y)\cos\left(\frac{m\pi}{h_1}y\right) \\[2mm] \dfrac{\partial\phi_2(0_-, y)}{\partial x}\cos\left(\dfrac{m\pi}{h_2}y\right) & = & \dfrac{\partial\phi_3(0_+, y)}{\partial x}\cos\left(\dfrac{m\pi}{h_2}y\right)\end{array}\right\}, \qquad (2.29)$$

$$\left.\begin{array}{rcl}\phi_3(b_-, y)\cos\left(\dfrac{m\pi}{h_2}y\right) & = & \phi_4(b_+, y)\cos\left(\frac{m\pi}{h_2}y\right) \\[2mm] \dfrac{\partial\phi_3(b_-, y)}{\partial x}\cos\left(\dfrac{m\pi}{h_3}y\right) & = & \dfrac{\partial\phi_4(b_+, y)}{\partial x}\cos\left(\dfrac{m\pi}{h_3}y\right)\end{array}\right\}, \qquad (2.30)$$

$$\left.\begin{array}{rcl}\phi_4(a_-, y)\cos\left(\dfrac{m\pi}{h_3}y\right) & = & \phi_5(a_+, y)\cos\left(\frac{m\pi}{h_3}y\right) \\[2mm] \dfrac{\partial\phi_4(a_-, y)}{\partial x}\cos\left(\dfrac{m\pi}{h_3}y\right) & = & \dfrac{\partial\phi_5(a_+, y)}{\partial x}\cos\left(\dfrac{m\pi}{h_3}y\right)\end{array}\right\}. \qquad (2.31)$$

After multiplication, integrate each equation in relations (2.28)-(2.31) over $(0, h_i)$ appropriately and using the wall condition (2.7) in relation (2.29) and the wall condition (2.10) in relation (2.30), we obtain

$$\left.\begin{array}{rcl}\displaystyle\int_0^{h_1}\phi_1(-a, y)\cos\left(\dfrac{m\pi}{h_1}y\right)dy & = & \displaystyle\int_0^{h_1}\phi_2(-a, y)\cos\left(\dfrac{m\pi}{h_1}y\right)dy, \\[4mm] \displaystyle\int_0^{h_1}\dfrac{\partial\phi_1(-a, y)}{\partial x}\cos\left(\dfrac{m\pi}{h_1}y\right)dy & = & \displaystyle\int_0^{h_1}\dfrac{\partial\phi_1(-a, y)}{\partial x}\cos\left(\dfrac{m\pi}{h_1}y\right)dy,\end{array}\right\} \qquad (2.32)$$

$$\left.\begin{array}{rcl}\displaystyle\int_0^{h_1}\phi_2(0, y)\cos\left(\dfrac{m\pi}{h_1}y\right)dy & = & \displaystyle\int_0^{h_1}\phi_3(0, y)\cos\left(\dfrac{m\pi}{h_1}y\right)dy, \\[4mm] \displaystyle\int_0^{h_1}\dfrac{\partial\phi_2(0, y)}{\partial x}\cos\left(\dfrac{m\pi}{h_2}y\right)dy & = & \displaystyle\int_0^{h_2}\dfrac{\partial\phi_3(0, y)}{\partial x}\cos\left(\dfrac{m\pi}{h_2}y\right)dy,\end{array}\right\} \qquad (2.33)$$

$$
\left. \begin{aligned}
\int_0^{h_2} \phi_3(b,y) \cos\left(\frac{m\pi}{h_2}y\right) dy &= \int_0^{h_2} \phi_4(b,y) \cos\left(\frac{m\pi}{h_2}y\right) dy, \\
\int_0^{h_2} \frac{\partial \phi_3(b,y)}{\partial x} \cos\left(\frac{m\pi}{h_3}y\right) dy &= \int_0^{h_3} \frac{\partial \phi_4(b,y)}{\partial x} \cos\left(\frac{m\pi}{h_3}y\right) dy,
\end{aligned} \right\} \tag{2.34}
$$

$$
\left. \begin{aligned}
\int_0^{h_3} \phi_4(a,y) \cos\left(\frac{m\pi}{h_3}y\right) dy &= \int_0^{h_3} \phi_5(a,y) \cos\left(\frac{m\pi}{h_3}y\right) dy, \\
\int_0^{h_3} \frac{\partial \phi_4(a,y)}{\partial x} \cos\left(\frac{m\pi}{h_3}y\right) dy &= \int_0^{h_3} \frac{\partial \phi_5(a,y)}{\partial x} \cos\left(\frac{m\pi}{h_3}y\right) dy.
\end{aligned} \right\} \tag{2.35}
$$

Here, the relations (2.32)-(2.35) produce a system of $(8N+8)$ linear algebraic equations with $(8N+8)$ unknowns $R, A_n, B_0, B_1, \hat{B}_n, \tilde{B}_n, C_0, C_1, \hat{C}_n, \tilde{C}_n, D_0, D_1, \hat{D}_n, \tilde{D}_n, T, E_n (n = 1, 2, \ldots, N)$. This requires the inversion of $(8N+8) \times (8N+8)$ complex valued matrix. The system of equations is solved by Gauss elimination method with the help of MATLAB.

It may be noted that the above system can have a unique solution if the occurrence of ill-conditioned matrix can be avoided. This situation can be avoided by choosing the appropriate values of the parameters.

2.2.2   Case-II: When waves incident from higher depth region

Here, the surface water wave propagating from $x = +\infty$ is incident on the dock (see Fig. 2.2). In this case, we will have the same equations as discussed in Case-I, except the far-field condition which is given by

$$
\phi_1(x,y) \sim \hat{T} e^{-ik_0(x+a)} \frac{\cosh k_0(h_1 - y)}{\cosh k_0 h_1} \qquad \text{as } x \to -\infty, \qquad (2.36)
$$

$$
\phi_5(x,y) \sim (e^{-ip_0(x-a)} + \hat{R} e^{ip_0(x-a)}) \frac{\cosh p_0(h_3 - y)}{\cosh p_0 h_3} \quad \text{as } x \to \infty, \qquad (2.37)
$$

where $\hat{R}$ and $\hat{T}$, respectively, denote the reflection and transmission coefficients for the Case-II. The Havelock's expansions for the different velocity potentials in the five regions with appropriate eigenfunctions are almost same as given in relations (2.23)-(2.27) with some modification in the velocity potentials $\phi_1(x,y)$ and $\phi_5(x,y)$ as given by:

$$
\phi_1(x,y) = \hat{T} e^{-ik_0(x+a)} \frac{\cosh k_0(h_1 - y)}{\cosh k_0 h_1} + \sum_{n=1}^{\infty} \widehat{E}_n e^{k_n(x+a)} \frac{\cos k_n(h_1 - y)}{\cos k_n h_1},
$$

$$
(-\infty < x < -a, \ 0 < y < h_1), \quad (2.38)
$$

$$
\phi_5(x,y) = (e^{-ip_0(x-a)} + \hat{R} e^{ip_0(x-a)}) \frac{\cosh p_0(h_3 - y)}{\cosh p_0 h_3} + \sum_{n=1}^{\infty} \widehat{A}_n e^{-p_n(x-a)} \frac{\cos p_n(h_3 - y)}{\cos p_n h_3},
$$

$$
(a < x < \infty, \ 0 < y < h_3). \qquad (2.39)
$$

Here also, on truncating the series to a finite number N (say) we left with $(8N+8)$ unknowns. The same procedure as described in the Section 2.2.1 for Case-I, is followed here to determine these unknowns.
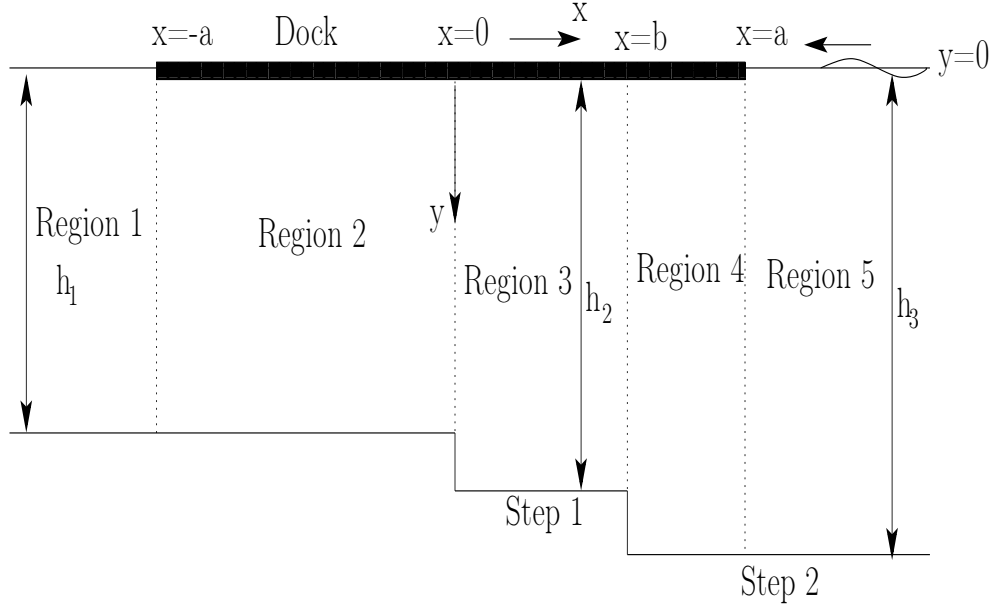
Figure 2.2: Definition sketch for Case II

2.3 Multiple steps at the bottom

Here, the problem of scattering of surface water waves by the edges of a finite floating dock over a M-step bottom topography is considered where the waves incident on the dock from the lower depth water region (see Fig. 2.3). The position of the finite floating dock is same as above. The positions of steps at the bottom are given by $a(j-3)/M \leq x \leq a(j-2)/M$, $y = h^{(j)} = h_1 + (j-2)h$, $j = 3, 4, ..., M+2$ where h is equal heights of all steps with $h^{(1)} = h^{(2)} = h_1$. We have taken $h^{(M+2)} = h^{(M+3)}$ here. The entire fluid domain is divided
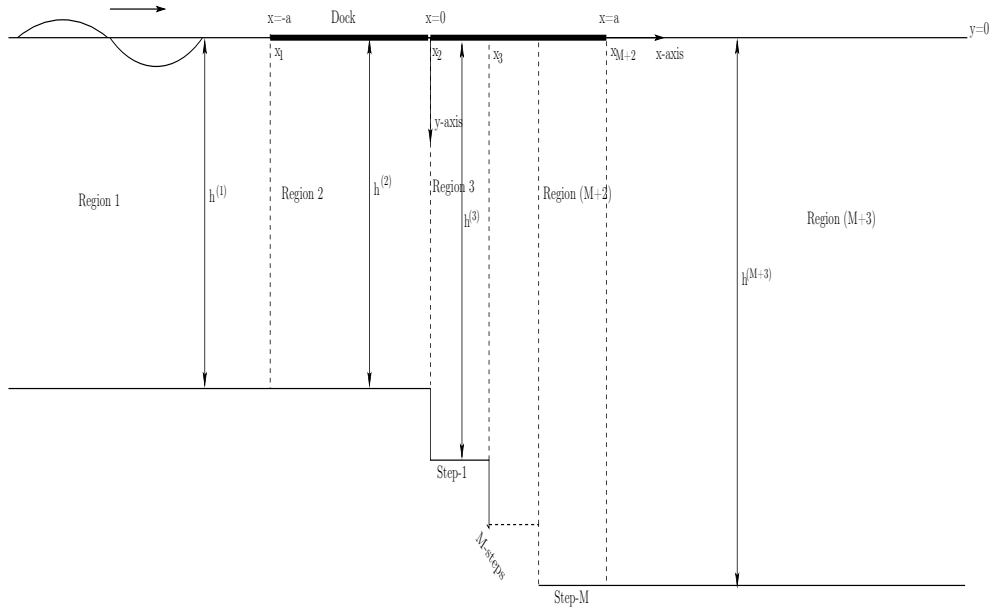
Figure 2.3: Definition sketch for multisteps at the bottom

into $M + 3$ regions:

(i) The open region 1: $-\infty < x < -a, 0 < y < h_1$

(ii) The covered region 2: $-a < x < 0, 0 < y < h_1$

(iii) Other covered regions 3,4,...,M+2:
$a(j-3)/M < x < a(j-2)/M, 0 < y < h_1 + (j-2)h, j = 3, 4, ..., M + 2$

(iv) The open region M+3: $a < x < \infty, 0 < y < h^{(M+3)}$.

The region $(x \le 0, 0 \le y \le h_1)$ denotes the lower depth water region whereas the region $(x \ge a(M-1)/M, 0 \le y \le h^{(M+3)})$ represents the higher depth water region. Here, the complex velocity potential $\phi(x, y)$ satisfies the Laplace's equation:

$$\frac{\partial^2 \phi_j}{\partial x^2} + \frac{\partial^2 \phi_j}{\partial y^2} = 0, \quad j = 1, 2, ..., M + 3, \quad \text{in the corresponding fluid region } j, \quad (2.40)$$

along with the following different boundary conditions:
at $y = 0$, the free surface conditions (excluding rigid dock position) are

$$\frac{\partial \phi_j}{\partial y} + K\phi_i = 0, \quad j = 1, M + 3, \quad (2.41)$$

at $y = 0$, $-a \le x \le a$, the rigid dock conditions are

$$\frac{\partial \phi_j}{\partial y} = 0, j = 2, 3, ..., M + 2, \quad (2.42)$$

the bottom conditions at $y = h^{(j)}$ as

$$\frac{\partial \phi_j}{\partial y} = 0, \quad j = 1, 2, ..., M + 3, \quad (2.43)$$

and conditions at the walls $x = x_{j-1}$ (where $x_{j-1} = a(j-3)/M$) of the stepped profile as

$$\frac{\partial \phi_j}{\partial x} = 0, j = 3, 4, ..., M + 2. \quad (2.44)$$

The edge conditions at the two ends of the dock is given by the relation

$$\frac{\partial \phi_j}{\partial y} \sim \widehat{A} \ln r \text{ as } r \to 0, \quad (2.45)$$

where $\widehat{A}$ is a constant with $r^2 = [(x + a)^2 + y^2]$ for $j = 1, 2$ and $r^2 = [(x - a)^2 + y^2]$ for $j = M + 2, M + 3$.
The velocity potentials ϕ_1 and ϕ_{M+3} satisfy the far filed conditions as given by

$$\phi_1(x, y) \sim (e^{ik_0(x+a)} + Re^{-ik_0(x+a)})\frac{\cosh k_0(h_1 - y)}{\cosh k_0 h_1}, \ x \to -\infty, \quad (2.46)$$

$$\phi_{M+3}(x, y) \sim Te^{ip_0(x-a)}\frac{\cosh p_0(h_3 - y)}{\cosh p_0 h_3}, \qquad x \to \infty. \quad (2.47)$$

where $k = k_0$ and $k = p_0$ are the positive real roots of the transcendental equations $K - k \tanh kh^{(1)} = 0$ and $K - k \tanh kh^{(M+3)} = 0$, respectively and R and T represent, respectively, the reflection and transmission coefficients to be determined here.

The other conditions that will be necessary to be applied to obtain the solution of the above problem are that the pressure and velocity are continuous across the interfaces $x = x_1 = -a, x = x_{j-1} = a(j-3)/M, \quad j = 3, ..., M+3$, which are given by

$$\left.\begin{array}{rcl}\phi_j(x_{j-}, y) & = & \phi_{j+1}(x_{j+}, y) \\[2mm] \dfrac{\partial \phi_j(x_{j-}, y)}{\partial x} & = & \dfrac{\partial \phi_{j+1}(x_{j+}, y)}{\partial x}\end{array}\right\} \; 0 < y < h^{(j)}, \; j = 1, 2, 3, ..., M+2. \qquad (2.48)$$

Assuming M steps of equal heights at the bottom and the wave is incident from lower depth region, the expressions of the velocity potential $\phi_j (j = 1, 2, ..., M+3)$ in all regions can be expressed as

$$\phi_1(x, y) = \left(e^{ik_0(x+a)} + Re^{-ik_0(x+a)}\right) \frac{\cosh k_0(h_1 - y)}{\cosh k_0 h_1} + \sum_{n=1}^{\infty} A_n e^{k_n(x+a)} \frac{\cos k_n(h_1 - y)}{\cos k_n h_1},$$

$$(-\infty < x < -a, \; 0 < y < h_1), \qquad (2.49)$$

$$\phi_2(x, y) = B_0 + B_1 \frac{x}{a} + \sum_{n=1}^{\infty} \left(\hat{B}_n e^{\frac{n\pi x}{h_1}} + \tilde{B}_n e^{\frac{-n\pi x}{h_1}}\right) \cos\left(\frac{n\pi}{h_1} y\right),$$

$$(-a < x < 0, \; 0 < y < h_1), \qquad (2.50)$$

$$\phi_j(x, y) = B_0^{(j)} + B_1^{(j)} \frac{x}{a} + \sum_{n=1}^{\infty} \left(\hat{B}_n^{(j)} e^{\frac{n\pi x}{h^{(j)}}} + \tilde{B}_n^{(j)} e^{\frac{-n\pi x}{h^{(j)}}}\right) \cos\left(\frac{n\pi}{h^{(j)}} y\right),$$

$$\left(\frac{a(j-3)}{M} < x < \frac{a(j-2)}{M}, \; 0 < y < h_1 + (j-2)h; 3 \le j \le M+2\right), \qquad (2.51)$$

$$\phi_{M+3}(x, y) = Te^{ip_0(x-a)} \frac{\cosh p_0(h_1 + Mh - y)}{\cosh p_0(h_1 + Mh)} + \sum_{n=1}^{\infty} E_n e^{-p_n(x-a)} \frac{\cos p_n(h_1 + Mh - y)}{\cos p_n(h_1 + Mh)},$$

$$(a < x < \infty, \; 0 < y < h_1 + Mh), \qquad (2.52)$$

where $R, A_n, B_0, B_1, \hat{B}_n, \tilde{B}_n, B_0^{(j)}, B_1^{(j)}, \hat{B}_n^{(j)}, \tilde{B}_n^{(j)}, T, E_n, (3 \le j \le M+2)$ are the unknown constants to be determined. Following the same procedure as described in the previous section, to produce a system of linear algebraic equations, we multiply the matching conditions by $\cos(m\pi y/h^{(j)}); (j = 1, 2, ..., M+3, m = 0, 1, 2, ..., N)$, then integrating over $(0, h^{(j)})$ appropriately and using wall conditions appropriately, we obtain $2(N+1)(M+1)$ number of equations in $2(N+1)(M+1)$ unknowns which need to be solved to determine the unknowns. In the case of incidence of wave from higher depth region we proceed in similar way as described in the Section 2.2.

2.4   Energy Balance Relation

For derivation of the energy balance relation for Case-I of the present problem, we use the Green's integral theorem:

$$\int_C \left(\phi \frac{\partial \phi^*}{\partial n} - \phi^* \frac{\partial \phi}{\partial n} \right) ds = 0 \tag{2.53}$$

where ϕ^* is the complex conjugate of ϕ, $\partial/\partial n$ represents the outward normal derivative to the boundary denoted by C of the fluid region

$$y = 0 \ (a < x < X); y = 0 \ (-a < x < a); y = 0 \ (-X < x < -a); x = -X \ (0 < y < h_1);$$
$$y = h_1 \ (-X < x < 0); x = 0 \ (h_1 < y < h_2); y = h_2 \ (0 < x < b); x = b \ (h_2 < y < h_3);$$
$$y = h_3 \ (b < x < X); x = X \ (0 < y < h_3).$$

Then, we take limit as $X \to \infty$.

The contributions from the lines $y = 0 \ (a < x < X)$; $y = 0 \ (-a < x < a)$ and $y = 0 \ (-X < x < -a)$ are zero.

There are no contributions from the lines $y = h_1 \ (-X < x < 0)$; $x = 0 \ (h_1 < y < h_2)$; $y = h_2 \ (0 < x < b)$; $x = b \ (h_2 < y < h_3)$ and $y = h_3 \ (b < x < X)$.

The contribution from the line $x = -X \ (0 < y < h_1)$ is

$$\int_0^h \left(\phi \frac{\partial \phi^*}{\partial x} - \phi^* \frac{\partial \phi}{\partial x} \right) dy = i(1 - |R|^2) \frac{2k_0 h_1 + \sinh 2k_0 h_1}{2 \cosh^2 k_0 h_1}, \tag{2.54}$$

and from the line $x = X \ (0 < y < h_3)$ is

$$\int_h^0 \left(\phi \frac{\partial \phi^*}{\partial x} - \phi^* \frac{\partial \phi}{\partial x} \right) dy = -i|T|^2 \frac{2p_0 h_3 + \sinh 2p_0 h_3}{2 \cosh^2 p_0 h_3}. \tag{2.55}$$

Hence, on combining all the contributions shown above, the relation (2.53) produces the energy balance relation as given by

$$|R|^2 + J_1 |T|^2 = 1, \tag{2.56}$$

where

$$J_1 = \left(\frac{2p_0 h_3 + \sinh 2p_0 h_3}{2k_0 h_1 + \sinh 2k_0 h_1} \right) \left(\frac{2 \cosh^2 k_0 h_1}{2 \cosh^2 p_0 h_3} \right).$$

Similarly, the energy balance relation can be derived for the Case-II, when the wave is incident on the dock from positive infinity and is given by

$$|\hat{R}|^2 + J_2 |\hat{T}|^2 = 1, \tag{2.57}$$

where

$$J_2 = \left(\frac{2k_0 h_1 + \sinh 2k_0 h_1}{2p_0 h_3 + \sinh 2p_0 h_3} \right) \left(\frac{2 \cosh^2 p_0 h_3}{2 \cosh^2 k_0 h_1} \right).$$

2.5 Numerical Results and Discussion

In this section, MATLAB programs are worked out to investigate the effects of the various system parameters such as dock length "a", width "b" of step-1, depth ratios h_2/h_1 and h_3/h_1 (or heights of the steps: $(h_2 - h_1)$ and $(h_3 - h_1)$), on the reflection and transmission coefficients. The main aim of the present investigation is to look how the incident wave energy is scattered by both obstacles, dock and two steps. Furthermore, the other important factors of the study, namely, force and moment on the dock over this two step-type bottom topography are also determined and plotted through graphs. For ensuring the correctness of the numerical results the energy identity relation is also derived and verified. Here, all the system parameters are non-dimensionalized by using h_1 as the length scale. The new non-dimensionalized parameters are $A = a/h_1$, $B = b/h_1$, $K' = Kh_1$, $H_2 = h_2/h_1$ and $H_3 = h_3/h_1$.

2.5.1 Convergence for N

In this section, the convergence study for N i.e. the number of evanescent modes is examined for the dock over two step-type bottom topography. In Table 2.1, the values of $|R|$ are tabulated against K' for various values of $N = 2, 3, 5, 6, 8$. The table shows that a sufficient accuracy in the present results is obtained with $N = 5$ for all the values of K' and almost same results are obtained for $N = 6, 7, 8$. Hence, $N = 5$ is taken throughout the study.

Table 2.1: $|R|$ versus K' for various values of $N = 2, 3, 5, 6, 8$ with $A = 1, B = 0.5, H_2 = 1.2, H_3 = 2$.

K'	$|R|(N=2)$	$|R|(N=3)$	$|R|(N=5)$	$|R|(N=6)$	$|R|(N=8)$
0.2	0.377478	0.414558	0.428097	0.428112	0.428122
0.4	0.524783	0.549555	0.569775	0.569782	0.569791
0.6	0.625412	0.651122	0.667499	0.667501	0.667511
0.8	0.690012	0.718745	0.735588	0.735600	0.735614
1.0	0.755322	0.769875	0.787637	0.787648	0.787655

2.5.2 Validation of the results

To validate the present model, the results of the present study are compared with the results available in the literature. It should be observed that if we consider the depth ratios equal to 1 (i.e. $H_2 = 1$ and $H_3 = 1$), the present problem reduces to the problem of scattering of water waves by a finite dock over horizontal bottom (Linton [76], for normal incidence). From the Fig. 2.4 and Table 2.2, it is observed that an excellent agreement is achieved between the present results and results of Linton [76], for normal incidence. Moreover, the energy balance relations (2.56) and (2.57) agree and provides a numerical check for the results obatained through numerical computations as shown in Table 2.3 and Table 2.4.

Table 2.2: Comparison of present results with Linton (2001) for different K' with fixed $A = 1, B = 0.5, H_2 = 1$ and $H_3 = 1$

K'	Linton (2001), for $\theta = 0$		Present results	
	$|R|$	$|T|$	$|R|$	$|T|$
0.2	0.4226	0.9062	0.4226	0.9062
0.4	0.5674	0.8234	0.5673	0.8235
0.6	0.6619	0.7495	0.6619	0.7496
0.8	0.7302	0.6831	0.7301	0.6833
1.0	0.7818	0.6234	0.7817	0.6236

Table 2.3: Verification of energy balance relation for Case I with $A = 1, B = 0.5$

K'	H_2	H_3	R	T	$|R|^2 + J_1|T|^2$
0.2	1	1	0.1759-0.3843i	0.9347-0.0034i	1.0000
0.4	1	1	0.3118-0.4739i	0.8724-0.0093i	1.0000
1.0	1	1	0.5623-0.5431i	0.7063-0.0335i	1.0000
0.2	1.65	2	0.2139-0.3499i	0.9851+0.0125i	1.0065
0.5	1.18	2	0.2851-0.5663i	0.7269-0.0174i	0.9991

Table 2.4: Verification of energy balance relation for Case II with $A = 1, B = 0.5$

K'	H_2	H_3	$\hat{R}$	$\hat{T}$	$|\hat{R}|^2 + J_2|\hat{T}|^2$
0.2	1	1	0.1759 - 0.3843i	0.8241 + 0.3771i	1.0000
0.4	1	1	0.3118 - 0.4739i	0.6879 + 0.4526i	1.0000
1.0	1	1	0.5623 - 0.5431i	0.4333 + 0.4485i	1.0000
3.3	2.5	3	0.8151 - 0.5495i	0.0713 + 0.1682i	1.0002
3.5	2.5	3	0.8291 - 0.5485i	0.0639 + 0.1651i	1.0200
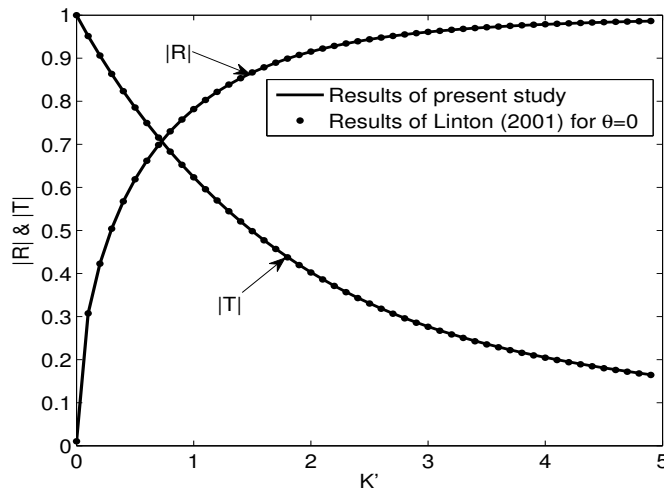
Figure 2.4: Comparison of present results with Linton (2001) for fixed $A = 1, B = 0.5$, $H_2 = 1$ and $H_3 = 1$

2.5.3 Effect of system parameters on the reflection and transmission coefficients

Case I: Waves incident from lower depth region

(a) (b)
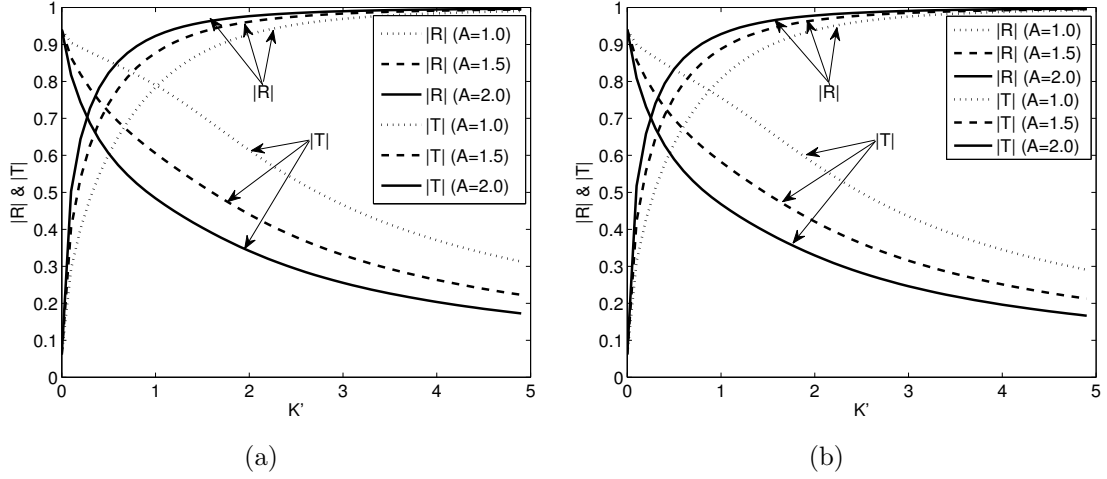
Figure 2.5: $|R|$ and $|T|$ with fixed $H_2 = 1.2$ and $H_3 = 2$ for different values of dock length A where in Fig. (a) $B = 0.2$ and in Fig. (b) $B = 0.5$.

(a) (b)
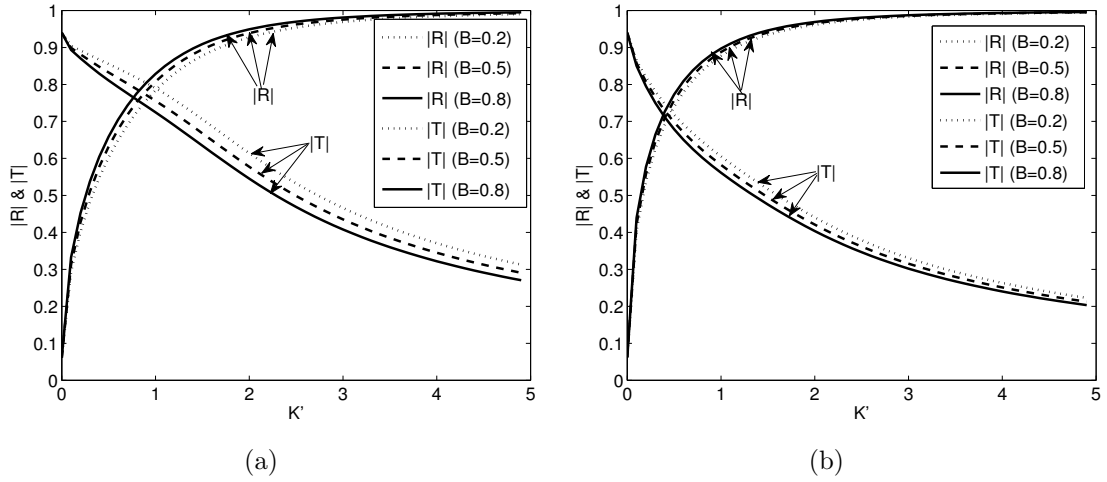
Figure 2.6: $|R|$ and $|T|$ with fixed $H_2 = 1.2$ and $H_3 = 2$ for different values of width B of step-1 where in (a) $A = 1.0$ and in (b) $A = 1.5$.

(i) **Effect of dock length**

Figs. 2.5a and 2.5b show the variation in the reflection coefficient $|R|$ and transmission coefficient $|T|$ against the wavenumber K' for different values of dock length $A = 1.0, 1.5, 2.0$. Here, $H_2 = 1.2$ and $H_3 = 2$ are kept fixed. From these figures, it is observed that the values of the reflection coefficient $|R|$ are very small for small K' (< 0.1) which is plausible, since for long waves the flow is uniform along the horizontal direction, i.e., the incident waves can not be observed by the floating dock and hence incident waves almost fully transmitted. The values of $|R|$ for K'
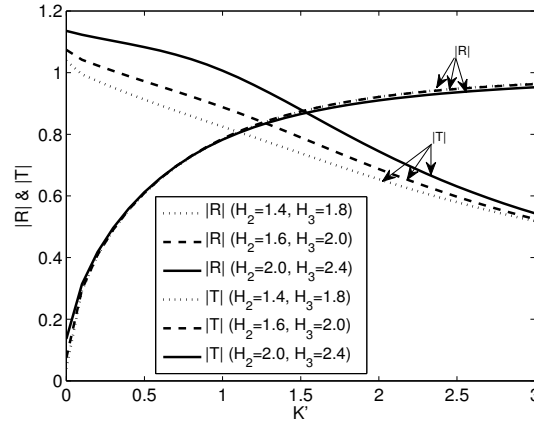
Figure 2.7: $|R|$ and $|T|$ against K' for different depth ratios with $A = 1$ and $B = 0.5$

(< 0.1) are nearly same for different values of A. It is also found that the reflection coefficient is increasing as the value of K' is increasing whereas the transmission coefficient is decreasing with increasing the value of K'. This is due to the fact that for large value of K', the incident wave is concentrated near the free surface and as such most of the incident wave energy is reflected by the floating dock. Furthermore, the values of $|R|$ are increasing and the values of $|T|$ are decreasing as the values of A (and B) are increasing for average values of K'. Hence, it is found that the values of $|R|$ are increasing and the values of $|T|$ are decreasing as the dock length is increasing which is plausible as longer the dock length produces more reflection.

(ii) **Effect of width of step-1**

The reflection coefficient $|R|$ and transmission coefficient $|T|$ are plotted against K' for different values of width of step-1 ($B = 0.2, 0.5, 0.8$) in Figs. 2.6a and 2.6b with fixed $H_2 = 1.2$ and $H_3 = 2$. In these figures we observe the similar behavior of the curves of $|R|$ and $|T|$ against K' as shown in Figs. 2.5a and 2.5b. It is also seen from these figures that the values of $|R|$ is increasing to a small extent as the value of B is increasing from 0.2 to 0.8. Because when step 2 is moving away from step 1, it has very less effect on the reflection coefficient. Similarly, $|T|$ is decreasing to a small extent as the width B is increasing. Hence, the width B has very less effect on reflection and transmission coefficients.

(iii) **Effect of water depth ratios and comparison between the flat bottom, 1-step bottom, 2-step bottom and M-steps bottom**

The variation of the water depths H_2 and H_3 on the reflection coefficient $|R|$ and transmission coefficient $|T|$ is shown in Fig. 2.7. From this figure, it is observed that the values of $|R|$ are decreasing slightly with increasing the values of K' while the values of $|T|$ are increasing as the values of K' are increasing. This may happen due to the fact that increasing the depth ratios creates more gap in the region $x > 0$ producing more transmission. The effect of different number of steps (i.e., flat

(a) (b)
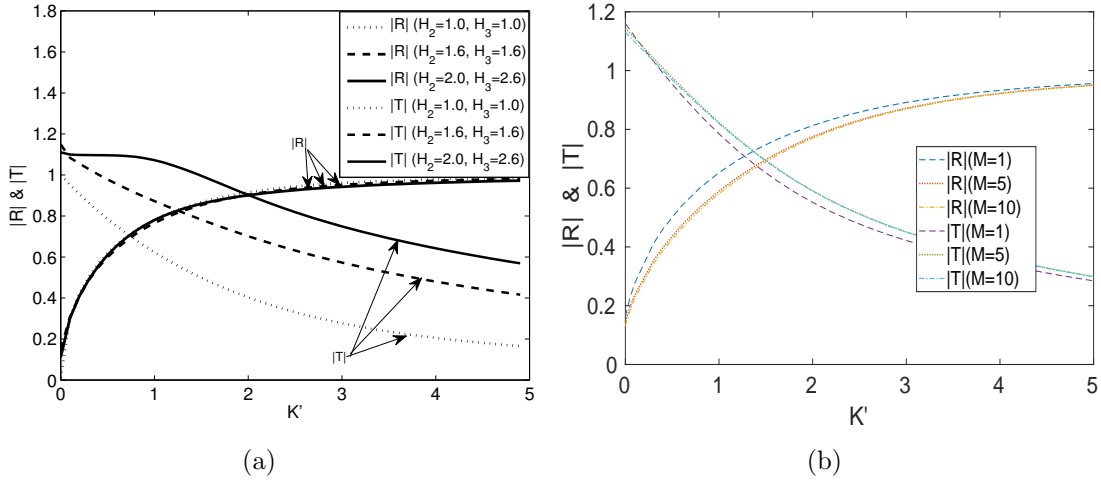
Figure 2.8: $|R|$ and $|T|$ against K' with $A = 1$ and $B = 0.5$ for (a) flat-type, 1-step and 2-step bottom (b) multi-stepped bottom.

bottom, 1-step bottom, 2-step bottom and M-steps bottom) is shown in Figs. 2.8a and 2.8b for Case-I only. In Fig. 2.8a, we consider the depth ratios $H_2 = H_3 = 1$ for flat bottom, $H_2 = H_3 \neq 1$ for 1-step bottom and $H_2 \neq H_3 \neq 1 (H_2 < H_3)$ for 2-step bottom. From this figure, it is found that the reflection coefficient is slightly decreasing as we go from flat bottom to 1-step bottom then to 2-step bottom. But the transmission coefficient is increasing as the number of steps are increasing, which is true because increasing the number of steps produces more transmitting fluid region causing more transmission. Although the transmission coefficient is increasing but the reflection coefficient is slightly decreasing by increasing the number of steps. In Fig. 2.8b, the more number of steps are considered, i.e. $M = 1, 5, 10$ (1-step bottom, 5-steps bottom and 10-steps bottom). In this case also, the same observation is obtained as in the Fig. 2.8a, i.e. the reflection coefficient is slightly decreasing and the transmission coefficient is increasing as the number of steps are increasing. This is plausible from the physical behaviour of the problem.

Case II: Waves incident from higher depth region
Here, the surface wave is incident on the dock from the higher depth region to lower depth region, i.e., wave is incident on the dock from positive infinity. The effect for various system parameters on the reflection $|\hat{R}|$ and transmission $|\hat{T}|$ coefficients is shown in Figs. 2.9, 2.10 and 2.11.

(i) **Effect of dock length**
The reflection and transmission coefficients against K' are depicted in Figs. 2.9a and 2.9b for different values of $A = 1.0, 1.5, 2.0$. Here, we have taken $H_2 = 1.3$ and $H_3 = 2$. It is observed that the reflection coefficient is increasing and transmission coefficient is decreasing with increasing the value of K' as observed in the case when the wave train is incident from lower depth region. It also seen that $|\hat{R}|$ is increasing and $|\hat{T}|$ decreasing as the value of the dock length is increasing. This is plausible
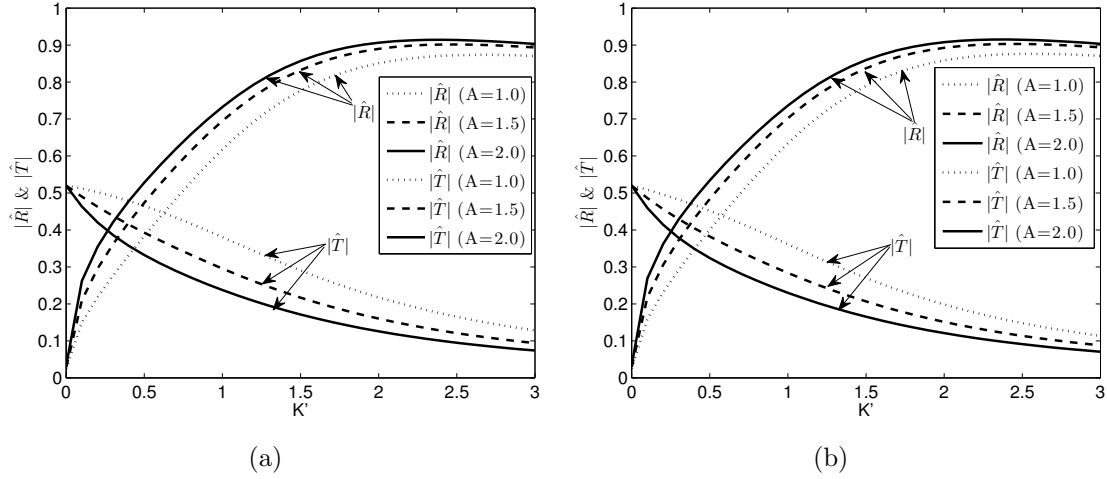
Figure 2.9: $|\hat{R}|$ and $|\hat{T}|$ against K' for fixed $H_2 = 1.3$ and $H_3 = 2$ with different (a) $B = 0.2$ and (b) $B = 0.5$.
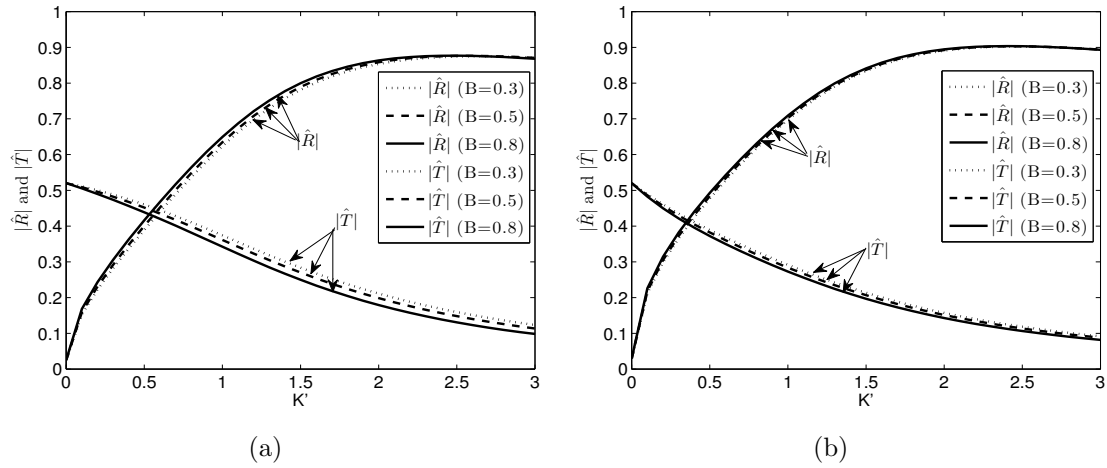
Figure 2.10: $|\hat{R}|$ and $|\hat{T}|$ against K' for fixed $H_2 = 1.3$ and $H_3 = 2$ with different (a) $A = 1.0$ and (b) $A = 1.5$.

from the fact that longer the length of the dock will certainly increase the reflection.

(ii) **Effect of width of step-1**

The values of reflection coefficient $|\hat{R}|$ and transmission coefficient $|\hat{T}|$ are depicted against K' in Figs. 2.10a and 2.10b for different values of width of step-1, $B = 0.3, 0.5, 0.8$. In each figure, the values of other parameters are $H_2 = 1.3$ and $H_3 = 2$. From these figures, it is found that the reflection coefficient is increasing slightly as the value of B is increasing form 0.3 to 0.8 and also the transmission coefficient is decreasing slightly. Both results are plausible as described in Case-I.

(iii) **Effect of water depth ratios**

Fig. 2.11 shows the variation of depth ratios H_2 and H_3 on $|\hat{R}|$ and $|\hat{T}|$ against K'. From this figure, it is observed that the values of $|\hat{R}|$ curves are increasing as the values of depth ratios are increasing whereas the values of $|\hat{T}|$ curves are decreasing.
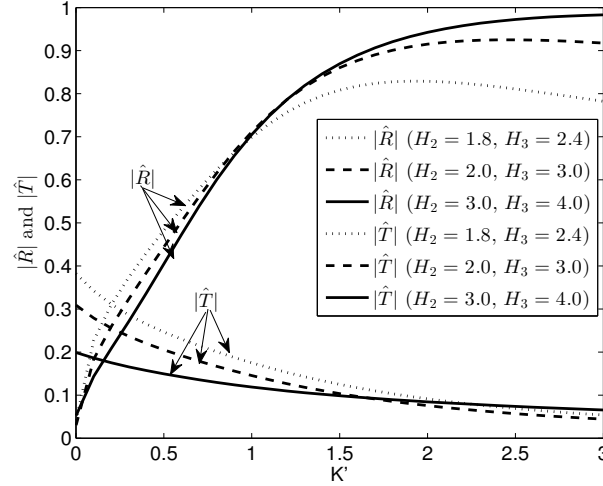
Figure 2.11: $|\hat{R}|$ and $|\hat{T}|$ against K' for different depth ratios with $A = 1$ and $B = 0.5$

This result is plausible from the physical understanding that larger the depth ratio will increase the height of side wall of the step producing more reflection and less transmission.

2.6 Force and Moment

Force and moment are the important factors in the study of water waves for designing the breakwaters. Here, the results are derived for the Case-I only (i.e., when wave is incident from lower depth region). Similarly, force and moment for Case-II can also be derived with proper modification in the velocity potentials as described in Section 2.2.2.

Force: The dimensionless vertical exciting force on the dock due to an incident wave is given by

$$
\begin{aligned}
F &= \frac{e^{-ik_0a}}{a} \int_{-a}^{a} \phi_j(x,0)dx \\
\Rightarrow F &= \frac{e^{-ik_0a}}{a} \left(\int_{-a}^{0} \phi_2(x,0)dx + \int_{0}^{b} \phi_3(x,0)dx + \int_{b}^{a} \phi_4(x,0)dx \right)
\end{aligned}
$$

$$
\begin{aligned}
\Rightarrow F = e^{-ik_0a} \Bigg\{ &B_0 - \frac{B_1}{2} + \sum_{n=1}^{\infty} \left[\hat{B}\left(1 - e^{\frac{-n\pi a}{h_1}}\right) - \tilde{B}\left(1 - e^{\frac{n\pi a}{h_1}}\right) \right] \frac{h_1}{an\pi} \\
&+ C_0 \frac{b}{a} + \frac{C_1}{2}\left(\frac{b}{a}\right)^2 + \sum_{n=1}^{\infty} \left[\hat{C}\left(e^{\frac{n\pi b}{h_2}} - 1\right) - \tilde{C}\left(e^{\frac{-n\pi b}{h_2}} - 1\right) \right] \frac{h_2}{an\pi} \\
&+ D_0\left(1 - \frac{b}{a}\right) + \frac{D_1}{2}\left(1 - \frac{b^2}{a^2}\right) + \sum_{n=1}^{\infty} \left[\hat{D}\left(e^{\frac{n\pi a}{h_3}} - e^{\frac{n\pi b}{h_3}}\right) \right. \\
&\left. - \tilde{D}\left(e^{\frac{-n\pi a}{h_3}} - e^{\frac{-n\pi b}{h_3}}\right) \right] \frac{h_3}{an\pi} \Bigg\}
\end{aligned}
$$

Fig. 2.12 shows the variation of the absolute value of dimensionless force $|F|$ against K' for
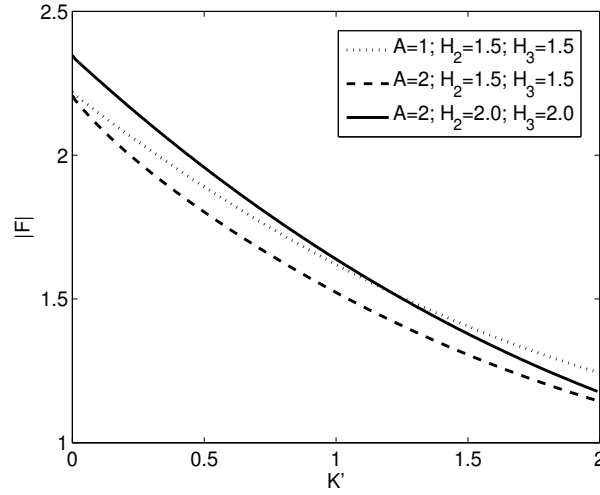
Figure 2.12: $|F|$ against K' for fixed $B = 0.5$

different values of the dock length $A = 1, 2$ and depth ratios $H_2 = 1.5, 2.0$, $H_3 = 1.5, 2.0$ with fixed $B = 0.5$. From this figure, it is observed that the force is decreasing with increasing the values of K' (Linton [76]). It is also found that the force is decreasing as the length of the dock is increasing (Linton [76]). This is plausible from the physical point of view.

Moment: The dimensionless vertical pitching moment on the dock due to an incident wave is given by

$$
\begin{aligned}
M &= \frac{e^{-ik_0a}}{a^2} \int_{-a}^{a} x\phi_j(x,0)dx \\
\Rightarrow M &= \frac{e^{-ik_0a}}{a^a} \left(\int_{-a}^{0} x\phi_2(x,0)dx + \int_{0}^{b} x\phi_3(x,0)dx + \int_{b}^{a} x\phi_4(x,0)dx \right)
\end{aligned}
$$

$$
\begin{aligned}
\Rightarrow M = e^{-ik_0a} &\left\{ -\frac{B_0}{2} + \frac{B_1}{3} + \sum_{n=1}^{\infty} \left[\hat{B} \left(e^{\frac{-n\pi a}{h_1}} (h_1 + n\pi a) - h_1 \right) \right. \right. \\
&- \left. \tilde{B} \left(e^{\frac{n\pi a}{h_1}} (h_1 - n\pi a) - h_1 \right) \right] \frac{h_1}{(an\pi)^2} + \frac{C_0}{2} \left(\frac{b}{a} \right)^2 + \frac{C_1}{3} \left(\frac{b}{a} \right)^3 \\
&+ \sum_{n=1}^{\infty} \left[\hat{C} \left(e^{\frac{n\pi b}{h_2}} (n\pi b - h_2) + h_2 \right) + \tilde{C} \left(e^{\frac{-n\pi b}{h_2}} (h_2 + n\pi b) - h_2 \right) \right] \frac{h_2}{(an\pi)^2} \\
&+ \frac{D_0}{2} \left(1 - \frac{b^2}{a^2} \right) + \frac{D_1}{3} \left(1 - \frac{b^3}{a^3} \right) + \sum_{n=1}^{\infty} \left[\hat{D} \left(e^{\frac{n\pi a}{h_3}} (n\pi a - h_3) - e^{\frac{n\pi b}{h_3}} (n\pi b - h_3) \right) \right. \\
&+ \left. \left. \tilde{D} \left(e^{\frac{-n\pi a}{h_3}} (n\pi a + h_3) - e^{\frac{-n\pi b}{h_3}} (n\pi b + h_3) \right) \right] \frac{h_3}{(an\pi)^2} \right\}
\end{aligned}
$$

The dimensionless moment on the finite dock is depicted against K' in Fig. 2.13. It is

Table 2.5: Force and moment for different K' with $A = 1, B = 0.5, H_2 = 1, H_3 = 1$

K'	Linton (2001), for $\theta = 0$		Present results	
	$|F|$	$|M|$	$|F|$	$|M|$
0.2	1.8844	0.2671	1.8842	0.2670
0.4	1.7738	0.3396	1.7734	0.3394
0.6	1.6689	0.3753	1.6684	0.3749
0.8	1.5704	0.3922	1.5696	0.3918
1.0	1.4788	0.3984	1.4779	0.3978
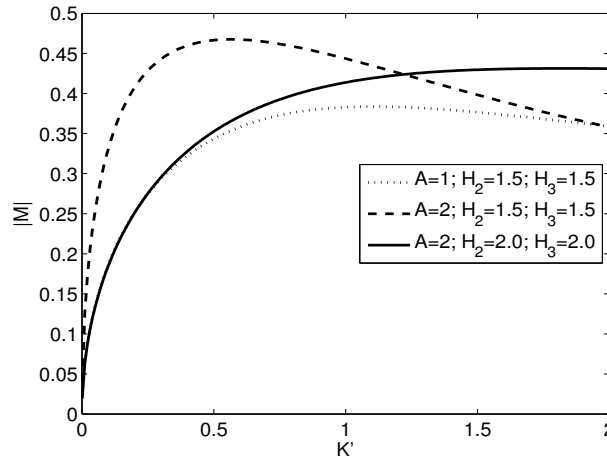
Figure 2.13: $|M|$ against K' for fixed $B = 0.5$

observed that the moment is increasing as the values of dock length A (Linton [76]) and the depth ratios H_2, H_3 are increasing. The values of force $|F|$ and moment $|M|$ are given in tabular form (Table 2.5) for different values of K'. Here, the other parameters $A = 1$, $B = 0.5$, $H_2 = 1 =$ and $H_3 = 1$ are kept fixed. It is found that the present results for force and moment are matching with Linton [76] correct up to three decimal places. This also ensures the correctness of the numerical results of the present problem.

2.7   Conclusion

The scattering of surface water waves by a finite dock is examined under the assumptions of the linearized water wave theory. In addition to finite dock, 2-step bottom topography is considered to analyze the effect of abrupt change in bottom topography on the wave propagation from lower depth region (Case-I) as well as from higher depth region (Case-II). It is observed that the reflection coefficient is decreasing slightly and transmission coefficient is increasing with increasing the depth ratios for Case-I. On the other hand, for Case-II, the reflection coefficient is increasing as the values of the depth ratios are increasing while the transmission coefficient is decreasing. The reflection coefficient is also increasing with increasing the values of K', dock length and width of

the step-1 whereas the transmission coefficient is decreasing for the same. Furthermore, this problem is generalized over $M-$steps and it is found that the transmission coefficient is increasing but the reflection coefficient is slightly decreasing by increasing the number of steps. The energy balance relation is also derived and verified. It is observed that the numerical results obtained for reflection and transmission coefficients satisfy the energy balance relation almost accurately. The present results are also validated through the results available in the literature. Further, this paper provides information towards the designing of horizontal breakwater over step topography towards the protection of seashore.

Chapter 3

Scattering of Water Waves by a Thin Vertical Barrier Over Stepped Bottom Topography

3.1 Introduction

In Chapter 2, the scattering of surface water waves for normal incidence by rigid horizontal dock over stepped bottom topography was considered for its solutions. In this chapter, instead of rigid dock, the interaction of obliquely incident surface waves by thin rigid vertical barrier over an impermeable stepped bottom is studied. The physical problem is formulated as mixed boundary value problem which involves Helmholtz equation as the governing equation. It is analyzed under the assumption of small amplitude water wave theory. The associated mixed boundary value problem is solved using the eigenfunction expansion of the velocity potential. The resulting system of equations is solved using algebraic least squares method giving rise the numerical values of the reflection and transmission coefficients by the barrier over step. The numerical values of these coefficients are compared with the known results of Rhee [115] and Losada [78]. The energy balance relation for the given problem is derived and verified numerically ensuring the correctness of the present results. A major part of the work presented in this chapter has been published in Kumar et al. [66].

3.2 Mathematical Formulation

Let us assume the fluid under consideration is homogeneous, incompressible, inviscid and the fluid motion is irrotational and also simple harmonic in time t. The Cartesian coordinate system is taken with mean free surface along the xz-plane and y-axis is vertically downwards (taken as positive) through the thin vertical rigid barrier of length d over the step bottom topography. The position of the step is at $x = 0, h_2 \leq y \leq h_1$ and the barrier is at $x = 0, 0 \leq y \leq d$. The fluid domain is divided into two regions such as $R_1 : -\infty < x \leq 0, \ 0 \leq y \leq h_1, \ R_2 : \ 0 \leq x < \infty, \ 0 \leq y \leq h_2$. Under the small amplitude theory of water waves, the velocity potential can be represented by $\Phi(x, y, z, t) = \Re\{\phi(x, y)e^{i(\mu z - \omega t)}\}$, where $\Re$ denotes the real part and ω is the angular frequency of the wave. The complex valued spatial potential $\phi(x, y)$ denoted as ϕ_1 for
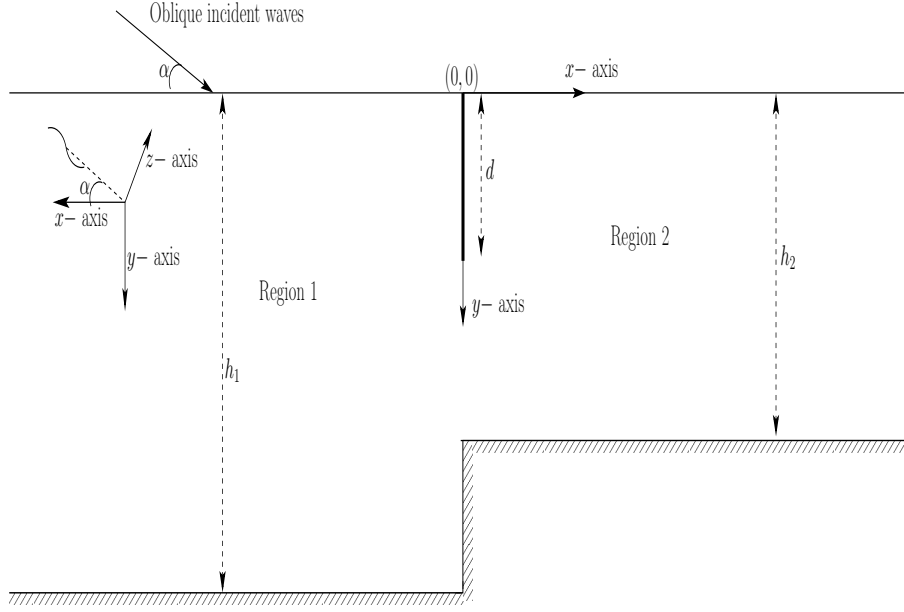
Figure 3.1: Schematic of the problem with rigid barrier over impermeable stepped bottom.

$x < 0$ and ϕ_2 for $x > 0$, satisfies the Helmholtz equation (Rhee [115])

$$\frac{\partial^2 \phi}{\partial x^2} + \frac{\partial^2 \phi}{\partial y^2} - \mu^2 \phi = 0 \quad \text{in the regions } R_j, \quad j = 1, 2, \tag{3.1}$$

where $\mu = k_0 \sin \alpha$, α is the angle of incidence with respect to x-axis and k_0 is the wave number of the incident wave. Also, $\phi_j(x, y)$, $j = 1, 2$, satisfies the boundary conditions (Losada et al. [78] and Rhee [115]) as defined below:

$$\frac{\partial \phi_1}{\partial y} + K\phi_1 = 0 \quad \text{on } y = 0, -\infty < x < 0; K = \omega^2/g, \tag{3.2}$$

$$\frac{\partial \phi_2}{\partial y} + K\phi_2 = 0 \quad \text{on } y = 0, \ 0 < x < \infty, \tag{3.3}$$

$$\frac{\partial \phi_1}{\partial y} = 0 \quad \text{on } y = h_1, -\infty < x < 0, \tag{3.4}$$

$$\frac{\partial \phi_2}{\partial y} = 0 \quad \text{on } y = h_2, \ 0 < x < \infty, \tag{3.5}$$

and the far-field conditions

$$\phi_1(x, y) \sim \frac{ig}{w}\{e^{is_0 x} + Re^{-is_0 x}\}\frac{\cosh k_0(y - h_1)}{\cosh k_0 h_1} \quad \text{as } x \to -\infty, \tag{3.6}$$

and

$$\phi_2(x, y) \sim \frac{ig}{w}\{Te^{iq_0 x}\}\frac{\cosh p_0(y - h_2)}{\cosh p_0 h_2} \quad \text{as } x \to \infty, \tag{3.7}$$

where $s_0 = \sqrt{k_0^2 - \mu^2}$, $q_0 = \sqrt{p_0^2 - \mu^2}$; k_0 and p_0 satisfy the respective transcendental equations $k \tanh k h_1 - K = 0$, and $k \tanh k h_2 - K = 0$, g is acceleration due to gravity and $|R|$ and $|T|$ respectively represent the reflection and transmission coefficients. The phase speed along the rays of the incident wave leading to Snell's law for refraction across

the step at the bottom, resulting $\mu = k_0 \sin \alpha = p_0 \sin \beta$ as mentioned by Kirby and Dalrymple [62].

In addition to this, the matching conditions at $x = 0$ due to continuity of pressure and velocity are:

$$\phi_1(0, y) = \phi_2(0, y), \quad d \le y \le h_2 \text{ (at the gap)}, \tag{3.8}$$

$$\frac{\partial \phi_1}{\partial x}(0, y) = \frac{\partial \phi_2}{\partial x}(0, y), \quad d \le y \le h_2 \text{ (at the gap)}, \tag{3.9}$$

$$\frac{\partial \phi_1}{\partial x}(0, y) = 0, \quad 0 \le y \le d \text{ (at the barrier)}, \tag{3.10}$$

$$\frac{\partial \phi_2}{\partial x}(0, y) = 0, \quad 0 \le y \le d \text{ (at the barrier)}, \tag{3.11}$$

$$\frac{\partial \phi_1}{\partial x}(0, y) = 0, \quad h_2 \le y \le h_1 \text{ (at the step)}. \tag{3.12}$$

In this problem, the singularity (Ray et al. [110]) at the edge of the vertical barrier is not considered. The study uses the Eqs. (3.1)-(3.12) to coin a system of equations and the system of equation will be solved numerically to determine R and T which is described in the next section.

3.3 Method of Solution

The Havelock's expansion for the velocity potential in regions R_j, $j = 1, 2$, are given by

$$\phi_1(x, y) = \frac{ig}{w} \Big[\{e^{is_0 x} + R e^{-is_0 x}\} f_0(y) + \sum_{n=1}^{\infty} A_n e^{-is_n x} f_n(y) \Big],$$

$$- \infty < x \le 0, 0 \le y \le h_1, \tag{3.13}$$

$$\phi_2(x, y) = \frac{ig}{w} \Big[\{T e^{iq_0 x}\} g_0(y) + \sum_{n=1}^{\infty} B_n e^{iq_n x} g_n(y) \Big], \quad 0 \le x < \infty, 0 \le y \le h_2, \tag{3.14}$$

with
$$f_n(y) = \frac{\cosh k_n(y - h_1)}{\cosh k_n h_1}, \quad g_n(y) = \frac{\cosh p_n(y - h_2)}{\cosh p_n h_2}; \quad n = 0, 1, 2, ... \tag{3.15}$$

and k_n & p_n, $n = 0, 1, 2, ...$ satisfy the transcendental equations

$$k \tanh k h_1 - K = 0 \text{ and } p \tanh p h_2 - K = 0,$$

respectively, where k_0, p_0 are real roots corresponding to propagating mode while k_n, p_n, $n = 1, 2, ...$ are purely imaginary roots corresponding to evanescent modes. Also, $s_n = \sqrt{k_n^2 - \mu^2}$, $q_n = \sqrt{p_n^2 - \mu^2}$ for $n = 1, 2, ...$. The unknowns R, A_n, T, B_n, $n = 1, 2, 3, ...$ are to be determined. After truncating the series to a finite number say N, we have $2N + 2$ number of unknowns.

Using the relations (3.13) and (3.14) in the conditions (3.8) − (3.12), we obtain

$$(1+R)f_0(y) + \sum_{n=1}^{N} A_n f_n(y) - T g_0(y) - \sum_{n=1}^{N} B_n g_n(y) = 0, \ d \leq y \leq h_2, \quad (3.16)$$

$$is_0(1-R)f_0(y) - \sum_{n=1}^{N} is_n A_n f_n(y) = 0, \ 0 \leq y \leq d, \quad (3.17)$$

$$iq_0 T g_0(y) + \sum_{n=1}^{N} iq_n B_n g_n(y) = 0, \ 0 \leq y \leq d, \quad (3.18)$$

$$is_0(1-R)f_0(y) - \sum_{n=1}^{N} is_n A_n f_n(y) - iq_0 T g_0(y) - \sum_{n=1}^{N} iq_n B_n g_n(y) = 0,$$

$$d \leq y \leq h_2, \quad (3.19)$$

$$is_0(1-R)f_0(y) - \sum_{n=1}^{N} is_n A_n f_n(y) = 0, \ h_2 \leq y \leq h_1. \quad (3.20)$$

Approximate solution of the $2N + 2$ unknowns appearing in Eqs. (3.16) − (3.20) can be obtained by the method of algebraic least-squares for which we consider infinite number of discretized points: (i) $\hat{y}_1, \hat{y}_2, \hat{y}_3, ...$ on the barrier $(0, d)$, (ii) $\tilde{y}_1, \tilde{y}_2, \tilde{y}_3, ...$ in the gap (d, h_2) and (iii) $\breve{y}_1, \breve{y}_2, \breve{y}_3, ...$ on the step (h_2, h_1), which lead to an overdetermined system with infinite number of equations in the matrix form as

$$A\vec{X} = \vec{b}, \quad (3.21)$$

where A is the coefficient matrix, $\vec{b}$ is the known vector and $\vec{X} = [R, A_n, T, B_n]$; $n = 1, 2, 3, ..., N$, is unknown vector to be determined. The least square solution is found for which the following normal system need to be solved:

$$A^* A \vec{X} = A^* \vec{b}, \quad (3.22)$$

where A^* denotes the conjugate transpose of A. Here, the system of equations (3.22) is solved by Gauss elimination method with the help of MATLAB. If A has linearly independent columns then the least-squares solution is unique and is given by

$$\vec{X} = (A^* A)^{-1} A^* b, \quad (3.23)$$

Here, it may be noted that, the ill-conditioned matrix can be avoided by choosing appropriate discretized points (see Section 5). The non-dimensional horizontal force per unit width of the barrier over the step-type bottom is given by

$$\frac{|F_h|}{\rho g h_1 A} = \frac{\omega}{g h_1} \left| \int_0^d (\phi_2(0, y) - \phi_1(0, y)) dy \right|. \quad (3.24)$$

3.4 Energy Balance Relation

The energy identity relating to reflection and transmission coefficients of the given problem, can be derived by using Green's integral theorem:

$$\int_{\Gamma} \left(\phi \frac{\partial \phi^*}{\partial n} - \phi^* \frac{\partial \phi}{\partial n} \right) dS = 0, \tag{3.25}$$

where $\frac{\partial}{\partial n}$ is the outward normal derivative to the boundary Γ, ϕ^* is the complex conjugate of ϕ, Γ is composed of $\{-X \leq x \leq 0, y = 0\} \cup \{x = -X, 0 \leq y \leq h_1\} \cup \{-X \leq x \leq 0, y = h_1\} \cup \{x = 0, h_2 \leq y \leq h_1\} \cup \{0 \leq x \leq X, 0 \leq y \leq h_2\} \cup \{x = X, 0 \leq y \leq h_2\} \cup \{0 \leq x \leq X, y = 0\} \cup \{x = 0^+, 0 \leq y \leq d\} \cup \{x = 0^-, 0 \leq y \leq d\}$ and then we take $X \to \infty$. The contribution to the integral (3.25) is zero due to the bottom as well as the barrier since $\frac{\partial \phi}{\partial n} = 0$ & $\frac{\partial \phi^*}{\partial n} = 0$. The contribution to the integral (3.25) at the free surface is zero. The contribution from the line $x = -X$, $0 \leq y \leq h_1$ is

$$\int_0^{h_1} \left(\phi_1 \frac{\partial \phi_1^*}{\partial x} - \phi_1^* \frac{\partial \phi_1}{\partial x} \right) dy = \frac{g^2}{\omega^2} \frac{is_0(|R|^2 - 1)}{2k_0 \cosh^2(k_0 h_1)} [2k_0 h_1 + \sinh(2k_0 h_1)]. \tag{3.26}$$

At the line $x = X$, $0 \leq y \leq h_2$, the integral gives rise to

$$\int_{h_2}^0 \left(\phi_2 \frac{\partial \phi_2^*}{\partial x} - \phi_2^* \frac{\partial \phi_2}{\partial x} \right) dy = \frac{g^2}{\omega^2} \frac{iq_0 |T|^2}{2p_0 \cosh^2(p_0 h_2)} [2p_0 h_2 + \sinh(2p_0 h_2)]. \tag{3.27}$$

On adding all of these contributions in Eq. (3.25), we get the energy identity as

$$|R|^2 + \delta \, |T|^2 = 1, \tag{3.28}$$

where $\delta = \frac{iq_0 k_0 (2p_0 h_2 + \sinh(2p_0 h_2))}{is_0 p_0 (2k_0 h_1 + \sinh(2k_0 h_1))} \frac{\cosh^2(k_0 h_1)}{\cosh^2(p_0 h_2)}$.

3.5 Numerical Results and Discussion

Here, the reflection $|R|$ coefficient and transmission $|T|$ coefficient are computed by solving the system given in Eq. (3.21) using algebraic least-squares method. The non-dimensional horizontal force on the barrier is computed numerically from the Eq. (3.24). These values are shown through tables and also through graphs for various values of parameters. For applying the algebraic least-square method, we consider different number of equally spaced discretized points, say m_1 points on the barrier: $\hat{y}_i = id/(m_1 - 1)$, $i = 0, 1, 2, ..., (m_1 - 1)$, m_2 points in the gap: $\tilde{y}_i = d + i(h_2 - d)/(m_2 - 1)$, $i = 0, 1, 2, ..., (m_2 - 1)$ and m_3 points on the step: $\breve{y}_i = h_2 + i(h_1 - h_2)/(m_3 - 1)$, $i = 0, 1, 2, ..., (m_3 - 1)$. Thus, from Eqs. (3.16)-(3.20), we obtain $2(m_1 + m_2) + m_3 = \hat{m}$ (say) equations in $2N + 2$ unknowns which are to be determined by solving the system (3.21). The non-dimensionalization of the physical parameters is made using both the depths h_1 & h_2. Here, the non-dimensional parameter are d/h_1, Kh_1, $H = h_2/h_1$, $p_0 h_2$.

(a)   (b)
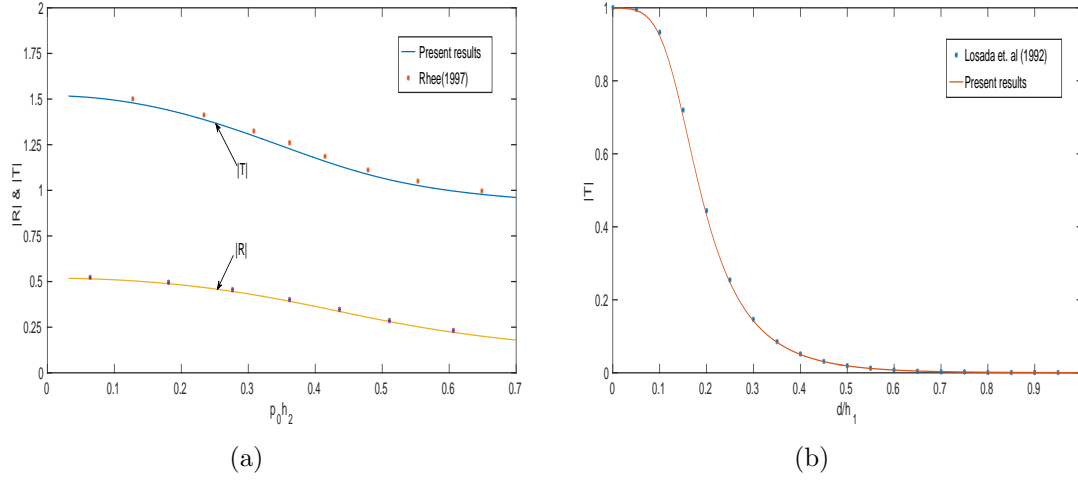
Figure 3.2: Comparison of the present results with (a) Rhee (1997) with $H = 0.1, \alpha = 0, d/h_1 = 0$ (b) Losada et al. (1992) with $H = 1.0, Kh_1 = 4.262, \alpha = 0$.

3.5.1 Validation

For validation of the present results, the results for a vertical step h_2/h_1 at the bottom topography in the absence of the barrier are compared with results of Rhee [115] in Fig. 3.2a. Here, $|R|$ and $|T|$ against $p_0 h_2$ are drawn where the present results (solid lines) fully coincide with Rhee [115] (stars), proving the correctness of present results. In Fig. 3.2b, the present results for $|T|$ are compared with Losada et al. [78] for vertical barrier over flat bed (in the absence of step). The transmission coefficient $|T|$ against the dimensionless barrier length d/h_1 for fixed $Kh_1 = 4.262$ and $\alpha = 0$ is presented in Fig. 3.2b, where the present results agree well with those of Losada et al. [78]. This proves the correctness of the present results. In Table 3.1, $|R|$ and $|T|$ are calculated for different non-dimensional values of Kh_1 and the results tabulated here show that the current numerical results verify the energy balance relation (3.28) showing again the correctness of the present results.

Kh_1	$|R|$	$|T|$	$|R|^2 + \gamma|T|^2$
0.5	0.2836709	0.971339	0.998969
1	0.542422	0.839165	0.996779
1.5	0.797381	0.595626	0.995996
2	0.938224	0.339009	0.997709
2.5	0.984274	0.172273	0.999051
3	0.996101	0.085408	0.999610
3.5	0.998994	0.042712	0.999828
4	0.999722	0.021717	0.999918
4.5	0.999916	0.011221	0.999959

Table 3.1: Verification of energy balance relation for $d/h_1 = 0.6, H = 0.9, \alpha = \pi/4$.

3.5.2   Convergence for N and (m_1, m_2, m_3)

The convergence of N (the number of evanescent modes) and the convergence of number of discretization points (m_1, m_2, m_3) are examined. In Table 3.2, the values of $|R|$ are given versus Kh_1 for various values of $N = 10, 20, 30, 55$ and 60 for fixed values of $d/h_1 = 0.6, H = 0.9, \alpha = \pi/4$. The tabular data show that the accuracy in $|R|$ upto two decimal places are obtained with $N = 55$ for all the values of Kh_1. Further, the Table 3.3 shows, the tabulated values of $|R|$ and $|T|$ versus Kh_1 for various values of (m_1, m_2, m_3) for fixed values of $d/h_1 = 0.3, H = 0.5, \alpha = 0$ and $N = 55$. The tabular data show that the accuracy in the results upto four decimal places are obtained with $(m_1, m_2, m_3) = (700, 700, 350)$.

Kh_1	$|R|(N = 10)$	$|R|(N = 20)$	$|R|(N = 30)$	$|R|(N = 55)$	$|R|(N = 60)$
0.5	0.301273	0.294279	0.289798	0.284316	0.283670
1	0.564326	0.556549	0.550659	0.543309	0.542421
1.5	0.810078	0.806768	0.802992	0.798008	0.797381
2	0.940626	0.941080	0.940057	0.938443	0.938224
2.5	0.983528	0.984619	0.984594	0.984321	0.984273
3	0.995167	0.995944	0.996081	0.996105	0.996100

Table 3.2: $|R|$ versus Kh_1 for various values of $N = 10, 20, 30, 55$ and 60.

Kh_1	(m_1, m_2, m_3)	$|R|$	$|T|$
0.1	(100,100,50)	0.197766	1.151433
	(200,200,100)	0.197685	1.151281
	(400,400,200)	0.197632	1.151208
	(700,700,350)	0.197599	1.151172
	(800,800,400)	0.197588	1.151156
0.5	(100,100,50)	0.294316	1.064908
	(200,200,100)	0.294429	1.064789
	(400,400,200)	0.294445	1.064757
	(700,700,350)	0.294438	1.064742
	(800,800,400)	0.294434	1.064736
0.7	(100,100,50)	0.342612	1.019294
	(200,200,100)	0.342789	1.019196
	(400,400,200)	0.342826	1.019186
	(700,700,350)	0.342827	1.019182
	(800,800,400)	0.342826	1.019180

Table 3.3: $|R|$ and $|T|$ versus Kh_1 for fixed $N = 55$ with different values of (m_1, m_2, m_3).

3.5.3   Influence of physical parameters on the reflection coefficient, transmission coefficient and force on the barrier over stepped bottom

Here, the reflection $|R|$ and transmission $|T|$ coefficients, and the force on the barrier are calculated numerically and plotted through different graphs for various values of the
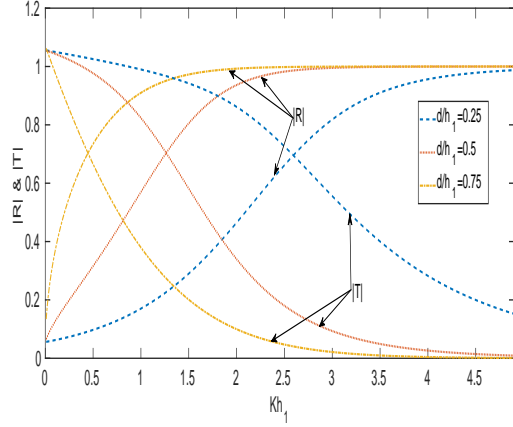
Figure 3.3: $|R|$ and $|T|$ varying against Kh_1 for $H = 0.8$ and $\alpha = 0$ with different barrier length.
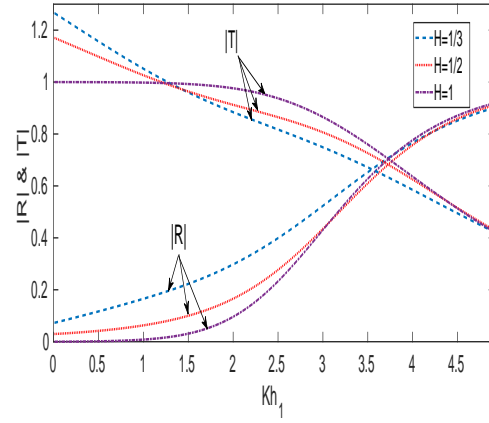
Figure 3.4: $|R|$ and $|T|$ varying against Kh_1 for $d/h_1 = 0.2$ and $\alpha = \pi/4$ with different H.
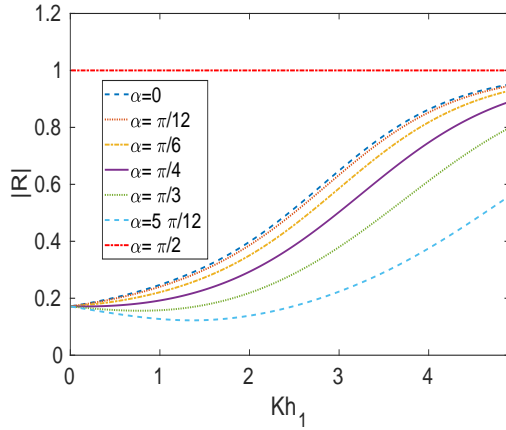
Figure 3.5: $|R|$ versus Kh_1 for $d/h_1 = 0.2$ and $H = 0.5$ with different α.
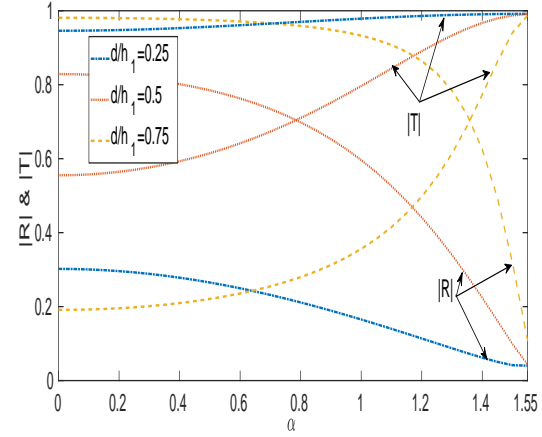
Figure 3.6: $|R|$ and $|T|$ versus α for $Kh_1 = 1.5$ and $H = 0.8$ with different barrier length.

parameters. The variation of $|R|$ & $|T|$ against the non-dimensional wave frequency Kh_1 for three different lengths of the barrier is shown in Fig. 3.3. It is observed that the reflection coefficient increases as the length of the barrier d/h_1 increases from 0.25 to 0.75. Consequently, the transmission coefficient decreases as the length of the barrier increases. Also, the reflection coefficient increases while transmission coefficient decreases as the non-dimensional wave frequency increases. Hence, larger frequency waves gets maximum reflection and minimum transmission. This may happen due to the fact that larger frequency waves almost confined near the free surface and hence gets comparatively more reflection and lesser transmission. In Fig. 3.4, the variation of reflection $|R|$ and transmission $|T|$ coefficients as a function of non-dimensional wave frequency Kh_1 by thin vertical barrier of length $d/h_1 = 0.2$ for three different step heights at the bottom is represented. The reflection coefficient $|R|$ decreases while transmission coefficient $|T|$ increases as the depth ratio H increases (i.e. the step height decreases). The effect of
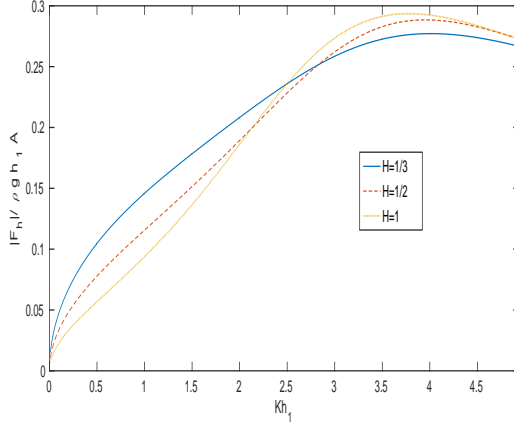
Figure 3.7: Dimensionless force varying against Kh_1 for $d/h_1 = 0.3$ and $\alpha = 0$ with different depth ratio H.
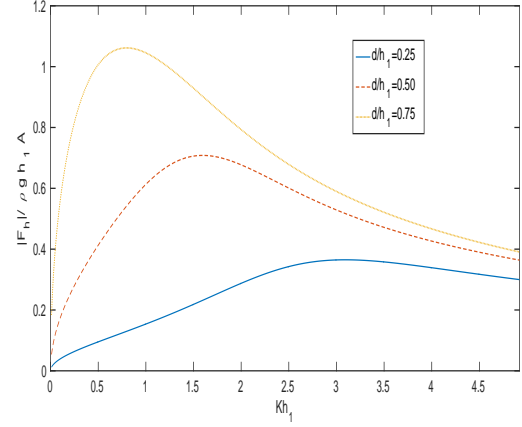
Figure 3.8: Dimensionless force varying against Kh_1 for $H = 0.8$ and $\alpha = 0$ with different barrier lengths.
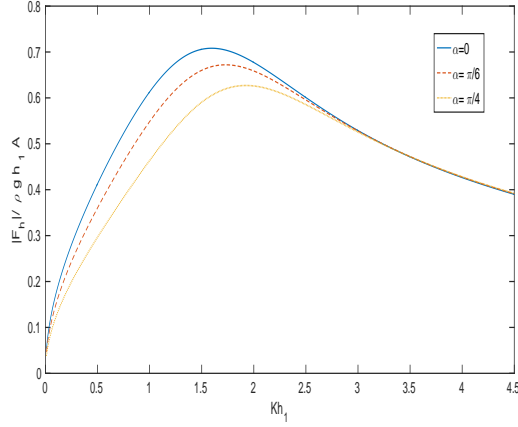
Figure 3.9: Dimensionless force versus Kh_1 for $d/h_1 = 0.4$ and $H = 0.8$ with different α.
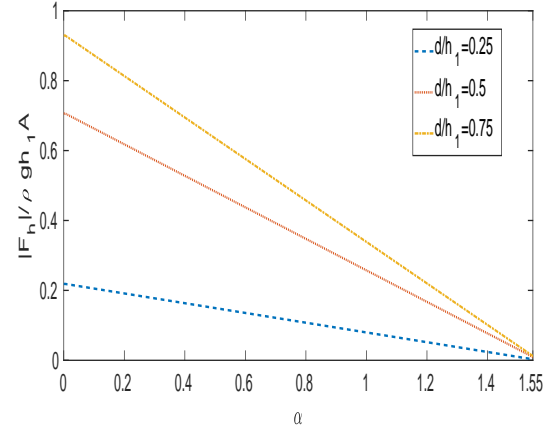
Figure 3.10: Dimensionless force versus α for $Kh_1 = 1.5$ and $H = 0.8$ with different barrier lengths.

depth ratio H on $|R|$ & $|T|$ is diminished as the value of Kh_1 becomes larger which may be due to the fact that the larger frequency waves i.e. waves with short wavelength are almost confined near the free surface and get lesser influenced due to the stepped bottom. It is also noticed that the pattern of transmission coefficient is also different for $Kh_1 < 1$, which may be due to phase shift in transmitted waves by altering depth ratio. Figure 3.5 shows $|R|$ versus Kh_1 for different values of angle of incidence. As the angle of incidence α increases, the reflection coefficient decreases. Also, there is more reflection for normal incidence case ($\alpha = 0$) in comparison to oblique incidence case. It is also observed that $|R|$ becomes unity for $\alpha = \pi/2$ for all the frequencies of incident waves, which validate the physical behaviour of the problem. In Fig. 3.6, the reflection coefficient monotonically decreases with the angle of incidence for all these dimensionless lengths of the barrier ranging from $0.25 - 0.75$. Consequently, the transmission coefficient monotonically increases with the angle of incidence for all these dimensionless lengths of

the barrier. The variation of the non-dimensional horizontal force $|F_h|/\rho g h_1 A$ against the non-dimensional wave frequency Kh_1 is reported in Fig. 3.7. For $Kh_1 < 2.5$, the force on the barrier decreases as H increases while for $Kh_1 > 2.5$, the force on the barrier increases as H increases. The pattern in the curves in Fig. 3.7 is changing because there may be a phase shift due to alteration of depth ratio for each curve. In Fig. 3.8, the variation of $|F_h|/\rho g h_1 A$ as a function of Kh_1 is shown for three different lengths of the barrier $d/h_1 = 0.25, 0.50, 075$. It is observed that the force on the barrier increases as the value of d/h_1 increases. It is also observed that as the length of the barrier increases, the reflection coefficient increases but force on the barrier also increases. Fig. 3.9 shows the non-dimensional horizontal force versus Kh_1 for three different angle of incidence $\alpha = 0, \pi/6, \pi/4$. The maximum value of the non-dimensional horizontal force on the barrier decreases as the angle incidence increases. In Fig. 3.10, the non-dimensional horizontal force versus angle of incidence for three different dimensionless lengths of the barrier ranging from $0.25 - 0.75$ is demonstrated. It is observed that the dimensionless force decreases versus angle of incidence for each dimensionless lengths of the barrier. It may also be constructed from Figs. 3.6 and 3.10 that the dimensionless force versus α decreases for each length of the barrier as the reflection coefficient decreases.

3.6   Conclusion

In this chapter, an oblique surface wave scattering by thin vertical rigid barrier over a step bottom topography is examined for its solution using matched eigenfunction expansion method by the aid of algebraic least squares method. The performance of the barrier over step is studied through various graphs of the reflection and transmission coefficients and non-dimensional horizontal force. The reflection coefficient increases as the length of the barrier and the step height increase while it decreases as the angle of incidence increases. Also, the maximum reflection occurs for normal incidence of the incident waves. The analysis of non-dimensional horizontal force per unit width of the barrier is also examined. As the length of the barrier over the step increases, the peak on force curves goes up. The non-dimensional horizontal force on the barrier decreases as the reflection coefficient due to the presence of the barrier decreases. Also, it is noticed that the force on the barrier is less for obliquely incidence waves in comparison of normal incidence waves. These results conclude that the barrier along with step works as an effective barrier to reflect more incident waves causing tranquillity zone along lee side, yielding less impact on seashore.

Chapter 4

Scattering of Water Waves by Two Thin Vertical Barriers Over Shelf Bottom Topography

4.1 Introduction

In the present chapter, the problem of Chapter-3 is considered for its solution where double barrier is considered instead of single barrier and shelf bottom topography is considered in place of stepped bottom topography. Here, two different configuration of the barriers are considered (i) surface piercing positions, and (ii) fully submerged positions. Further, the problem is generalized for an array of surface piercing barriers. The associated mixed boundary value problem is solved with the aid of method involving eigenfunction expansions of the velocity potential and orthogonality relation of the eigenfunctions. The resulting system of algebraic equations is solved using least square method to find the physical quantities i.e. reflection and transmission coefficients, free surface elevation and non-dimensional horizontal force experienced by the barriers. The energy balance relation is derived from Green's integral theorem and the numerically calculated results satisfy this relation, which ensures the correctness of the present results. Also, the obtained results are compared with the results available in the literature of Das [27] and also compared with the results of Chapter-3, for validation purpose. The major part of this chapter is published in Kumar et al. [67].

4.2 Mathematical Formulation

Here, the rectangular cartesian coordinate system is chosen in which the mean free surface of the water coincides with xz-plane and the positive direction of the y-axis is taken vertically downwards. A pair of surface piercing thin vertical barriers i.e. front and rear, of lengths d_1 and d_2 are placed at $x = \mp a$ respectively over shelf bottom topography. The whole fluid domain is divided into three regions as

$R_1 : -\infty < x \leq -a, 0 \leq y \leq h_1$; $R_2 : -a \leq x \leq a, 0 \leq y \leq h_2$;

$R_3 : a \leq x \leq \infty, 0 \leq y \leq h_3$.

We assume that the fluid under consideration is homogeneous, incompressible, and inviscid and the fluid motion is irrotational and simple harmonic in time
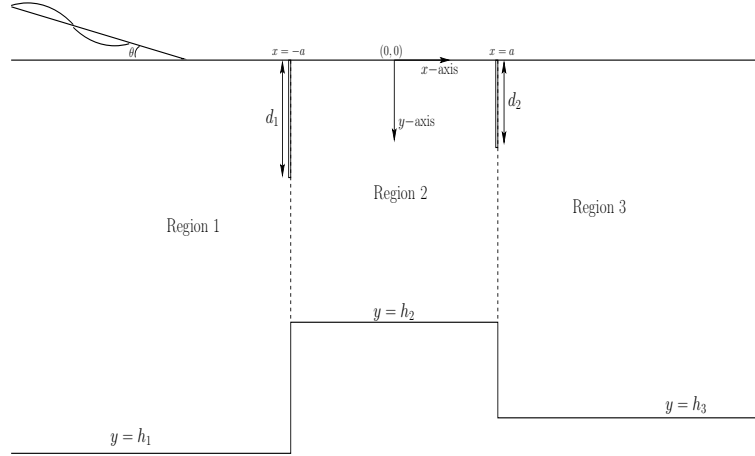
Figure 4.1: Two unequal thin vertical barriers over asymmetric shelf bottom topography.

t. It is also assumed that the barriers and the shelf profile are infinitely long in z-direction and therefore the characteristic behaviour remains the same along z-axis. Under the linearised wave theory of water waves, the velocity potential may be represented by $\Phi_j(x, y, z, t) = \Re\{\phi_j(x, y, z)e^{-i\omega t + i\mu z}\}$, where $\Re$ denotes the real part, ω is the angular frequency, θ is the angle of incidence and $\mu = k_0^{(1)} \sin\theta$, μ is the z component of the wave number $k_0^{(1)}$ associated with the incident wave given by $\psi(x, y, z, t) = \Re\{[\cosh k_0^{(1)}(y - h_1)/\cosh k_0^{(1)} h_1]e^{ik_{0x}^{(1)}x - i\omega t + i\mu z}\}$, where $k_{0x}^{(1)} = k_0^{(1)} \cos\theta = \sqrt{(k_0^{(1)})^2 - \mu^2}$ ($k_{0x}^{(1)}$ is the x component of the wave number $k_0^{(1)}$ associated with the incident wave) and $k = k_0^{(1)}$ is the unique positive real root of $k \tanh kh_1 - K = 0$ and $\phi_j(x, y)$ satisfies the Helmholtz equation

$$\frac{\partial^2 \phi_j}{\partial x^2} + \frac{\partial^2 \phi_j}{\partial y^2} - \mu^2 \phi_j = 0 \quad \text{in each fluid region } R_j, \quad j = 1, 2, 3, \tag{4.1}$$

along with the boundary conditions

$$\frac{\partial \phi_j}{\partial y} + K\phi_j = 0 \quad \text{on } y = 0 \text{ in } R_j, \ j = 1, 2, 3, \tag{4.2}$$

$$\frac{\partial \phi_1}{\partial y} = 0 \quad \text{on } y = h_1, \quad -\infty < x \leq -a, \tag{4.3}$$

$$\frac{\partial \phi_2}{\partial y} = 0 \quad \text{on } y = h_2, \quad -a \leq x \leq a, \tag{4.4}$$

$$\frac{\partial \phi_3}{\partial y} = 0 \quad \text{on } y = h_3, \quad a \leq x \leq \infty. \tag{4.5}$$

The matching conditions due to continuity of pressure and velocity are

$$\phi_1(-a, y) = \phi_2(-a, y), \quad d_1 \leq y \leq h_2, \tag{4.6}$$

$$\phi_{1x}(-a, y) = \phi_{2x}(-a, y), \quad d_1 \leq y \leq h_2, \tag{4.7}$$

$$\phi_{1x}(-a, y) = \phi_{2x}(-a, y) = 0, \quad 0 \leq y \leq d_1, \tag{4.8}$$

$$\phi_2(a, y) = \phi_3(a, y), \quad d_2 \leq y \leq h_2, \tag{4.9}$$

$$\phi_{2x}(a, y) = \phi_{3x}(a, y), \quad d_2 \le y \le h_2, \tag{4.10}$$

$$\phi_{2x}(a, y) = \phi_{3x}(a, y) = 0, \quad 0 \le y \le d_2, \tag{4.11}$$

the vertical wall conditions at the bottom are

$$\phi_{1x}(-a, y) = 0, \quad h_2 \le y \le h_1, \tag{4.12}$$

$$\phi_{3x}(a, y) = 0, \quad h_2 \le y \le h_3, \tag{4.13}$$

and the far field conditions are

$$\phi_1(x, y) \sim [e^{ik_{0x}^{(1)}(x+a)} + Re^{-ik_{0x}^{(1)}(x+a)}]\frac{\cosh k_0^{(1)}(y - h_1)}{\cosh k_0^{(1)} h_1} \quad \text{as} \ \ x \to -\infty, \tag{4.14}$$

$$\phi_3(x, y) \sim [Te^{ik_{0x}^{(3)}(x-a)}]\frac{\cosh k_0^{(3)}(y - h_3)}{\cosh k_0^{(3)} h_3} \quad \text{as} \ \ x \to \infty. \tag{4.15}$$

Here $|R|$ and $|T|$ are the reflection and transmission coefficients associated with reflected and transmitted waves respectively which have to determined and $k_0^{(3)}$ satisfies the transcendental equation $k \tanh kh_3 - K = 0$, where $K = \omega^2/g$ with g as acceleration due to gravity, and $k_{0x}^{(3)} = k_0^{(3)} \cos\theta = \sqrt{(k_0^{(3)})^2 - \mu^2}$. In this problem, the singularity (Ray et al. [110]) at the edges of the vertical barriers is not considered.

4.3 Method of Solution

The Havelock's expansions for the velocity potentials in regions R_j, $j = 1, 2, 3$ are given by

$$\phi_1(x, y) = [e^{ik_{0x}^{(1)}(x+a)} + Re^{-ik_{0x}^{(1)}(x+a)}]f_0^{(1)}(y) + \sum_{n=1}^{\infty} A_n e^{k_{nx}^{(1)}(x+a)} f_n^{(1)}(y);$$

$$-\infty < x \le -a, \ 0 \le y \le h_1, \tag{4.16}$$

$$\phi_2(x, y) = [B_0 e^{ik_{0x}^{(2)}(x+a)} + C_0 e^{-ik_{0x}^{(2)}(x-a)}]f_0^{(2)}(y) + \sum_{n=1}^{\infty}[B_n e^{-k_{nx}^{(2)}(x+a)}$$

$$+ C_n e^{k_{nx}^{(2)}(x-a)}]f_n^{(2)}(y); \quad -a \le x \le a, \ 0 \le y \le h_2, \tag{4.17}$$

$$\phi_3(x, y) = [Te^{ik_{0x}^{(3)}(x-a)}]f_0^{(3)}(y) + \sum_{n=1}^{\infty} D_n e^{-k_{nx}^{(3)}(x-a)} f_n^{(3)}(y);$$

$$a \le x < \infty, \ 0 \le y \le h_3. \tag{4.18}$$

with

$$f_0^{(j)}(y) = \frac{\cosh k_0^{(j)}(y - h_j)}{\cosh k_0^{(j)} h_j}, \ f_n^{(j)}(y) = \frac{\cos k_n^{(j)}(y - h_j)}{\cos k_n^{(j)} h_j}, \ j = 1, 2, 3; \ n = 1, 2, 3, \dots$$

and $k_0^{(j)}$, $k_n^{(j)}$ are the roots of the transcendental equations $k_0^{(j)} \tanh k_0^{(j)} h_j - K = 0$ and $k_n^{(j)} \tan k_n^{(j)} h_j + K = 0$, $j = 1, 2, 3$, respectively, $k_{0x}^{(j)} = \sqrt{(k_0^{(j)})^2 - \mu^2}$ and $k_{nx}^{(j)} = \sqrt{(k_n^{(j)})^2 + \mu^2}$, $j = 1, 2, 3$. Here $R, A_n, B_0, B_n, C_0, C_n, T, D_n$, $n = 1, 2, \ldots$ are unknowns to be determined. After truncating the number of evanescent modes present in Eqs. $(4.16 - 4.18)$ to a finite number say N, we have $4N + 4$ number of unknowns.

Substituting the series relations $(4.16) - (4.18)$ in the conditions $(4.6) - (4.13)$ and multiplying either $f_m^{(1)}$ or $f_m^{(2)}$ or $f_m^{(3)}$ suitably as given below, then integrating over the appropriate intervals and then applying the orthogonality relation of eigenfunctions wherever possible, we obtain

$$\int_{d_1}^{h_2} \phi_1(-a, y) f_m^{(2)}(y) dy = \int_{d_1}^{h_2} \phi_2(-a, y) f_m^{(2)}(y) dy, \qquad (4.19)$$

$$\int_0^{h_1} \phi_{1x}(-a, y) f_m^{(1)}(y) dy = \int_0^{h_2} \phi_{2x}(-a, y) f_m^{(1)}(y) dy, \qquad (4.20)$$

$$\int_{d_2}^{h_2} \phi_2(a, y) f_m^{(2)}(y) dy = \int_{d_2}^{h_2} \phi_3(a, y) f_m^{(2)}(y) dy, \qquad (4.21)$$

$$\int_0^{h_2} \phi_{2x}(a, y) f_m^{(3)}(y) dy = \int_0^{h_3} \phi_{3x}(a, y) f_m^{(3)}(y) dy, \qquad (4.22)$$

$$\int_0^{d_1} \phi_{1x}(-a, y) f_m^{(1)}(y) dy = 0, \qquad (4.23)$$

$$\int_0^{d_1} \phi_{2x}(-a, y) f_m^{(2)}(y) dy = 0, \qquad (4.24)$$

$$\int_0^{d_2} \phi_{2x}(a, y) f_m^{(2)}(y) dy = 0, \qquad (4.25)$$

$$\int_0^{d_2} \phi_{3x}(a, y) f_m^{(3)}(y) dy = 0, \qquad (4.26)$$

where $m = 0, 1, 2, \ldots, N$. On simplifying the relations $(4.19) - (4.26)$, an over-determined system of $8N + 8$ equations in $4N + 4$ unknowns is obtained as follows:

$$A\vec{X} = \vec{b}, \qquad (4.27)$$

where A is the coefficient matrix, $\vec{b}$ is the known vector and $\vec{X} = [R, A_n, B_0, B_n, C_0, C_n, T, D_n]'$, $n = 1, 2, \ldots, N$ is the unknown vector to be determined.

The least square solution for the above system (4.27) gives rise the following normal system which need to be solved:

$$A^* A \vec{X} = A^* \vec{b}, \qquad (4.28)$$

where A^* denotes the conjugate transpose of A. If A has linearly independent columns, then the least square solution is unique and given by

$$\vec{X} = (A^* A)^{-1} A^* \vec{b}. \qquad (4.29)$$

Here, it may be noted that to utilize the least square approach described above successfully, the occurrence of ill-conditioned matrices must be avoided. This can be avoided by choosing appropriate values of parameters. Here, the system of equations (4.28) is solved by Gauss elimination method with the help of MATLAB. The numerical values of the unknowns $\vec{X} = [R, A_n, B_0, B_n, C_0, C_n, T, D_n]'$ are obtained, for which the error is given by

$$E = || A\vec{X} - \vec{b} ||, \tag{4.30}$$

where $||.||$ is the Euclidean norm.

Now, the horizontal force on the front and rear barriers can be calculated using the following Bernoulli's equation under the given assumptions

$$-\frac{\partial \Phi}{\partial t} + gy + \frac{P}{\rho} = \text{constant} \tag{4.31}$$

where P is the pressure and ρ is the density of the fluid. Therefore the non-dimensional horizontal forces per unit width at the front and rear barriers are respectively given by

$$\frac{|F_f|}{\rho gh_1^2} = \frac{\omega}{gh_1^2} \left| \int_0^{d_1} (\phi_2(-a, y) - \phi_1(-a, y)) dy \right| \tag{4.32}$$

$$\frac{|F_r|}{\rho gh_1^2} = \frac{\omega}{gh_1^2} \left| \int_0^{d_2} (\phi_3(a, y) - \phi_2(a, y)) dy \right| \tag{4.33}$$

The free surface elevations η_j in each of regions R_j can be calculated by

$$\eta_j = -\frac{i\omega}{g} \phi_j(x, 0), \quad j = 1, 2, 3. \tag{4.34}$$

4.3.1 Fully submerged barriers
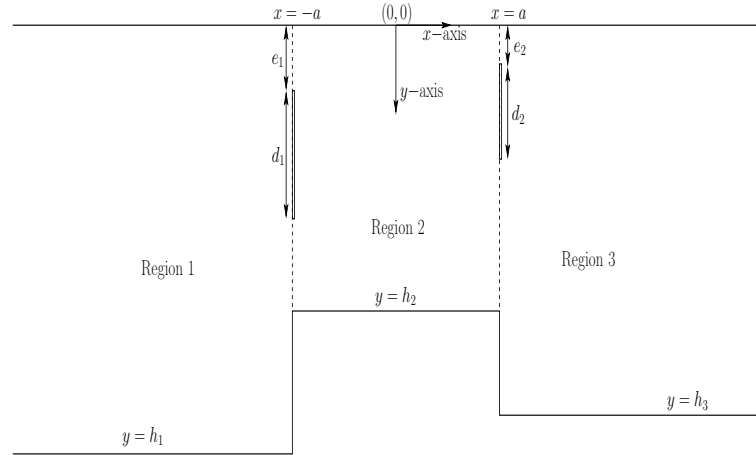
Figure 4.2: Schematic of the barriers with depth of submergence.

In this case, the depth of submergence of the front and rear barriers are respectively e_1

and e_2 and the modified matching conditions are

$$\phi_1(-a, y) = \phi_2(-a, y), \quad y \in [0, e_1] \cup [e_1 + d_1, h_2], \tag{4.35}$$

$$\phi_{1x}(-a, y) = \phi_{2x}(-a, y), \quad y \in [0, e_1] \cup [e_1 + d_1, h_2], \tag{4.36}$$

$$\phi_{1x}(-a, y) = \phi_{2x}(-a, y) = 0, \quad y \in [e_1, e_1 + d_1], \tag{4.37}$$

$$\phi_2(a, y) = \phi_3(a, y), \quad y \in [0, e_2] \cup [e_2 + d_2, h_2], \tag{4.38}$$

$$\phi_{2x}(a, y) = \phi_{3x}(a, y), \quad y \in [0, e_2] \cup [e_2 + d_2, h_2], \tag{4.39}$$

$$\phi_{2x}(a, y) = \phi_{3x}(a, y) = 0, \quad y \in [e_2, e_2 + d_2]. \tag{4.40}$$

Utilizing the relations $(4.16) - (4.18)$ in the matching conditions $(4.35) - (4.40)$ and the wall conditions $(4.12) - (4.13)$ and then using the orthogonality relation of eigenfunctions, we obtain

$$\int_0^{e_1} \phi_1(-a, y) f_m^{(2)}(y) dy + \int_{e_1+d_1}^{h_2} \phi_1(-a, y) f_m^{(2)}(y) dy = \int_0^{e_2} \phi_2(-a, y) f_m^{(2)}(y) dy$$

$$+ \int_{e_2+d_2}^{h_2} \phi_2(-a, y) f_m^{(2)}(y) dy, \tag{4.41}$$

$$\int_0^{h_1} \phi_{1x}(-a, y) f_m^{(1)}(y) dy = \int_0^{h_2} \phi_{2x}(-a, y) f_m^{(1)}(y) dy, \tag{4.42}$$

$$\int_0^{e_2} \phi_2(a, y) f_m^{(2)}(y) dy + \int_{e_2+d_2}^{h_2} \phi_2(a, y) f_m^{(2)}(y) dy = \int_0^{e_2} \phi_3(a, y) f_m^{(2)}(y) dy$$

$$+ \int_{e_2+d_2}^{h_2} \phi_3(a, y) f_m^{(2)}(y) dy, \tag{4.43}$$

$$\int_0^{h_2} \phi_{2x}(a, y) f_m^{(3)}(y) dy = \int_0^{h_3} \phi_{3x}(a, y) f_m^{(3)}(y) dy, \tag{4.44}$$

$$\int_{e_1}^{e_1+d_1} \phi_{1x}(-a, y) f_m^{(1)}(y) dy = 0, \tag{4.45}$$

$$\int_{e_1}^{e_1+d_1} \phi_{2x}(-a, y) f_m^{(2)}(y) dy = 0, \tag{4.46}$$

$$\int_{e_2}^{e_2+d_2} \phi_{2x}(a, y) f_m^{(2)}(y) dy = 0, \tag{4.47}$$

$$\int_{e_2}^{e_2+d_2} \phi_{3x}(a, y) f_m^{(3)}(y) dy = 0. \tag{4.48}$$

where $m = 0, 1, 2, ..., N$. In the similar pattern as employed in previous section, the system of equations can be solved to obtain the unknown physical quantities.

4.3.2 Array of surface piercing vertical barriers over the shelf bottom

In this case, the surface piercing rigid thin vertical barriers (M-pairs) of equal length d are placed at equidistant over the shelf bottom topography (see Fig. 4.3). The positions
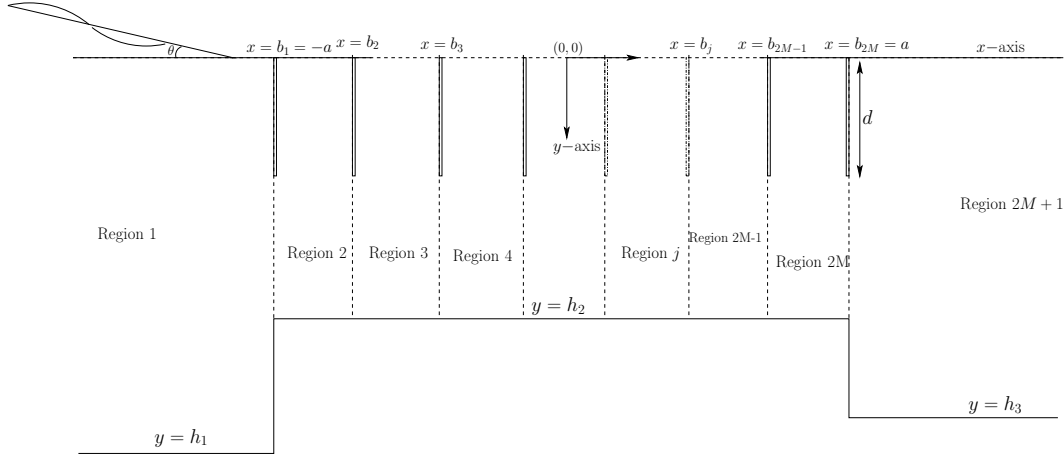
Figure 4.3: Schematic for the array of surface piercing barriers over shelf bottom topography.

of these barriers are at $x = b_j$, where $b_j = -a + (2(j-1)a/(2M-1))$, $j = 1, 2, ..., 2M$ i.e. $b_1 = -a$, $b_{2M} = a$. Here, the whole fluid domain is divided into $2M + 1$ regions as $R_1 : -\infty < x \leq b_1, 0 \leq y \leq h_1$, $R_j : b_{j-1} \leq x \leq b_j, 0 \leq y \leq h_2, j = 2, 3, ..., 2M$, $R_{2M+1} : b_{2M} \leq x < \infty, 0 \leq y \leq h_3$.

The complex valued potential $\phi_j(x, y)$ satisfies the Helmholtz equation:

$$\frac{\partial^2 \phi_j}{\partial x^2} + \frac{\partial^2 \phi_j}{\partial y^2} - \mu^2 \phi_j = 0 \quad \text{in each fluid region } R_j, \quad j = 1, 2, ..., 2M + 1, \tag{4.49}$$

along with the boundary conditions

$$\frac{\partial \phi_j}{\partial y} + K\phi_j = 0 \quad \text{on } y = 0 \text{ in } R_j, \ j = 1, 2, ..., 2M + 1, \tag{4.50}$$

$$\frac{\partial \phi_1}{\partial y} = 0 \quad \text{on } y = h_1, \ -\infty < x \leq b_1, \tag{4.51}$$

$$\frac{\partial \phi_j}{\partial y} = 0 \quad \text{on } y = h_2, \ b_{j-1} \leq x \leq b_j, j = 2, 3, ..., 2M, \tag{4.52}$$

$$\frac{\partial \phi_{2M+1}}{\partial y} = 0 \quad \text{on } y = h_3, \ b_{2M} \leq x < \infty. \tag{4.53}$$

The matching conditions due to continuity of pressure and velocity are

$$\phi_j(b_j, y) = \phi_{j+1}(b_j, y), \quad d \leq y \leq h_2, \tag{4.54}$$

$$\phi_{jx}(b_j, y) = \phi_{(j+1)x}(b_j, y), \quad d \leq y \leq h_2, \tag{4.55}$$

$$\phi_{jx}(b_j, y) = \phi_{(j+1)x}(b_j, y) = 0, \quad 0 \leq y \leq d; j = 1, 2, ..., 2M, \tag{4.56}$$

the vertical wall conditions of the shelf bottom are

$$\phi_{1x}(b_1, y) = 0, \quad h_2 \leq y \leq h_1, \tag{4.57}$$

$$\phi_{(2M+1)x}(b_{2M}, y) = 0, \quad h_2 \leq y \leq h_3, \tag{4.58}$$

and the far field conditions are

$$\phi_1(x,y) \sim [e^{ik_{0x}^{(1)}(x-b_1)} + Re^{-ik_{0x}^{(1)}(x-b_1)}]\frac{\cosh k_0^{(1)}(y-h_1)}{\cosh k_0^{(1)}h_1} \quad \text{as} \ \ x \to -\infty, \qquad (4.59)$$

$$\phi_{2M+1}(x,y) \sim [Te^{ik_{0x}^{(3)}(x-b_{2M})}]\frac{\cosh k_0^{(3)}(y-h_3)}{\cosh k_0^{(3)}h_3} \quad \text{as} \ \ x \to \infty. \qquad (4.60)$$

The expressions for the velocity potentials ϕ_j $(j=1,2,...,2M+1)$ in each of the regions can be expressed as

$$\phi_1(x,y) = [e^{ik_{0x}^{(1)}(x-b_1)} + Re^{-ik_{0x}^{(1)}(x-b_1)}]f_0^{(1)}(y) + \sum_{n=1}^{\infty} A_n e^{k_{nx}^{(1)}(x-b_1)}f_n^{(1)}(y);$$

$$-\infty < x \le b_1, \ 0 \le y \le h_1, \ (4.61)$$

$$\phi_j(x,y) = [B_0^{(j-1)}e^{ik_{0x}^{(2)}(x-b_{j-1})} + C_0^{(j-1)}e^{-ik_{0x}^{(2)}(x-b_j)}]f_0^{(2)}(y) + \sum_{n=1}^{\infty}[B_n^{(j-1)}e^{-k_{nx}^{(2)}(x-b_{j-1})}$$

$$+C_n^{(j-1)}e^{k_{nx}^{(2)}(x-b_j)}]f_n^{(2)}(y); b_{j-1} \le x \le b_j, \ 0 \le y \le h_2, j = 2,3,...,2M, \ (4.62)$$

$$\phi_{2M+1}(x,y) = [Te^{ik_{0x}^{(3)}(x-b_{2M})}]f_0^{(3)}(y) + \sum_{n=1}^{\infty} D_n e^{-k_{nx}^{(3)}(x-b_{2M})}f_n^{(3)}(y);$$

$$b_{2M} \le x < \infty, \ 0 \le y \le h_3. \ (4.63)$$

where $R, A_n, B_0^{(j-1)}, B_n^{(j-1)}, C_0^{(j-1)}, C_n^{(j-1)}, T, D_n, \ n = 1,2,...$ $(2 \le j \le 2M)$ are the unknowns to be determined. Now, following the same procedure as described in the previous Section 3, and utilizing the matching and wall conditions along with orthogonality of eigenfunctions, we obtained a system of $8M(N+1)$ algebraic equations with $4M(N+1)$ unknowns which need to be solved to determine the unknown physical quantities. In particular, for $M=1$, the problem of array of vertical barriers reduces to the problem of a pair of vertical barriers over the shelf bottom topography.

4.4   Energy Balance Relation

In this section, the energy balance relation is derived for the configuration of two barrier over shelf bottom topography (see Fig. 4.1) to check the accuracy in numerically calculated values.

Using Green's integral theorem

$$\int_{\Gamma} \left(\phi \frac{\partial \phi^*}{\partial n} - \phi^* \frac{\partial \phi}{\partial n} \right) d\Gamma = 0 \qquad (4.64)$$

where ϕ^* is the complex conjugate of ϕ and $\frac{\partial}{\partial n}$ is the outward normal derivative to the boundary Γ where Γ is given as

$\Gamma \equiv \{-X \le x \le -a, y = 0\} \cup \{x = -X, 0 \le y \le h_1\} \cup \{-X \le x \le -a, y = h_1\}$
$\quad \cup \{x = -a, h_2 \le y \le h_3\} \cup \{-a \le x \le a, y = h_2\} \cup \{x = a, h_2 \le y \le h_3\}$

$$\cup \{a \le x \le X, y = h_3\} \cup \{x = X, 0 \le y \le h_3\} \cup \{a \le x \le X, y = 0\}$$
$$\cup C_2 \cup \{-a \le x \le a, y = 0\} \cup C_1,$$

here, $C_2 = \{x = a^+, 0 \le y \le d_2\} \cup \{x = a^-, 0 \le y \le d_2\}$ and $C_1 = \{x = -a^+, 0 \le y \le d_1\} \cup \{x = -a^-, 0 \le y \le d_1\}$ are the curves enclosing the submerged part of the rear and front barriers respectively.

The contribution to the integral (4.64) is zero due to the bottom condition and the front and rear barriers conditions.

The contribution to the integral (4.64) due to the free surface is zero as

$$\int_X^{-X} [\phi\{-K\phi^*\} - \phi^*\{-K\phi\}] = 0. \tag{4.65}$$

The contribution of the line $x = -X$, $0 \le y \le h_1$ is

$$\int_0^{h_1} \left(\phi_1 \frac{\partial \phi_1^*}{\partial x} - \phi_1^* \frac{\partial \phi_1}{\partial x}\right) dy = \frac{ik_{0x}^{(1)}(|R|^2 - 1)}{2k_0^{(1)} \cosh^2(k_0^{(1)} h_1)} [2k_0^{(1)} h_1 + \sinh(2k_0^{(1)} h_1)]. \tag{4.66}$$

The contribution of the line $x = X$, $0 \le y \le h_3$ is

$$\int_{h_3}^0 \left(\phi_3 \frac{\partial \phi_3^*}{\partial x} - \phi_3^* \frac{\partial \phi_3}{\partial x}\right) dy = \frac{ik_{0x}^{(3)} |T|^2}{2k_0^{(3)} \cosh^2(k_0^{(3)} h_3)} [2k_0^{(3)} h_3 + \sinh(2k_0^{(3)} h_3)]. \tag{4.67}$$

On adding, all of these contributions in Eq. (4.64), the energy balance relation is derived as

$$|R|^2 + \gamma |T|^2 = 1, \tag{4.68}$$

where $\gamma = \frac{k_{0x}^{(3)} k_0^{(1)} (2k_0^{(3)} h_3 + \sinh(2k_0^{(3)} h_3))}{k_{0x}^{(1)} k_0^{(3)} (2k_0^{(1)} h_1 + \sinh(2k_0^{(1)} h_1))} \frac{\cosh^2 k_0^{(1)} h_1}{\cosh^2 k_0^{(3)} h_3}$.

4.5 Numerical Results and Discussion

The non-dimensionalisation of all the system parameters is done by using h_1 as the length scale. It may be noticed that, in the non-dimensional form, the depth ratio $h_3/h_1 = 1$ gives rise to a symmetric shelf bottom profile while the depth ratios $h_2/h_1 = h_3/h_1 = 1$ gives rise to a flat bottom profile. We denote $d_1 = d_2 = d$ ($d_1/h_1 = d_2/h_1 = d/h_1$ in non-dimensional form) for the identical length of the barriers.

4.5.1 Convergence for N

In this section, the convergence study of N i.e. the number of evanescent modes is examined for configuration of two barriers over shelf topography. In Table 4.1, the values of $|R|$ are tabulated against Kh_1 for various values of $N = 5, 25, 45, 75, 80, 85$ for symmetric shelf bottom topography. The table shows that the accuracy in the present results upto four decimal places are obtained with $N = 80$ for all the values of Kh_1. Hence, $N = 80$ is taken throughout the study. The identical length of the barriers is represented by $d(= d_1 = d_2)$ and $k_0^{(1)}$ is taken as k_0 for simplicity.

4.5.2 Validation

To validate the present results with the available results in literature $|R|$ are plotted versus Kh_1 in Fig. 4.4. In Fig. 4.4, the obtained results are compared with the results obtained by Das et. al. [27] for two thin vertical barriers over the flat bottom. This figure shows that the present results are in good agreement with the known results as a particular case in literature. The particular case of the present problem which is thin vertical barrier over a step (by taking $h_2/h_1 = h_3/h_1$ and the front barrier only) is compared with the results of Chapter-3 in Fig. 4.5. This shows an excellent agreement between the present results and the results of Chapter-3. In Table 4.2, $|R|$ and $|T|$ are tabulated for different values of k_0h_1. This table depicts that the present results satisfy the energy balance relation as stated in Eq. (4.68). This also proves the correctness of the present results.
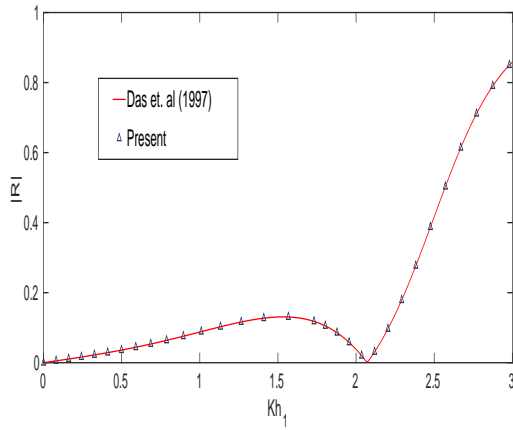
Figure 4.4: Validation of present results for $d/h_1 = 0.2$, $a/h_1 = 0.3$, $\theta = 0$ over flat bottom.
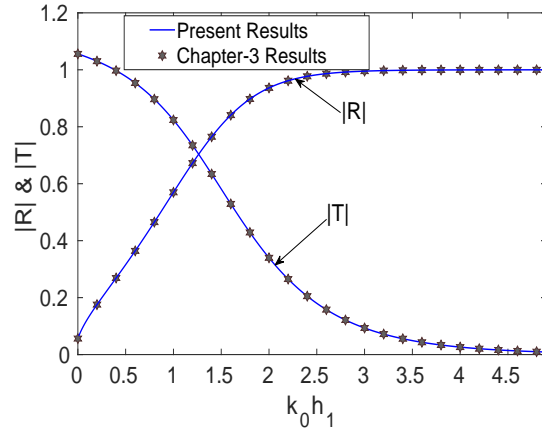
Figure 4.5: Validation of present results for $d_1/h_1 = 0.5$, $d_2/h_1 = 0$, $\theta = 0$ over a step $h_2/h_1 = 0.8$ and $h_3 = h_2$.

Table 4.1: $|R|$ versus Kh_1 for different values of $N = 5, 25, 45, 75, 80, 85$ ($d_1/h_1 = 0.2$, $d_2/h_1 = 0.3$, $h_2/h_1 = 0.8$, $a/h_1 = 0.5$, $\theta = 0$).

Kh_1	$|R|(N=5)$	$|R|(N=25)$	$|R|(N=45)$	$|R|(N=75)$	$|R|(N=80)$	$|R|(N=85)$
0.1	0.081730	0.074503	0.072928	0.072017	0.071919	0.071908
0.3	0.149369	0.135156	0.132137	0.130824	0.130788	0.130768
0.5	0.204106	0.183369	0.179066	0.176943	0.176872	0.176858
0.7	0.255945	0.228519	0.222937	0.218782	0.218705	0.218698
0.9	0.306924	0.272943	0.266094	0.262858	0.262799	0.262768
1.1	0.356064	0.316801	0.308791	0.304659	0.304486	0.304467
1.3	0.399229	0.358613	0.349744	0.346622	0.346586	0.346555
1.5	0.427206	0.395299	0.385152	0.377224	0.377198	0.377165
1.7	0.419549	0.422043	0.414011	0.408267	0.408087	0.407989
1.9	0.329387	0.434203	0.430019	0.428778	0.428599	0.428565

Table 4.2: Verification of energy balance relation for a pair of thin vertical barriers over symmetric shelf bottom topography ($d_1/h_1 = 0.2, d_2/h_1 = 0.3, h_2/h_1 = 0.8, a/h_1 = 0.2, \theta = 0$).

Kh_1	$|R|$	$|T|$	$|R|^2 + \gamma|T|^2$
0.1	0.071919	0.994826	0.999999
0.3	0.130788	0.982893	0.999999
0.5	0.176872	0.968715	0.999999
0.7	0.218705	0.952168	1.000000
0.9	0.262799	0.930936	1.000000
1.1	0.304486	0.907288	1.000000
1.3	0.346586	0.879877	0.999999
1.5	0.377198	0.857721	1.000000
1.7	0.408267	0.833465	1.000000
1.9	0.428599	0.816302	1.000000

4.5.3 Effect of various parameters on the reflection and transmission coefficients
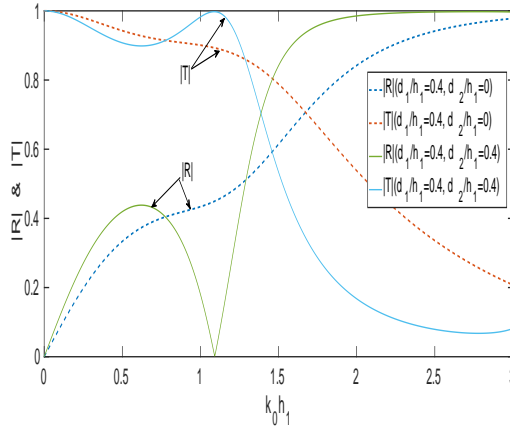
Figure 4.6: Comparison between single and double barriers over symmetric shelf bottom for $h_2/h_1 = 0.6, a/h_1 = 0.5, \theta = 0$.
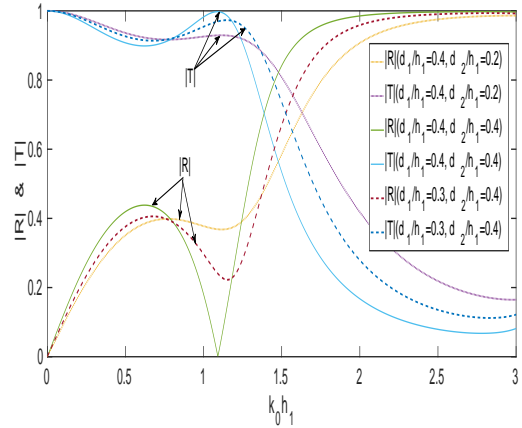
Figure 4.7: $|R|$ & $|T|$ for surface piercing barriers over symmetric shelf bottom for $h_2/h_1 = 0.6, a/h_1 = 0.5, \theta = 0$.

Figs. 4.6 and 4.7 show the variation of reflection $|R|$ & transmission $|T|$ coefficients as a function of non-dimensional wave number $k_0 h_1$ for different lengths of the barriers. In Fig. 4.6, a comparison is made between single and double barriers. It is noticed that local maxima in $|R|$ increases when there are two barriers instead of single barrier. Therefore, local minima in $|T|$ decreases for the same. This may happen due to the mutual interaction between the incident and reflected waves between the barriers. Therefore, a pair of thin vertical barriers are more effective to reflect more incident wave energy in comparison to a single thin vertical barrier. It is also noticed from Figs. 4.6 and 4.7 that the phenomena of zero reflection occurs for the identical lengths of the barriers i.e. $d/h_1 = 0.4$ which may be due to the constructive/destructive interference of the incident and reflected

Figure 4.8: Comparison between surface piercing & submerged barriers over symmetric shelf bottom for $d_1/h_1 = 0.2, d_2/h_1 = 0.3, h_2/h_1 = 0.6, a/h_1 = 0.3, \theta = 0$.

Figure 4.9: Submerged barriers over symmetric shelf bottom for $d/h_1 = 0.3$, $h_2/h_1 = 0.8, a/h_1 = 0.5, \theta = 0$.

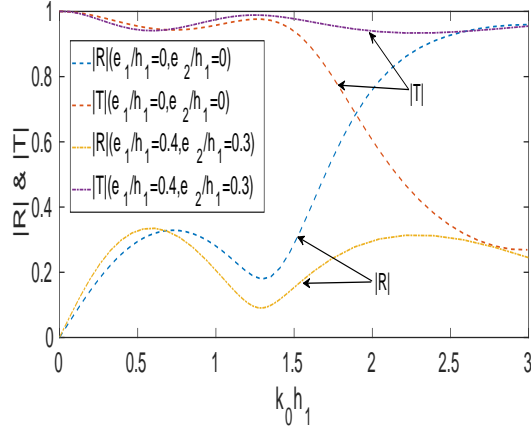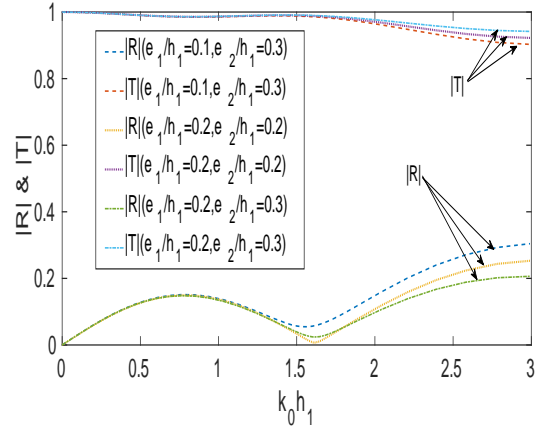waves between the barriers. Hence, the identical lengths of the barriers should be avoided in construction of breakwater to avoid zero reflection i.e. full transmission towards the protection of seashore. Fig. 4.8 demonstrates the variation of $|R|$ & $|T|$ versus $k_0 h_1$ for two different positions, surface piercing i.e. $e_1/h_1 = e_2/h_1 = 0$ and bottom standing i.e. $e_1/h_1 = 0.4, e_2/h_1 = 0.3$, of the barriers. It is observed that surface piercing barriers are more effective to reflect incident wave energy as comparison to bottom standing barriers which may be due to the fact that for larger values of wave number i.e. shorter waves almost confined near the free surface and produce more reflection due to the surface piercing barriers. Fig. 4.9 shows the effect of depth of submergence i.e. $e_1/h_1, e_2/h_1$ on $|R|$ & $|T|$. It is observed that reflection coefficient decreases as the depth of submergence increases which may be due to the same fact as mentioned towards Fig. 4.8. In Fig. 4.10, the variation of $|R|$ & $|T|$ versus $k_0 h_1$ for $M = 1, 2$ & 3, number of pairs of surface piercing barriers over the shelf bottom is demonstrated. It is observed that as $M = 1, 2, 3$ (single, double and triple pair of barriers) increases the local maxima's in $|R|$ increases while local minima's in $|T|$ decreases. Also, the figure demonstrates that zero reflection can be avoided by increasing the number of pairs of barriers. In next part, we will discuss the effect of various parameters on reflection and transmission coefficients.

(i) **Effect of the depth ratios**

The variation of $|R|$ & $|T|$ as a function of non-dimensional wave number $k_0 h_1$ for three different depth ratios h_2/h_1 over symmetric shelf bottom topography is shown in Fig. 4.11. It is observed that local maxima in $|R|$ increases and local minima in $|T|$ decreases as the depth ratio h_2/h_1 decreases. This may happen due to the mutual interaction between the incident and reflected waves between the barriers. It is also noticed that the effect of h_2/h_1 diminishes as the value of wavenumber becomes larger which may be due to the fact that larger wave number waves i.e. shorter waves almost confined near the free surface and get very less influenced due

to the bottom topography. A significant phase shift in the oscillatory pattern of $|R|$ & $|T|$ is also observed as the depth ratio h_2/h_1 decreases. This phase shift may happen due to the mutual interaction of waves of different wavenumbers generated over the shelf bottom topography. In Fig. 4.12, $|R|$ & $|T|$ are plotted against k_0h_1
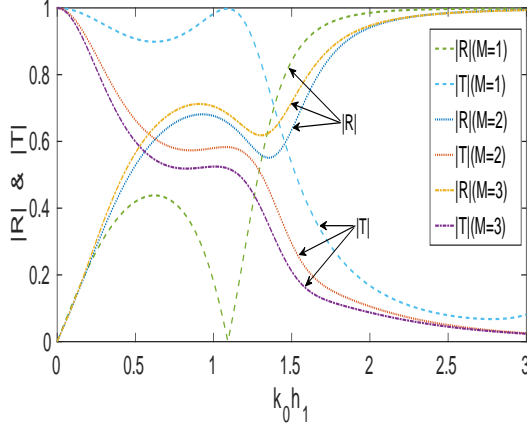

Figure 4.10: $|R|$ and $|T|$ versus k_0h_1 for $d/h_1 = 0.4, h_2/h_1 = 0.6, a/h_1 = 0.5, \theta = 0$ over symmetric shelf bottom.
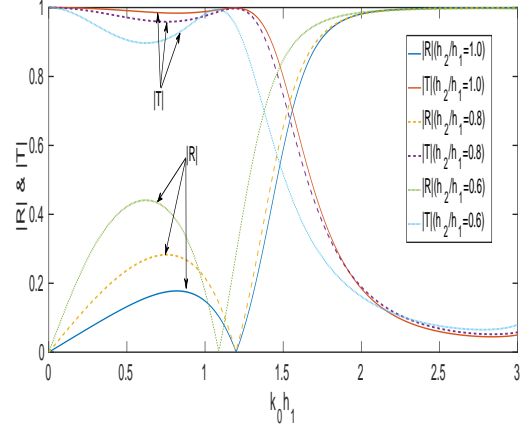
Figure 4.11: $|R|$ and $|T|$ versus k_0h_1 for $d/h_1 = 0.4, a/h_1 = 0.5, \theta = 0$ over symmetric shelf bottom.

for different values of h_3/h_1. It is noticed that local maxima in $|R|$ increases and local minima in $|T|$ decreases as h_3/h_1 decreases. This may happen due to the same fact as mentioned towards Fig. 4.11. Also, it is noticed that the phenomena of zero reflection occur only for symmetric shelf bottom topography i.e. for $h_3/h_1 = 1.0$. Hence, symmetrical design of shelf bottom topography may be avoided to avoid zero reflection i.e. full transmission. In Fig. 4.13, the influence of depth ratio h_2/h_1 on $|R|$ & $|T|$ versus k_0h_1 is shown for asymmetric shelf bottom topography. It is observed that local maxima in $|R|$ increases as h_2/h_1 decreases while the local minima in $|T|$ decreases. Here, the phenomena of zero reflection is absent because of asymmetric shelf bottom profile.

(ii) **Effect of the length of the barriers**

The effect of the length of the barriers on $|R|$ & $|T|$ against the wave number k_0h_1 is analysed in Fig. 4.14 and 4.15 respectively. It is observed that local maxima in $|R|$ increases as the length of the barriers d/h_1 increases as shown in Fig. 4.14. Consequently, local minima in the oscillatory pattern of $|T|$ decreases for the same as shown in Fig. 4.15. This may happen due to the same fact as mentioned in Fig. 4.11. Moreover, a significant phase shift in the oscillatory pattern of $|R|$ & $|T|$ is observed as d/h_1 increases. This phase shift may happen due to the mutual interaction of waves of different wave numbers generated between the barriers. Fig. 4.16 shows the variation of $|R|$ & $|T|$ against the length of the barriers d/h_1 for different wave numbers $k_0h_1 = 1.6218, 2.0653, 2.5318, 3.0144$ over symmetric shelf bottom topography. As the value of k_0h_1 becomes larger, $|R|$ increases and $|T|$ decreases. This may happen due to the fact that larger wave numbers waves i.e. shorter waves
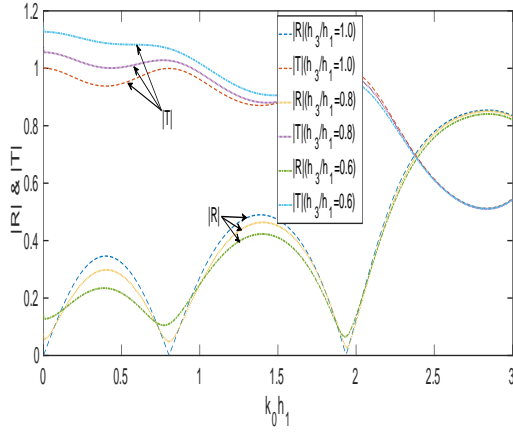
Figure 4.12: $|R|$ and $|T|$ versus $k_0 h_1$ for $d_1/h_1 = d_2/h_1 = 0.2$, $h_2/h_1 = 0.5$, $a/h_1 = 1.0$, $\theta = 0$ for different h_3/h_1.
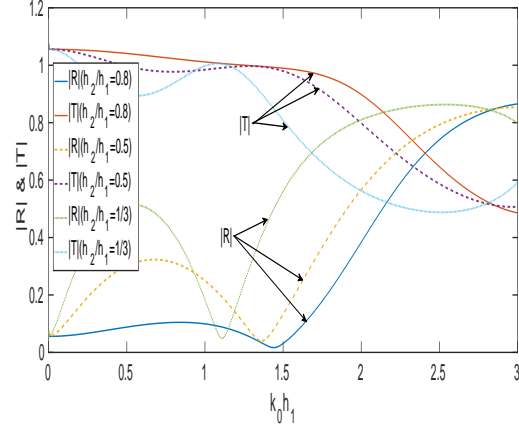
Figure 4.13: $|R|$ and $|T|$ versus $k_0 h_1$ for $d_1/h_1 = d_2/h_1 = 0.2$, $a/h_1 = 0.5$, $\theta = 0$ for different h_2/h_1 for asymmetric shelf $h_3/h_1 = 0.8$.
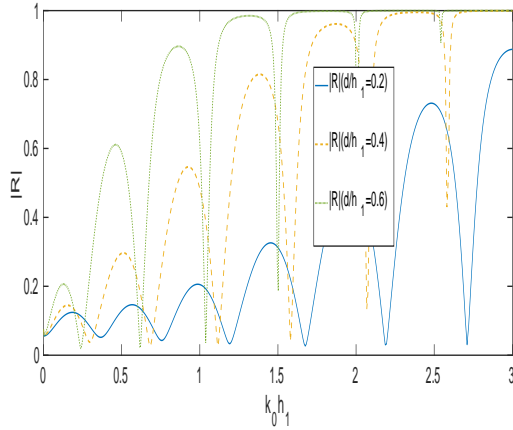
Figure 4.14: $|R|$ versus $k_0 h_1$ for $h_2/h_1 = 0.7$, $h_3/h_1 = 0.8$, $a/h_1 = 3.0$, $\theta = 0$ for different d/h_1.
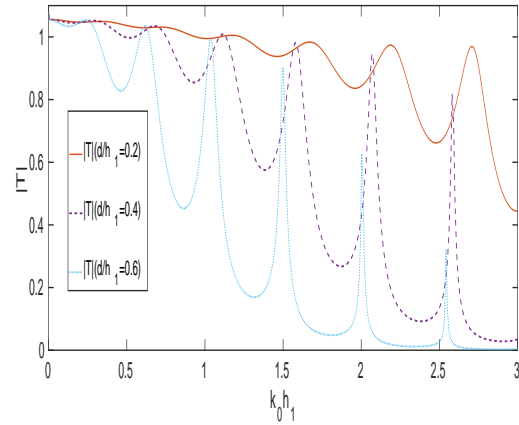
Figure 4.15: $|T|$ versus $k_0 h_1$ for $h_2/h_1 = 0.7$, $h_3/h_1 = 0.8$, $a/h_1 = 3.0$, $\theta = 0$ for different d/h_1.

confined more towards the free surface and this makes barriers more effective towards the reflection of incidence waves. Hence, less transmission is observed.

(iii) **Effect of the gap between the barriers**

The effect of the gap between the barriers on $|R|$ & $|T|$ is analysed in Figs. 4.17, 4.18 and 4.19. Figs. 4.17 and 4.18, respectively, show the variation of $|R|$ & $|T|$ against $k_0 h_1$ for different gaps between the barriers. In both the figures, the periodic oscillatory pattern for $|R|$ & $|T|$ increases as a/h_1 increases. This is due to the mutual interaction between the incident and reflected waves between the barriers. Fig. 4.19 shows the variation of $|R|$ & $|T|$ against a/h_1 for different lengths of the barriers. This depicts that for certain values of gap length the maximum reflection occurs due mutual interaction of incident and reflected waves between the barriers.

(iv) **Effect of the angle of incidence**
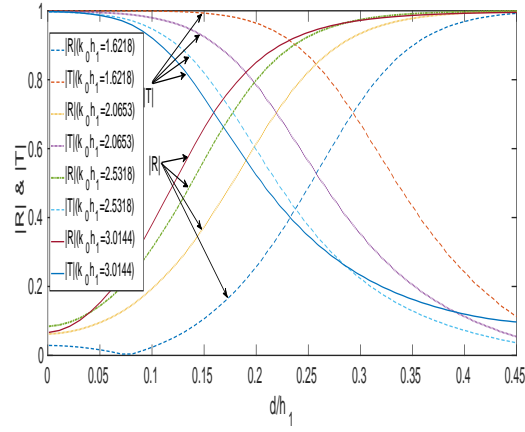
Figure 4.16: $|R|$ and $|T|$ versus d/h_1 for $h_2/h_1 = 0.5, a/h_1 = 0.5, \theta = 0$ for different wave numbers over the symmetric shelf bottom.
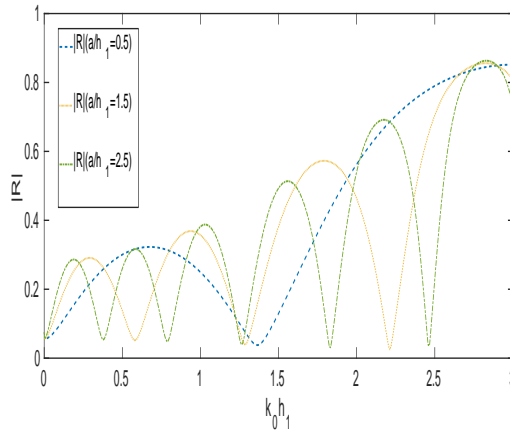
Figure 4.17: $|R|$ versus $k_0 h_1$ for $h_2/h_1 = 0.5, h_3/h_1 = 0.8, d/h_1 = 0.2, \theta = 0$ for different gaps between the barriers.
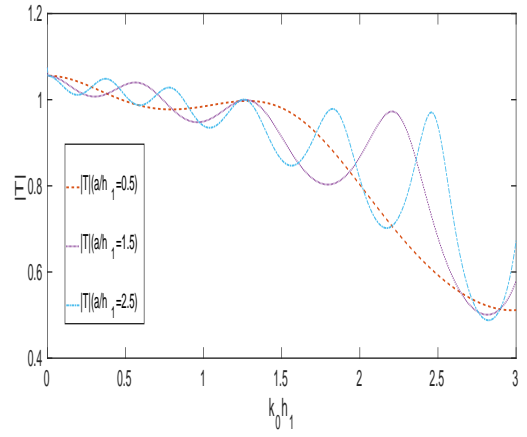
Figure 4.18: $|T|$ versus $k_0 h_1$ for $h_2/h_1 = 0.5, h_3/h_1 = 0.8, d_1/h_1 = 0.2, \theta = 0$ for different gaps between the barriers.
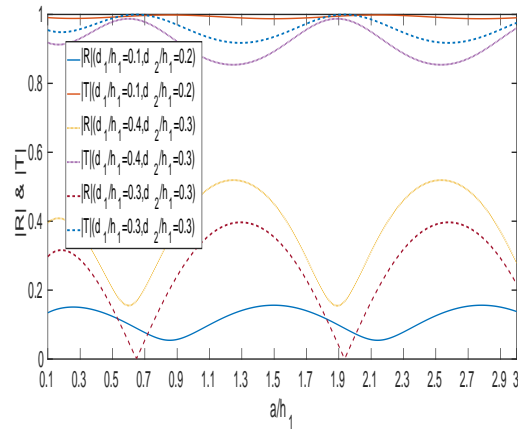
Figure 4.19: $|R|$ and $|T|$ versus a/h_1 for different lengths of the barriers over symmetric shelf for $h_2/h_1 = 0.8, Kh_1 = 1.0, \theta = 0$.

The effect of angle of incidence on $|R|$ & $|T|$ is shown through Fig. 4.20. It is observed that as the angle of incidence increases, the local maxima in $|R|$ decreases while the local minima in $|T|$ increases.
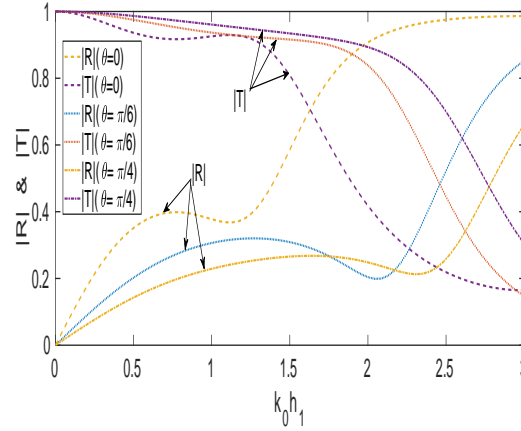
Figure 4.20: $|R|$ and $|T|$ versus $k_0 h_1$ for different angle of incidence for $d_1/h_1 = 0.4, d_2/h_1 = 0.2, h_2/h_1 = 0.6, a/h_1 = 0.5$.

4.5.4 Free Surface Elevation Profiles

Fig. 4.21 shows the behaviour of free surface wave elevation η_j in each of region $j = 1, 2, 3$ i.e. before the front barrier, between the barriers and after the rear barrier for different lengths of the identical barriers. It is noticed that the wave amplitude $\Re(\eta_1)$ before the front barrier increases while the wave amplitude after the rear barrier $\Re(\eta_3)$ decreases as d/h_1 increases. It is also noticed that wave elevation after the rear barrier is less in comparison to wave elevation before the front barrier which shows that less energy is transmitted to seashore. This fulfill the aim of our present study.

4.5.5 Force on the Barriers

Here, the effect of various system parameters on the non-dimensional horizontal force experienced by the front and rear barriers is observed in Figs. 4.22-4.24. The effect of the length of the barriers d/h_1 on the non-dimensional horizontal force on the front barrier ($|F_f|/\rho g h_1^2$) and the rear barrier ($|F_r|/\rho g h_1^2$) against the wavenumber $k_0 h_1$ is demonstrated respectively in Figs. 4.22a and 4.22b. Here, it is observed that the global maxima in both the force curves for front and rear barriers increases as the length of the barriers d/h_1 increases. This is possibly due to the mutual interaction of incident and reflected waves between the barriers. It is also observed that amplitude of the force on the rear barrier is less in comparison to the front barrier. Further, the variation of the non-dimensional horizontal force experienced by the front and rear barriers versus length of the identical barriers d/h_1 is plotted
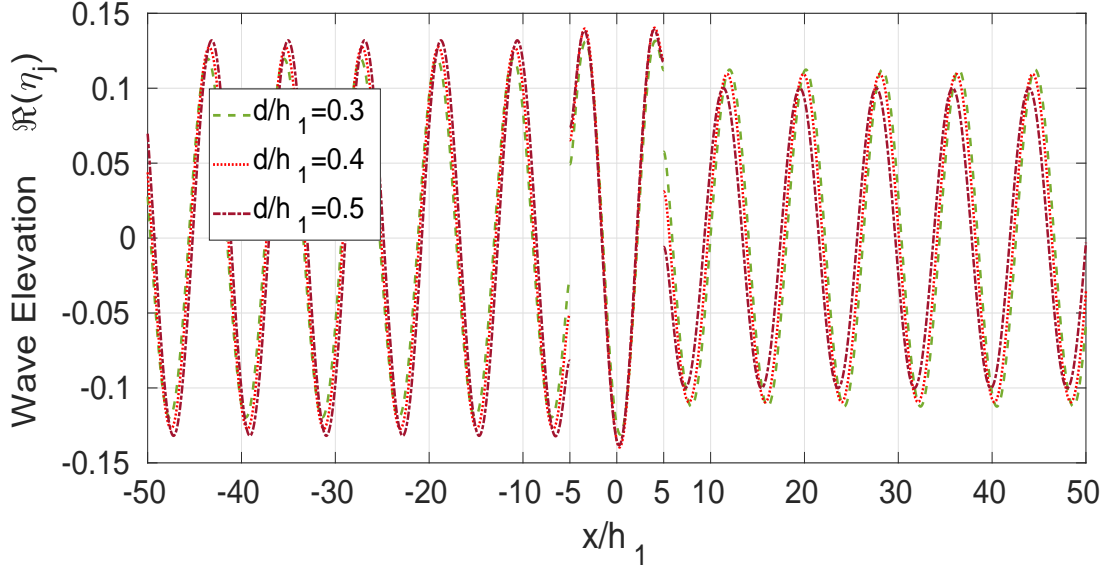
Figure 4.21: Surface elevation for different d/h_1 over symmetric shelf bottom for $h_2/h_1 = 0.8, a/h_1 = 5.0, Kh_1 = 0.5, \theta = 0$.
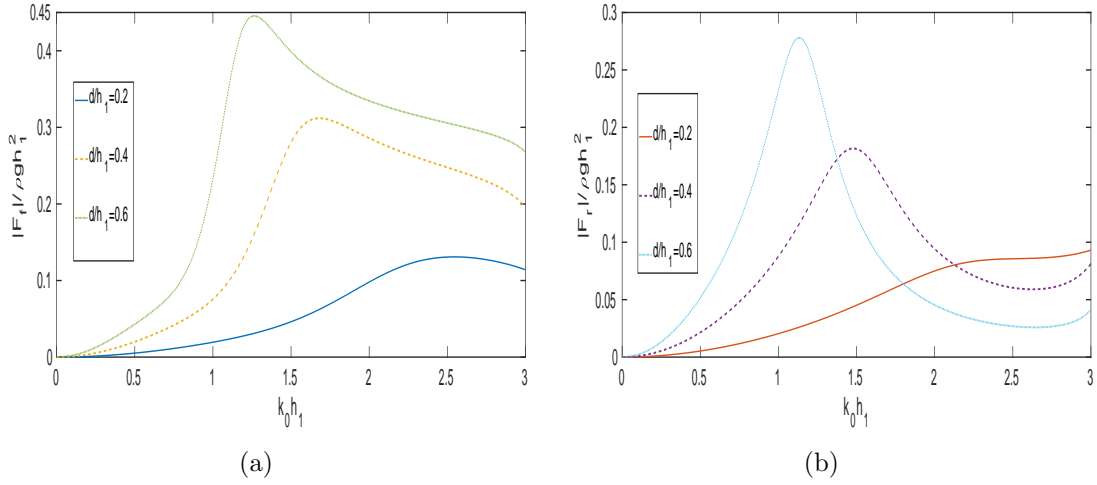
Figure 4.22: Force versus k_0h_1 for different d/h_1 for $a/h_1 = 0.5, \theta = 0$ over the flat bottom where in Fig. (a) Force on front barrier and in Fig. (b) Force on rear barrier.

respectively in Figs. 4.23a and 4.23b for different k_0h_1. Both the figures depict that the amplitude of horizontal force on the front and rear barriers increases as the wave number becomes larger. This may happen due to the fact that waves with larger wavenumbers i.e. shorter waves are confined near the free surface and create more pressure on the barriers. Further, the forces experienced by the front and rear barriers versus the gap between the barriers a/h_1 are plotted respectively in Figs. 4.24a and 4.24b for different d/h_1. These figures depict that for certain values of gap length, maximum force on the front and rear barriers occurs.

(a)   (b)
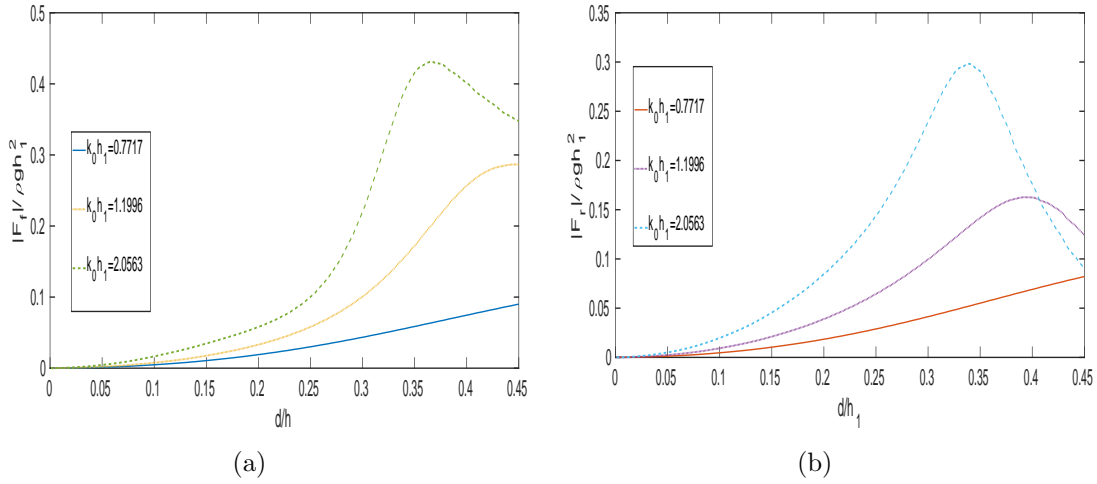
Figure 4.23: Force versus d/h_1 for different wave numbers for $h_2/h_1 = 0.5, a/h_1 = 1.5, \theta = 0$ over symmetric shelf bottom where in Fig. (a) Force on front barrier and in Fig. (b) Force on rear barrier.

(a)   (b)
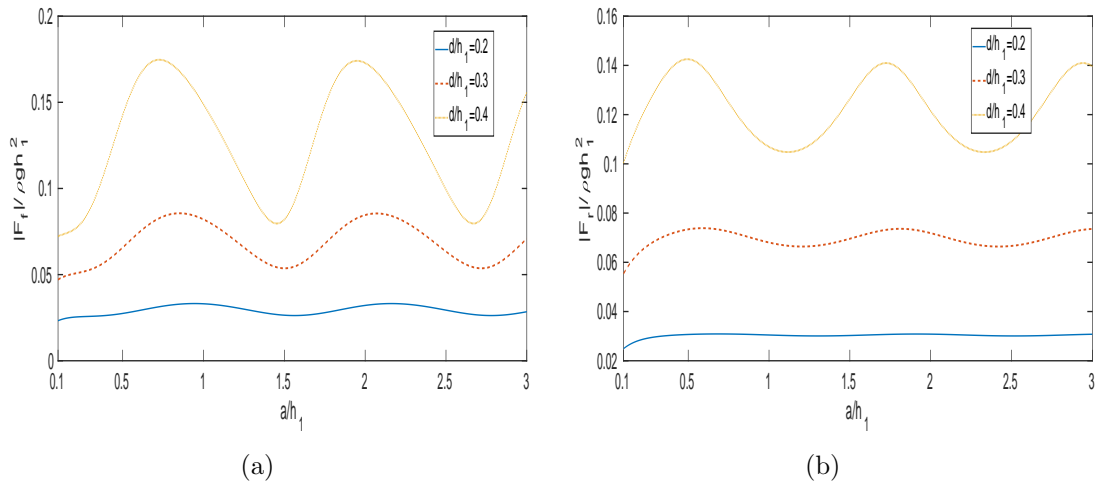
Figure 4.24: Force versus a/h_1 for different d/h_1 for $h_2/h_1 = 0.8, Kh_1 = 1.0, \theta = 0$ over symmetric shelf bottom topography where in Fig. (a) Force on front barrier and in Fig. (b) Force on rear barrier.

4.6   Conclusion

In this chapter, the problem of scattering of surface waves by two thin vertical barriers over a shelf bottom topography is examined for its solution with the aid of eigenfunction expansion method and least square method. The numerical values of the reflection and transmission coefficients are plotted through different graphs to analyse the influence of various system parameters. For identical barriers over the symmetric shelf bottom, the zeros in the reflection curve are observed. The zeros in the reflection curve can be avoided by using non-identical barriers or asymmetric shelf bottom topography. Hence, less energy will be transmitted to seashore i.e. less impact on the seashore. It is also noticed that more energy is reflected by a pair of barriers as compared to a single barrier.

Hence, less incident wave energy is transmitted to the lee side, yielding less impact on the seashore. Increasing the length of the barriers produces more reflection and consequently less transmission to the lee side. As the gap between the barriers increases, it causes more number of oscillations on both the reflection and transmission coefficients curves. The local maxima in reflection curve decreases as the angle of incidence increases. Also, the reflection coefficient decreases as the depth of submergence of the barriers increases. Furthermore, this problem is generalized for an array of surface piercing barriers (M-pair) over shelf bottom topography. It is noticed that local maxima in reflection curve increases as additional pairs of surface piercing barriers are considered between the barriers. It is also observed that the wave amplitude after the barriers can be decreased with the increased length of the barriers. The analysis of non-dimensional horizontal force per unit width of the front and rear barriers is also observed. As the length of the barrier increases, the global maxima on the force curves for both the front and rear barriers increases. Moreover, it is noticed that the front barrier experience more force as compared to the rear barrier.

Chapter 5

Scattering of water waves by two vertical barriers over arbitrary bottom topography

5.1 Introduction

In Chapter 4, the scattering of obliquely incident surface water waves by two vertical barriers over a shelf type bottom topography was investigated for its solutions. In this chapter, instead of shelf bottom profile, the arbitrary bottom profile is considered and hence different methodology is applied here to solve the problem. A finite element model is developed by formulating well-posed boundary value problem in a finite domain where the finite domain is obtained after truncating the radiation boundary conditions at a finite distance. The scattered potential is determined computationally and is further used to obtain the numerical values of the reflection and transmission coefficients and the force o the barriers. The energy balance relation is derived from Green's integral theorem, which ensures the correctness of the present numerical results. The obtained results are compared with the results available in the literature Das [27] for validation purpose. The physical quantities reflection and transmission coefficients, force on the barriers are calculated for two particular forms namely, parabolic hump and rectangular hump bottom profile. The study reveals, the number of zeros on the reflection and transmission curves are investigated concerning the gap between the identical or non-identical barriers. The effect of the gap between the barriers, height of the bottom topography, thickness of the barriers, length of the barriers and angle of incidence on the reflection and transmission coefficients, and the non-dimensional horizontal force on the front and rear barriers have been investigated using this model. This study will be helpful to handle similar problems arising in the area of applied mathematics and fluid mechanics.

5.2 Mathematical Formulation

The problem is analysed in a three-dimensional Cartesian coordinate system (x, y, z) such that the undisturbed free surface of water coincides with xz-plane and the y-axis is vertically downward. We consider oblique incidence of progressive wave train that makes an angle α with the positive x-axis to a pair of surface piercing vertical barriers in

the presence of the bottom topography which is arbitrary. Let d_1 and d_2 are drafts and $x = -l, l$ are positions of the front and rear barriers respectively, and b is the thickness of the front as well as the rear barrier. It is assumed that the barriers and the bottom topography are infinitely long in the z-direction and therefore the characteristic behaviour remains the same along the z-direction. Suppose the fluid under our consideration is
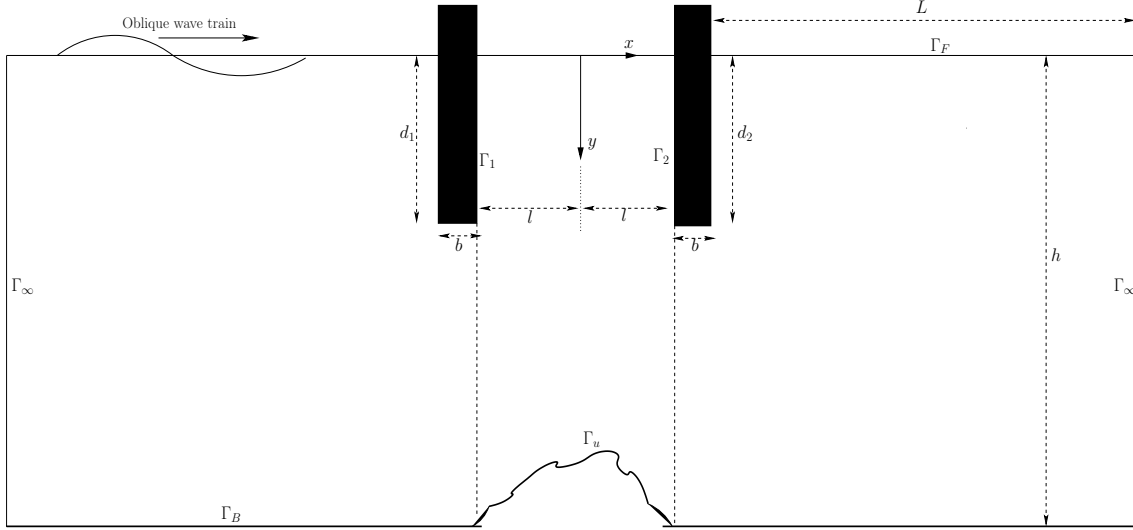
Figure 5.1: Schematic of the problem.

inviscid, incompressible, and the motion is irrotational and time harmonic with angular frequency ω and also along the z-direction. Therefore, the velocity potential $\Phi(x, y, z, t) = \Re[\phi(x, y)e^{i(\mu z - \omega t)}]$, where $\Re$ denotes the real part and μ is the component of the incident wave number k_0 along z-direction, $\mu = k_0 \sin \alpha$. Here, the spatial velocity potential $\phi(x, y)$ is taken as the sum of the incident wave potential denoted by $\phi_{inc}(x, y)$ and the scattered wave potential denoted by $\phi_{sc}(x, y)$ such that

$$\phi(x, y) = \phi_{inc}(x, y) + \phi_{sc}(x, y) \tag{5.1}$$

where $\phi_{inc}(x, y) = -\frac{Ag}{\omega} \frac{\cosh(k_0(y-h))}{\cosh(k_0 h)} e^{i(k_0 \cos \alpha)x}$, A is the amplitude of the incident wave, g is acceleration due to gravity, h is the finite depth of water away from the arbitrary undulated profile and k_0 is the wave number of the incident wave, which is the positive real root of the dispersion equation in k as

$$\omega^2 h/g = kh \tanh(kh). \tag{5.2}$$

The scattered velocity potential $\phi_{sc}(x, y)$ satisfies the Helmholtz equation given by

$$\frac{\partial^2 \phi_{sc}}{\partial x^2} + \frac{\partial^2 \phi_{sc}}{\partial y^2} - \mu^2 \phi_{sc} = 0, \text{ within the fluid domain } \Omega. \tag{5.3}$$

Apart from the governing differential equation, the scattered potential must satisfies the following boundary conditions:

$$\frac{\partial \phi_{sc}}{\partial y} + \frac{\omega^2}{g} \phi_{sc} = 0, \quad \text{on the free surface,} \tag{5.4}$$

$$\frac{\partial \phi_{sc}}{\partial y} = 0, \text{ on the flat bottom,} \tag{5.5}$$

$$\frac{\partial \phi_{sc}}{\partial n} = -\frac{\partial \phi_{inc}}{\partial n}, \quad \text{on the barriers and arbitrary bottom,} \tag{5.6}$$

where n represents the unit outward normal on the barriers and the arbitrary bottom. Finally, we impose the following radiation boundary conditions on the scattered potential at infinity to make the solution unique:

$$\frac{\partial \phi_{sc}}{\partial x} \pm (ik_0 \cos \alpha) \phi_{sc} = 0, \text{ on infinite boundaries i.e. } x \to \mp\infty. \tag{5.7}$$

But, we impose the radiation boundary conditions (5.7) at a finite distance from the barriers as the local disturbances decay sufficiently in a finite distance, say L, which is proven in Section 5.5. Thus, we have a well-posed boundary value problem, which is defined in a finite domain after truncating the infinite domain as shown in Fig. 5.1, where Γ_F, (Γ_1, Γ_2), Γ_B, Γ_u, Γ_∞ are respectively, the free surface, front and rear barriers boundary, flat bottom boundary, undulated arbitrary bottom boundary, and radiation boundaries. Let us rewrite the final formulation for the implementation of the finite element method after dropping the subscript 'sc' from 'ϕ_{sc}' as follows:

$$\frac{\partial^2 \phi}{\partial x^2} + \frac{\partial^2 \phi}{\partial y^2} - \mu^2 \phi = 0, \text{ in } \Omega \tag{5.8}$$

$$\frac{\partial \phi}{\partial n} + \frac{\omega^2}{g} \phi = 0, \quad \text{on } \Gamma_F \tag{5.9}$$

$$\frac{\partial \phi}{\partial n} = 0, \text{ on } \Gamma_B \tag{5.10}$$

$$\frac{\partial \phi}{\partial n} = -\frac{\partial \phi_{inc}}{\partial n}, \text{ on } \Gamma_S (= \Gamma_u \cup \Gamma_1 \cup \Gamma_2) \tag{5.11}$$

$$\frac{\partial \phi}{\partial n} - (ik_0 \cos \alpha) \phi = 0, \text{ on } \Gamma_\infty \tag{5.12}$$

Now, we aim to solve the boundary value problem $(5.8) - (5.12)$ to determine the scattered potential ϕ. The singularity (Ray et al. [110]) at the edges of the vertical barriers is not taken.

5.3   Method of Solution

We employ the finite element method to solve this problem of having arbitrary bottom topography between the surface piercing barriers.

For the present study, a two-dimensional finite element method (FEM) is employed to solve

the boundary value problem for the scattered velocity potential. There are commonly two ways, namely variational method and weighted residual method, to construct the integral formulation for the governing differential equation. As the approximated potential is substituted into the governing equation with the boundary conditions, residual occurs at each node which is forced to be equal to zero by employing the weighted residual method. The scattered velocity potential ϕ is approximated as a linear combination of the shape functions $N_i^e(x, y)$ and the nodal values ϕ_i^e over each typical element, e as

$$\hat{\phi}^e = \sum_{i=1}^{n_e} \phi_i^e N_i^e(x, y) \tag{5.13}$$

where $\hat{\phi}^e$ denotes the approximated scattered velocity potential and n_e the number of nodes over an element.

Now, on calculating the weighted residual of the governing differential equation (5.8) using the weight function, $w \equiv w(x, y)$, over each element and forcing it to zero, we obtain

$$0 = \int_{\Omega^e} -w \left(\frac{\partial^2 \hat{\phi}^e}{\partial x^2} + \frac{\partial^2 \hat{\phi}^e}{\partial y^2} - \mu^2 \hat{\phi}^e \right) d\Omega^e \tag{5.14}$$

$$\Rightarrow 0 = \int_{\Omega^e} \left(\frac{\partial w}{\partial x} \frac{\partial \hat{\phi}^e}{\partial x} + \frac{\partial w}{\partial y} \frac{\partial \hat{\phi}^e}{\partial y} + \mu^2 w \hat{\phi}^e \right) d\Omega^e - \int_{\Gamma^e} w \frac{\partial \hat{\phi}^e}{\partial n} d\Gamma^e \tag{5.15}$$

where Ω^e and Γ^e represent the domain and boundary of a typical element in which the corresponding integrations are taken, respectively. The second integral term (corresponding to the boundaries) may be written as

$$\int_{\Gamma^e} w \frac{\partial \hat{\phi}^e}{\partial n} d\Gamma^e = -\frac{w^2}{g} \int_{\Gamma_F^e} w \hat{\phi}^e d\Gamma_F^e + 0 + \int_{\Gamma_\infty^e} w(ik_0 cos\alpha) \hat{\phi}^e d\Gamma_\infty^e + Q^e \tag{5.16}$$

where

$$Q^e = \int_{\Gamma_S^e} w \left(-\frac{\partial \phi_{inc}}{\partial n} \right) d\Gamma_S^e. \tag{5.17}$$

The weight functions $w(x, y)$ are to be chosen as a set of linearly independent functions. In Galerkin approach, $w = N_j (j = 1, 2, 3, ..., n_e)$ are taken as the choice of weight functions. Now, substituting expressions (5.13) and (5.16) into equation (5.15), and on simplifying, we get

$$\sum_{i=1}^{n_e} \phi_i^e \left[\int_{\Omega^e} \left(\frac{\partial N_i^e}{\partial x} \frac{\partial N_j^e}{\partial x} + \frac{\partial N_i^e}{\partial y} \frac{\partial N_j^e}{\partial y} + \mu^2 N_i^e N_j^e \right) d\Omega^e + \frac{w^2}{g} \int_{\Gamma_F^e} N_i^e N_j^e d\Gamma_F^e - \right.$$

$$ik_0 \cos\alpha \int_{\Gamma_\infty^e} N_i^e N_j^e d\Gamma_\infty^e \Bigg] = \int_{\Gamma_S^e} N_j^e \left(-\frac{\partial \phi_{inc}}{\partial n} \right) d\Gamma_S^e \tag{5.18}$$

where $j = 1, 2, 3, ..., n_e$,

$$\Rightarrow \sum_{i=1}^{n_e} \phi_i^e \left[\int_{\Omega^e} \left(\frac{\partial N_i^e}{\partial x} \frac{\partial N_j^e}{\partial x} + \frac{\partial N_i^e}{\partial y} \frac{\partial N_j^e}{\partial y} + \mu^2 N_i^e N_j^e \right) d\Omega^e + \frac{w^2}{g} \int_{\Gamma_F^e} N_i^e N_j^e d\Gamma_F^e - \right.$$

$$- ik_0 cos\alpha \int_{\Gamma_\infty^e} N_i^e N_j^e d\Gamma_\infty^e \bigg] = -Q_j^e. \tag{5.19}$$

The computational domain of the problem is divided into finite elements by using two types of isoparametric* elements. The quadratic bar and quadratic quadrilateral elements corresponding to the boundaries and the inner domain, respectively. The local and global coordinate systems for isoparametrisation are defined in Fig. 5.2 and the shape functions of each node in any element in the local system are given below:

the shape functions for Quadratic Bar Element are

$$N_1^e = \frac{-s(1-s)}{2}, \ N_2^e = (1-s)(1+s), \ N_3^e = \frac{s(1+s)}{2} \tag{5.20}$$

whereas, the shape functions for Quadratic Quadrilateral Element are

$$N_1^e = -\frac{1}{4}(1-s)(1-t)(1+s+t), \ N_2^e = \frac{1}{2}(1-s^2)(1-t),$$

$$N_3^e = -\frac{1}{4}(1+s)(1-t)(1-s+t), \ N_4^e = \frac{1}{2}(1+s)(1-t^2),$$

$$N_5^e = -\frac{1}{4}(1+s)(1+t)(1-s-t), \ N_6^e = \frac{1}{2}(1-s^2)(1+t),$$
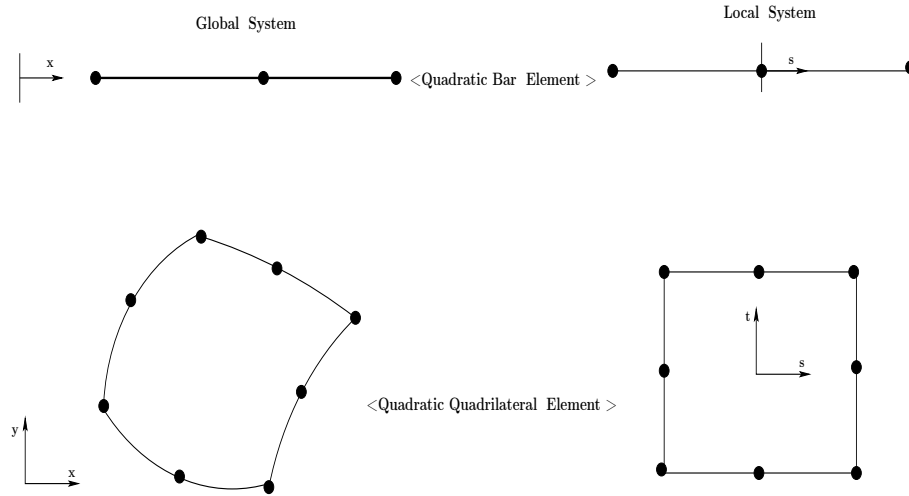
Figure 5.2: Quadratic Bar and Quadrilateral Element

$$N_7^e = -\frac{1}{4}(1-s)(1+t)(1+s-t), \ N_8^e = \frac{1}{2}(1-s^2)(1-t). \tag{5.21}$$

From equation (5.19), we derive the element stiffness matrix $[k_{ij}^e]$ and the load vector Q_j^e for the unknown nodal values ϕ_i^e for each element in the form as

$$[k_{ij}^e]_{n_e \times n_e} \{\phi_i^e\}_{n_e \times 1} = \{Q_j^e\}_{n_e \times 1} \tag{5.22}$$

---

*The same element is used to approximate the geometry as well as the dependent unknown.

where

$$k_{ij}^e = \int_{\Omega^e} \left(\frac{\partial N_i^e}{\partial x}\frac{\partial N_j^e}{\partial x} + \frac{\partial N_i^e}{\partial y}\frac{\partial N_j^e}{\partial y} + \mu^2 N_i^e N_j^e \right) d\Omega^e + \frac{w^2}{g} \int_{\Gamma_F^e} N_i^e N_j^e d\Gamma_F^e - ik_0 cos\alpha \int_{\Gamma_\infty^e} N_i^e N_j^e d\Gamma_\infty^e$$

and

$$Q_j^e = \int_{\Gamma_S^e} N_j^e \left(-\frac{\partial \phi_{inc}}{\partial n} \right) d\Gamma_S^e \tag{5.23}$$

which is further assembled to get a global stiffness matrix $[K_{ij}]$ and global load vector $\{Q_j\}$ over the elements and has to solve for unknown global nodal values. Once the scattered potential is determined, the behaviour of the reflected and transmitted waves can be investigated. The reflection and transmission coefficients of monochromatic surface waves are calculated by using the following relations:

$$|R| = \frac{\omega}{Ag}\frac{\cosh k_0 h}{\cosh k_0(y_0 - h)}|\phi(-L, y_0)| \tag{5.24}$$

and

$$|T| = \frac{\omega}{Ag}\frac{\cosh k_0 h}{\cosh k_0(y_0 - h)}\left| \frac{Ag}{\omega}\frac{\cosh k_0(y_0 - h)}{\cosh k_0 h} - e^{-i(k_0 \cos\alpha)x}\phi(L, y_0) \right| \tag{5.25}$$

where $y_0 \in [0, h]$ be any point. The horizontal force on the front and rear barriers are derived from the Bernoulli's equation for the unit amplitude of the incident waves. In non-dimensional form, the horizontal force on the front barrier $\frac{|F_f|}{\rho g h A}$ and the rear barrier $\frac{|F_r|}{\rho g h A}$ per unit width, respectively given by the integrals:

$$\frac{|F_f|}{\rho g h A} = \frac{\omega}{gh}\left| \int_0^{d_1} (\phi(-b - l, y) - \phi(-l, y))dy \right| \tag{5.26}$$

and

$$\frac{|F_r|}{\rho g h A} = \frac{\omega}{gh}\left| \int_0^{d_2} (\phi(b + l, y) - \phi(l, y))dy \right| \tag{5.27}$$

which are further solved numerically using Simpson's 1/3 rule.

5.4   Energy Balance Relation

Using Green's identity,

$$\int_\Gamma \left(\phi\frac{\partial \phi^*}{\partial n} - \phi^*\frac{\partial \phi}{\partial n} \right)d\Gamma = 0 \tag{5.28}$$

where $\phi^*(x, y)$ is the complex conjugate of the velocity potential $\phi(x, y)$ and $\frac{\partial}{\partial n}$ is the outward normal derivative to the boundary Γ which is boundary of the fluid region Ω.

The contribution to the integral (5.28) due to the free surface Γ_F is zero as

$$\int_{\Gamma_F} [\phi\{-\frac{\omega^2}{g}\phi^*\} - \phi^*\{-\frac{\omega^2}{g}\phi\}]dx = 0 \tag{5.29}$$

The contribution to the integral (5.28) due to the bottom $\Gamma_u \cup \Gamma_B$ and the front and rear barriers $\Gamma_1 \cup \Gamma_2$ is also zero as $\frac{\partial \phi}{\partial n} = \frac{\partial \phi^*}{\partial n} = 0$ on the bottom and as well as on both the barriers.

The contribution from the left radiation boundary is

$$\int_0^h \left(\phi\frac{\partial \phi^*}{\partial x} - \phi^*\frac{\partial \phi}{\partial x}\right)dy = \frac{A^2 g^2}{\omega^2}\frac{ik_0\cos\alpha(|R|^2 - 1)}{2k_0\cosh^2 k_0 h}[2k_0 h + \sinh 2k_0 h] \tag{5.30}$$

The contribution from the right radiation boundary is

$$\int_h^0 \left(\phi\frac{\partial \phi^*}{\partial x} - \phi^*\frac{\partial \phi}{\partial x}\right)dy = \frac{A^2 g^2}{\omega^2}\frac{ik_0\cos\alpha|T|^2}{2k_0\cosh^2 k_0 h}[2k_0 h + \sinh 2k_0 h] \tag{5.31}$$

On adding, all of these contributions in equation (5.28), we get the energy balance relation as given by

$$|R|^2 + |T|^2 = 1. \tag{5.32}$$

5.5 Numerical Results and Discussion

The arbitrary bottom profile is of two kinds, namely Type-I: Parabolic hump and Type-II: Rectangular hump respectively.

Type-I: The parabolic hump profile is given by

$$x(s) = s, \quad y(s) = \frac{c_0}{l^2}s^2 + (-c_0 + h), \quad \text{for} \quad -l \le s \le l. \tag{5.33}$$

Type-II: The rectangular hump profile is given by

$$x(s) = -l, \quad y(s) = s, \quad \text{for} \quad h - c_0 \le s \le h,$$

$$x(s) = s, \quad y(s) = h - c_0, \quad \text{for} \quad -l < s < l, \tag{5.34}$$

$$x(s) = l, \quad y(s) = s, \quad \text{for} \quad h - c_0 \le s \le h.$$

where c_0 is the height of the hump of bottom topography. The depth of the regions on both sides of the hump are equal. The non-dimensionalization of the physical parameters is done using the finite depth h of the fluid domain as d_1/h, d_2/h, $d/h(= d_1/h = d_2/h)$, b/h, l/h, L/h, c_0/h, $k_0 h$, $\omega^2 h/g$. It may be noted that, in non-dimensional form, $c_0/h = 0$ gives rise to flat bottom profile.

5.5.1   Convergence

The given problem of scattering of surface water waves by two vertical barriers over arbitrary bottom topography is formulated using FEM. The radiation boundaries are kept at a finite distance as the local disturbances due to barriers and the undulated bottom topography decay sufficiently within a finite distance. The analysis of the data in Table 5.1 depicts that a distance of four times the depth of the water is sufficient to keep the radiation boundaries for sufficient accuracy in the results and the same was stated by Bai [2]. The discretization of the computational domain has been done using two type of elements namely, quadratic quadrilateral elements within domain and quadratic bar elements at the boundaries. The mesh element size is progressively refined to the next higher level and its effect on the convergence of finite element solution has been analysed in Table 5.2. The total number of elements in the computational domain which is represented by N_e are increased as $4666, 8531, 12651$ and 18401 corresponding to $314, 474, 604$ and 750 elements on the boundaries respectively. The elements shape is parsimoniously kept square by keeping aspect ratio near to unity. The table shows that the accuracy in the present results for some given parameters upto four decimal places is obtained with $N_e = 12651$ for all the values of $k_0 h$.

Table 5.1: Effect of the distance L/h of the radiation boundary conditions from the barriers on the finite element solutions through $|R|$ ($c_0/h = 0.2, d_1/h = d_2/h = 0.2, b/h = 0.1, \alpha = 0$) for Type-I profile

Table 5.1(a): $l/h = 0.3$

$k_0 h$	$L/h = 0.1$	$L/h = 1$	$L/h = 2$	$L/h = 3$	$L/h = 4$	$L/h = 5$
0.5	0.276504	0.137907	0.137883	0.137851	0.136123	0.136064
1.0	0.462780	0.248362	0.251669	0.251940	0.249328	0.249295
1.5	0.473928	0.240563	0.256132	0.256492	0.251086	0.251027
2.0	0.650512	0.198451	0.155694	0.157147	0.178574	0.178646
2.5	1.144556	0.876928	0.859516	0.861297	0.870637	0.870648

Table 5.1(b): $l/h = 1.5$

$k_0 h$	$L/h = 0.1$	$L/h = 1$	$L/h = 2$	$L/h = 3$	$L/h = 4$	$L/h = 5$
0.5	0.149939	0.074437	0.075582	0.076514	0.076521	0.076520
1.0	0.519346	0.234490	0.228199	0.230084	0.230107	0.230108
1.5	0.548457	0.141532	0.129115	0.123400	0.123482	0.123485
2.0	1.020788	0.760138	0.759746	0.758679	0.758634	0.758631
2.5	1.064250	0.747572	0.753650	0.738450	0.738187	0.738203

5.5.2   Validation

In order to validate the present method, the model developed here is first applied to compute the reflection coefficient of scattering of normal incidence waves by two thin

Table 5.2: Covergence of number of element N_e through $|R|$ with respect to N ($c_0/h = 0.2, d_1/h = d_2/h = 0.2, b/h = 0.1, L/h = 4, \alpha = 0$) for Type-I profile

Table 5.2(a): $l/h = 0.3$

$k_0 h$	$N_e = 4666$	$N_e = 8531$	$N_e = 12651$	$N_e = 18401$
		$|R|$		
0.5	0.135083	0.136123	0.138081	0.138129
1.0	0.247737	0.249328	0.253401	0.253447
1.5	0.247922	0.251086	0.259496	0.259515
2.0	0.190514	0.178574	0.144996	0.145025
2.5	1.064250	0.870637	0.855389	0.855417

Table 5.2(b): $l/h = 1.5$

$k_0 h$	$N_e = 4666$	$N_e = 8531$	$N_e = 12651$	$N_e = 18401$
		$|R|$		
0.5	0.075310	0.075883	0.076781	0.076852
1.0	0.227398	0.228449	0.231057	0.231172
1.5	0.132235	0.128878	0.120396	0.120338
2.0	0.761662	0.760697	0.757534	0.757497
2.5	0.764996	0.755722	0.727747	0.727684

vertical barriers over the uniform bottom. This particular model is similar to Fig. 5.1 in the absence of undulation at the bottom. In the two thin barriers, the drafts $d_1/h = d_2/h = 0.2$ and positions $l/h = 0.3$ are considered for this particular case. The reflection coefficient calculated from the present model is compared with those predicted by Das et al. [27] as shown in Fig. 5.3. A good agreement is observed and this validates the present model. Another comparison is made with Tran et al. [132] who considered two thin identical barriers over sinusoidal bottom topography. This particular case can be obtained from the present model by considering the drafts of the barriers as $d_1/h = d_2/h = 0.2$ and the arbitrary bottom profile as sinusoidal profile. The comparison is shown in Fig. 5.4, where an excellent agreement between the reflection coefficients is observed. Moreover, the energy identity relation $|R|^2 + |T|^2 = 1$ agrees and provides a numerical check for the results obtained through numerical computations as shown in Fig. 5.5. For Figs. 5.3 and 5.5, the distance between thin vertical identical barriers is $0.6h$. In the next section, the effects of the undulated profile, thickness and length of the vertical barriers are examined and an analysis for the number of zeros on $|R|$ & $|T|$ versus gap between the barriers is performed.

5.5.3 Influence of various parameters on the reflection and transmission coefficients

The scattering of surface waves by two surface-piercing thin vertical barriers having the depth of submergence d_1 and d_2 over Type-I bottom profile for normal incidence waves for different values of l/h, $|R|$ is plotted versus $k_0 h$ in Figs. 5.6 and 5.8 and $|T|$ is plotted
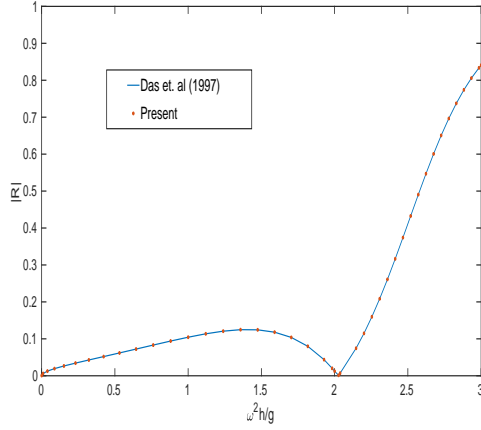
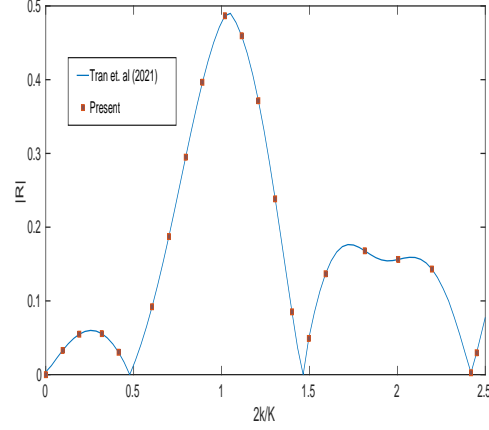Figure 5.3: Comparison between the present results and Das et. al (1997).

Figure 5.4: Comparison between the present results and Tran et. al (2021).
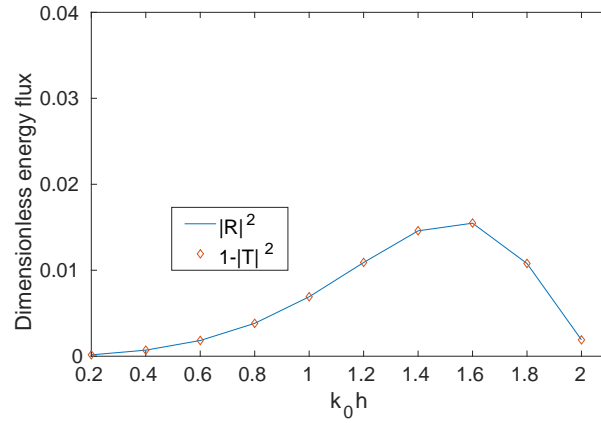
Figure 5.5: Conservation of wave energy for scattering by two thin identical barriers $d/h = 0.2$, $c_0/h = 0.1$ over Type-I hump.

versus k_0h in Figs. 5.7 and 5.9. For the case of two identical barriers i.e. $d/h = 0.2$, the zeros on the curve $|R|$ *vs* k_0h exist, and the number of zeros increases as the gap between the barriers increases as shown in Fig. 5.6. Corresponding to the zeros on the reflection curve, there exist zeros on the transmission curve $|T|$ *vs* k_0h as shown in Fig. 5.7. This may happen due to the constructive and/or destructive interference between incident and reflected waves between the barriers. These zeros of the reflection curve should be avoided for the protection of coastal structures. It is also observed that as the gap between the barriers increases the lower frequency zeros of $|T|$ curve coalesce in pairs as shown in Fig. 5.7. When the depths of submergence of the barriers are different i.e. $d_1/h = 0.18$, $d_2/h = 0.2$, Figs. 5.8 and 5.9 both show the non existence of the zeros on the reflection and transmission curves respectively. However, the minima's and maxima's still appear on both the curves and the number of maxima's and minima's increases as the gap between the barriers increases. This is due to the mutual interaction between the incident and reflected waves.   As the reflection and transmission coefficients

Figure 5.6: $|R|$ versus $k_0 h$ for $d_1/h = d_2/h = 0.2, c_0/h = 0.1, \alpha = 0$ for different positions of the barriers.
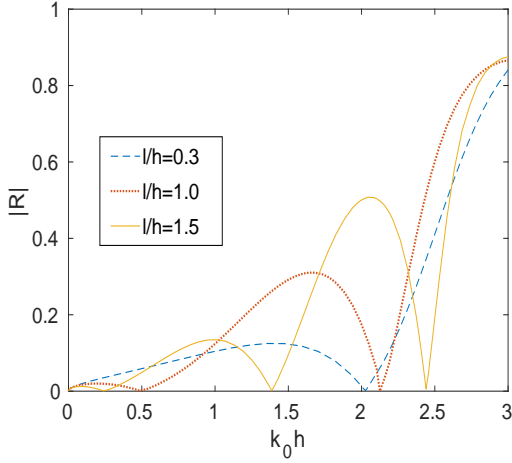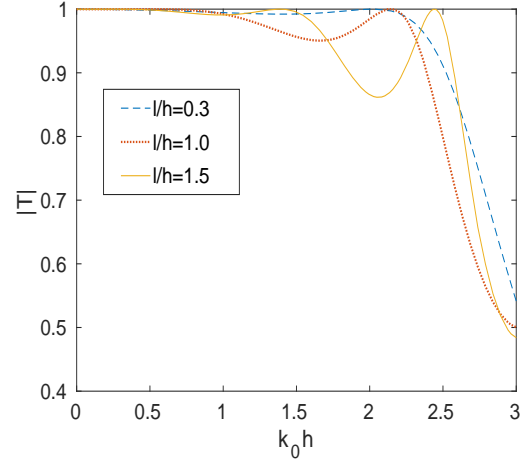

Figure 5.7: $|T|$ versus $k_0 h$ for $d_1/h = d_2/h = 0.2, c_0/h = 0.1, \alpha = 0$ for different positions of the barriers.
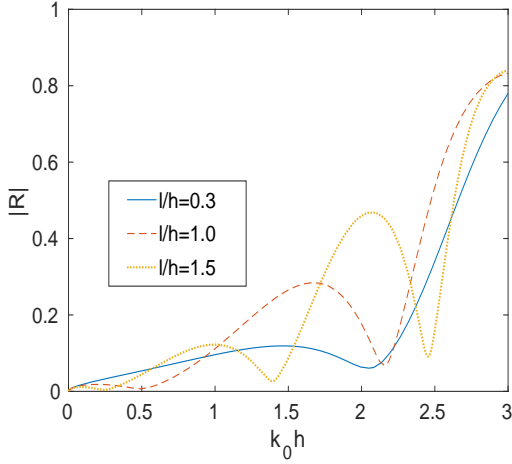
Figure 5.8: $|R|$ versus $k_0 h$ for $d_1/h = 0.18$, $d_2/h = 0.2, c_0/h = 0.1, \alpha = 0$ for different positions of the barriers.
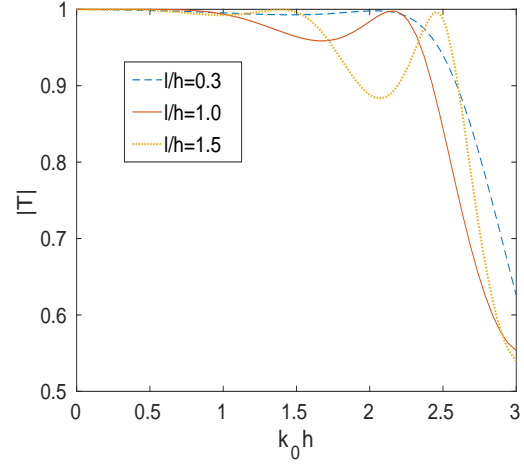
Figure 5.9: $|T|$ versus $k_0 h$ for $d_1/h = 0.18$, $d_2/h = 0.2, c_0/h = 0.1, \alpha = 0$ for different positions of the barriers.

satisfy the energy conservation identity, therefore transmission coefficient curves are not presented in the following results now onwards. Figs. 5.10 and 5.11 show the effect of bottom topography on $|R|$. In Fig. 5.10, the variation of $|R|$ as a function of $k_0 h$ by two thin vertical barriers for different heights c_0/h of the parabolic hump at the bottom is shown. The value of $|R|$ increases as c_0/h increases for the wavenumbers $0 < k_0 h < 2$. While the effect on the reflection coefficient is negligible for the incident waves with larger wavenumbers $k_0 h > 2.2$. The possible reason may be that the larger wavenumbers incident waves are confined near the free surface. In Fig. 5.11, $|R|$ is plotted versus $k_0 h$ for different heights of the rectangular hump at the bottom. It is again observed that $|R|$ increases as c_0/h increases for smaller wave numbers while $|R|$ is negligibly affected due to the waves with larger wavenumbers.   In Fig. 5.12, $|R|$ is presented versus $k_0 h$ for three different thicknesses b/h of the barriers. It is clearly noticed that $|R|$ increases as b/h increases.
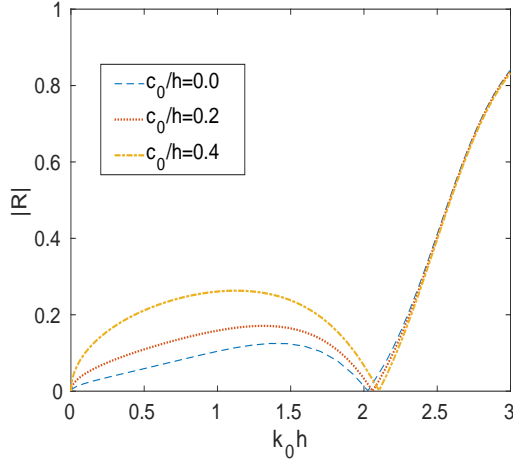
Figure 5.10: $|R|$ versus k_0h for thin barriers $d_1/h = d_2/h = 0.2, l/h = 0.3, \alpha = 0$ for different heights of Type-I hump.
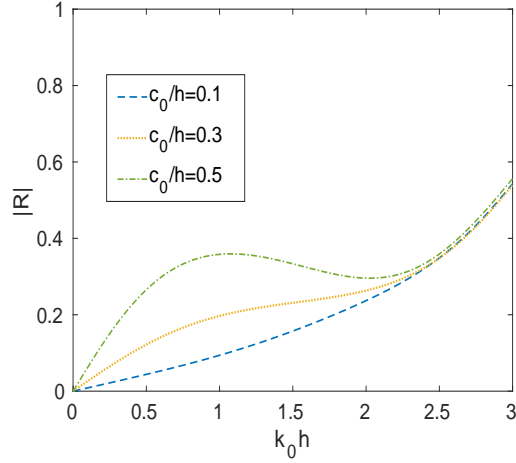
Figure 5.11: $|R|$ versus k_0h for thin barriers $d_1/h = 0.1, d_2/h = 0.2, l/h = 0.5, \alpha = 0$ for different heights of Type-II hump.
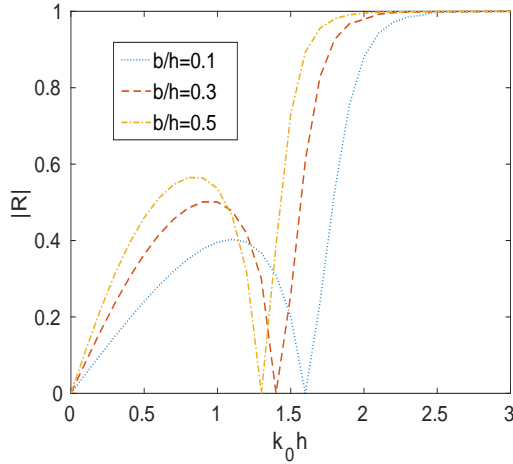
Figure 5.12: $|R|$ versus k_0h for $d_1/h = d_2/h = 0.3, c_0/h = 0.3, l/h = 0.3, \alpha = 0$ for different thickness of the barriers (Type-I).
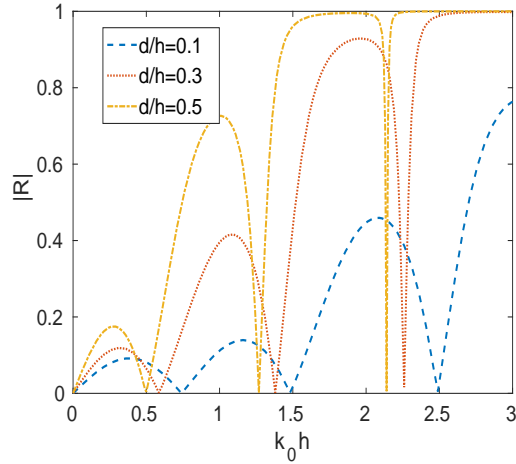
Figure 5.13: $|R|$ versus k_0h for $b/h = 0.1$, $c_0/h = 0.2, l/h = 1.5, \alpha = 0$ for different drafts of the barriers (Type-I).

This may happen due to the mutual interaction of incident and reflected waves between the barriers. Also, a phase shift is noticed in $|R|$ that may happen due to the mutual interaction of waves of different wavenumbers generated over the parabolic hump bottom topography. In Fig. 5.13, $|R|$ is presented versus k_0h for three different drafts of the identical barriers. The local maxima in $|R|$ increase as the drafts d/h of the barriers increases. This may happen due to the mutual interaction of incident and reflected waves between the barriers. Also, significant phase shifts in the oscillatory pattern of $|R|$ are observed as the length of barriers increases. This phase shift may happen due to the same as mentioned towards Fig. 5.12.

The effect of angle of incidence α on $|R|$ against k_0h is shown in Figs. 5.14 and 5.15 for barriers over the parabolic and rectangular hump bottom topography respectively. As $\alpha = 0, \pi/6, \pi/4$ increases, the first local maxima in $|R|$ decreases. After that local maxima

in $|R|$ increase as α increases. This may happen due to the fact that the constructive and/or destructive interference between incident and reflected waves occurs between the barriers. The local maxima's in $|R|$ shift toward the right as α increases. This phase shift in $|R|$ may occur due to the same fact as mentioned towards Fig. 5.12. In Fig. 5.15, the local maxima's in $|R|$ decreases as $\alpha = \pi/18, \pi/6, \pi/4$ increases. It is also noticed that the phenomena of zero reflection do not appear due to the use of non-identical barriers.
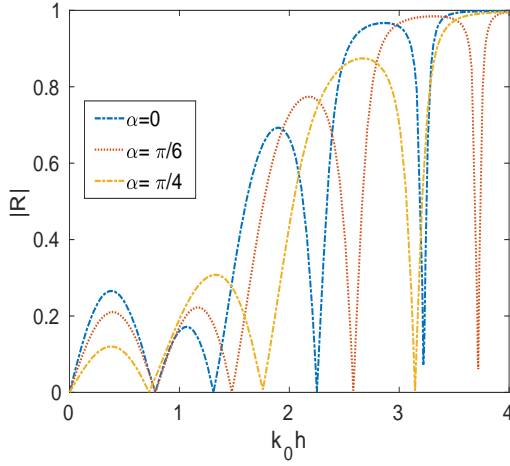
Figure 5.14: $|R|$ versus k_0h for $d_1/h = d_2/h = 0.2, b/h = 0.1, c_0/h = 0.5, l/h = 1.5$ for different angle of incidence (Type-I).
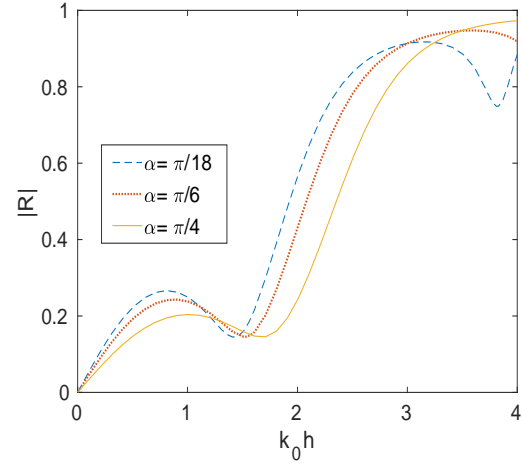
Figure 5.15: $|R|$ versus k_0h for $d_1/h = 0.1, d_2/h = 0.2, b/h = 0.1, c_0/h = 0.3, l/h = 0.5$ for different angle of incidence (Type-II).

5.5.4 Force on the barriers

Figs. 5.16a and 5.16b show the variation of non-dimensional horizontal force on the front and rear barriers versus $\omega^2 h/g$ for $d_1/h = 0.1$, $d_2/h = 0.2$, $b/h = 0$, $\alpha = \pi/6$, $l/h = 0.25$ for the flat bottom $c_0/h = 0$ and parabolic bottom $c_0/h = 0.3$. The peak in both of these plots refers to the resonant motion due to the mutual interaction between the incident and reflected waves between the vertical barriers. A good agreement of these force profiles with Wang et al. [141], when the parameter are the same as that of, again proves the correctness of the present method. Figs. 5.17a and 5.17b show the variation of the non-dimensional horizontal force on the barriers versus the length of the barriers d/h for the front and rear barriers respectively over the rectangular hump bottom topography for three different wavenumbers $k_0h = 0.7717, 1.1996, 2.0563$. It is observed that the peak for both the force curves the front and rear barriers go high as the value of the wavenumber becomes larger. This may be due to the fact that incident wave energy with higher wavenumbers is confined near the free surface. It is also noticed that the force on the front barrier is more in comparison to the force on the rear barrier. Figs. 5.18a and 5.18b show the variation of the non-dimensional horizontal force against k_0h for three different values of the heights of the parabolic hump on the front and rear barriers, respectively. The value of the horizontal force does not change significantly for the wavenumbers $0 < k_0h < 1.2$ and $0 < k_0h < 1.7$, respectively, on the front and rear barriers but as the value of the
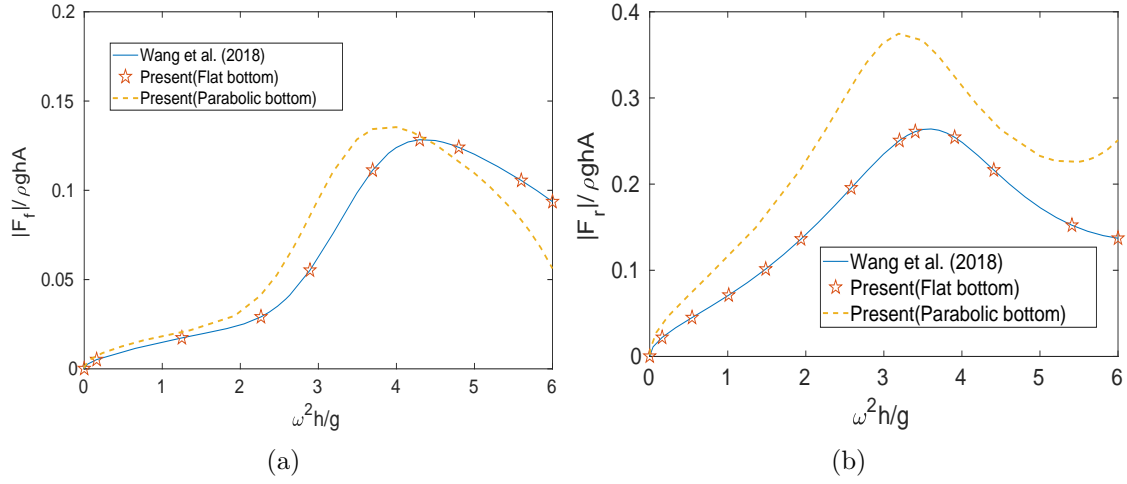
Figure 5.16: Non-dimensional horizontal force versus $\omega^2 h/g$ where in Fig. (a) Force on front barrier, and in Fig. (b) Force on rear barrier.
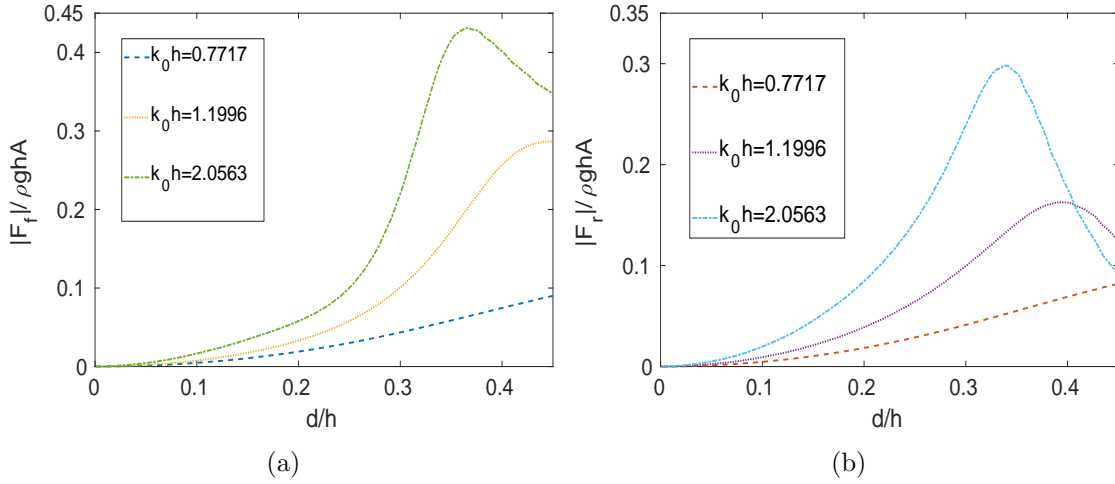
Figure 5.17: Non-dimensional horizontal force on the barriers versus d/h for $c_0/h = 0.5, b/h = 0, l/h = 0.75$ for three different wave numbers over Type-II hump where in Fig. (a) Force on front barrier, and in Fig. (b) Force on rear barrier.

wavenumbers gets relatively larger, both the force profiles get fluctuates. The force on the front barrier is more in comparison to the rear barrier. Both of the figures show that local maxima's on these decrease as the height of the parabolic hump increases.

5.6 Conclusion

In this chapter, a finite element method is employed to examine the scattering of obliquely incident surface waves by two vertical barriers over an arbitrary bottom topography. The results are obtained for two particular cases of the arbitrary bottom topography: parabolic hump and rectangular hump. The radiation boundary conditions are kept at a finite distance from the vertical barriers as the local disturbances decay sufficiently within a distance of four times the depth of the water. It is observed that the zeros on the reflection
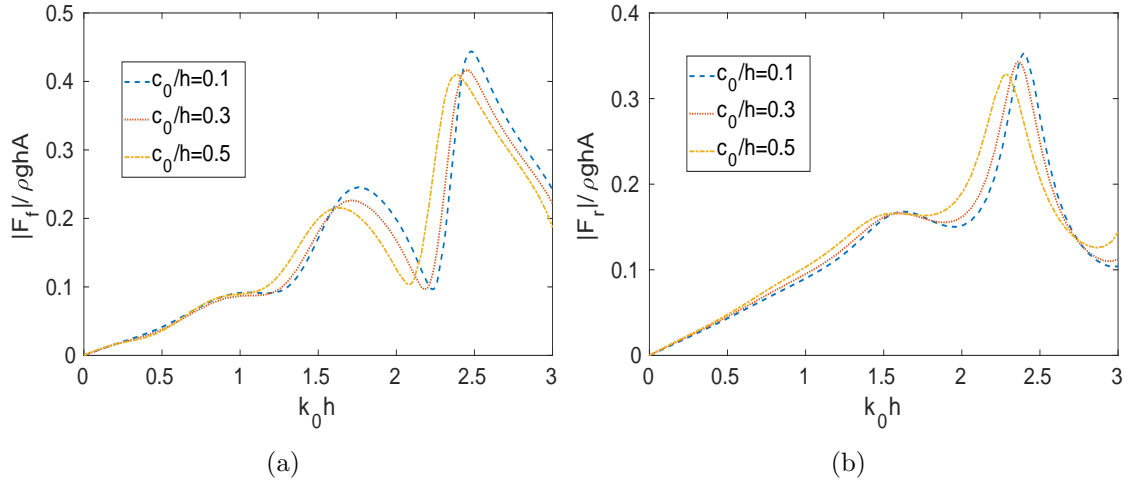
Figure 5.18: Non-dimensional horizontal force on the barriers versus $k_0 h$ for $d_1/h = d_2/h = 0.2, b/h = 0.1, \alpha = 0, l/h = 1.5$ for different heights of Type-I hump where in Fig. (a) Force on front barrier, and in Fig. (b) Force on rear barrier.

and transmission curves exist for the identical barriers and the number of zeros increases as the gap between them increases. Also, the lower frequency zeros of the transmission curve coalesce in pairs as the gap between the barriers increases. The study reveals that the reflection coefficient increases due to the height of bottom topography for smaller wave numbers while it has negligible effect for larger wavenumbers. This means, for larger wavenumbers, the water depth throughout the region can be seen as deep enough. It is noticed that the reflection coefficient increases with the drafts and thickness of the barriers. Also, the influence of the angle of incidence on the reflection coefficient has been demonstrated. In addition to this, the effect of the height of the hump and the drafts of the barriers on the non-dimensional horizontal force on the front and rear barriers is observed through different plots. Also, it should be noticed that the front barrier experiences more force in comparison to the rear barrier. This study will be helpful to solve similar problems arising in the area of applied mathematics and physics.

Chapter 6

Summary and Future Work

A brief summary of the mathematical techniques and the major results derived in this thesis are highlighted in the first section of this chapter. The scope of the future work is highlighted in the subsequent section.

6.1   Summary of the present work

The research work considered in this thesis are presented in various chapters and the results are highlighted in the section namely, conclusion in each chapter. Here, a brief summary of work done in the entire thesis is highlighted.

In Chapter 2, a study on the scattering of surface water waves by a finite dock in finite depth of water is examined under the assumptions of the linearized water wave theory for normal incident of waves. In addition to finite dock, 2-step bottom topography is considered to analyze the effect of abrupt change in bottom topography on the wave propagation from lower depth region as well as from higher depth region. It is observed that the reflection coefficient is decreasing slightly and transmission coefficient is increasing with increasing the depth ratios for wave propagation from lower depth region. On the other hand, for wave propagation from higher depth region, the reflection coefficient is increasing as the values of the depth ratios are increasing while the transmission coefficient is decreasing. The reflection coefficient is also increasing by increasing the wavenumber, dock length and width of the step whereas the transmission coefficient is decreasing for the same. Furthermore, this problem is generalized for multi-steps and it is found that the transmission coefficient is increasing but the reflection coefficient is slightly decreasing by increasing the number of steps. The energy balance relation is also derived and verified. It is observed that the numerical results obtained for reflection and transmission coefficients satisfy the energy balance relation almost accurately. The present results are also validated through the results available in the literature. Thus, the horizontal breakwater can be designed for the protection of seashore.

Chapter 3 deals with the scattering of oblique incident surface gravity waves by a thin vertical rigid barrier over a stepped bottom topography with the aid of matched eigenfunction expansion method using algebraic least squares method. The performance of the barrier over stepped bottom is studied through various graphs of the reflection and transmission coefficients and non-dimensional horizontal force. The reflection coefficient increases as the length of the barrier and the step height increase while it decreases as the angle of incidence increases. It is observed that the maximum reflection occurs for

normal incidence of the incident waves. The analysis of non-dimensional horizontal force per unit width of the barrier is also examined. As the length of the barrier over the step increases, the absolute maximum of force curves goes on increasing. The non-dimensional horizontal force on the barrier decreases as the reflection coefficient due to the presence of the barrier decreases. Also, it is noticed that the force on the barrier is less for obliquely incidence waves in comparison of normal incidence waves. Therefore, the barrier over stepped bottom may be utilize to effectively reflect the incident waves and causes a calm zone along lee side, yielding less impact on seashore.

In Chapter 4, the problem of scattering of water waves by two thin vertical barriers over a shelf-type bottom topography is examined for its solution using the eigenfunction expansion method and the least square approach. The numerical values of the reflection and transmission coefficients are plotted through different graphs to demonstrate the influence of various system parameters. For identical length of the barriers over symmetric shelf bottom, the zeros in the reflection curve occur. These zeros in the reflection curve may be avoided by using non-identical length of the barriers or asymmetric shelf bottom topography. It is also observed that more energy is reflected by a pair of barriers in comparison to single barrier. On increasing the length of the barriers, more reflection and consequently less transmission occurs to the lee side. As the gap between the barriers increases, it causes more number of oscillations on both the reflection and transmission coefficients curves. The local maxima in reflection curve decreases as the angle of incidence increases. Also, the reflection coefficient decreases as the depth of submergence of the barriers increases. Furthermore, the problem is generalized for an array of surface piercing barriers over shelf bottom topography. It is noticed that local maxima in reflection curve increases as additional pairs of surface piercing barriers are considered between the barriers. It is also observed that the wave amplitude after the barriers can be decreased with the increased length of the barriers. The analysis of non-dimensional horizontal force per unit width of the front and rear barriers is also observed. It is shown that the front barrier experience more force as compared to the rear barrier.

In Chapter 5 deals with the scattering of obliquely incident surface waves by two vertical barriers over an arbitrary bottom topography. The finite element method is employed to obtain the numerical results. The radiation boundary conditions are kept at a finite distance from the vertical barriers as the local disturbances decay sufficiently within a distance. The numerical results are analyzed through different plots and tables for parabolic and rectangular type hump bottom profiles. It is observed that the zeros on the reflection and transmission curves exist for identical length of the barriers and these zeros increases as the gap between the barriers increases. Also, the lower frequency zeros of the transmission curve coalesce in pairs as the gap between the barriers increases. The study reveals that the reflection coefficient increases due to the height of bottom topography for smaller wave numbers while it has a negligible effect for larger wavenumbers. This means for larger wavenumbers the water depth throughout the region can be seen as deep enough. It is noticed that the reflection coefficient increases with the drafts and thickness

of the barriers. Also, the influence of the angle of incidence on the reflection coefficient has been observed. In addition to this, the effect of the hump height and the drafts of the barriers on the non-dimensional horizontal force on the front and rear barriers is studied. The energy balance relation is derived using Green's integral theorem, which ensures the correctness of the present numerical results. The obtained results are compared with the results available in the literature for validation purpose.

6.2 Scope of future work

The possible extension related to scope of future research work of some of the problems are given below. Hence, the scope of future research work can be taken up as follows:

1. The problem involving scattering of water waves by thin inclined barriers in the presence of undulating bottom topography using hypersingular integral equation approach can be considered.

2. The problem of diffraction of water waves by thin/thick inclined barriers incorporating time dependence using boundary element method can be examined.

3. The problem of scattering of water waves by thin inclined barriers in the presence of undulating bottom in two layer fluids using hypersingular integral equation approach can be investigated.

4. The non-linear theory for scattering of water waves by vertical barrier(s) over arbitrary bottom topography using finite element method can be developed.

5. Similar problems arising in other areas of engineering applications can be investigated using the mathematical procedure developed here.

References

[1] Au, M.; Brebbia, C. Numerical prediction of wave forces using the boundary element method. *Applied Mathematical Modelling.* **1982**, 6(4), 218-228.

[2] Bai, K. J. Diffraction of oblique waves by an infinite cylinder, *J. Fluid Mech.* **1975**, 68(3), 513-535.

[3] Banerjea, S. Scattering of water waves by a vertical wall with gaps. *The Journal of the Australian Mathematical Society. Series B. Applied Mathematics.* **1996**, 37(4), 512-529.

[4] Bartholomeusz, E. The reflexion of long waves at a step. *Mathematical Proceedings of the Cambridge Philosophical Society*, Cambridge Univ Press. **1958**, 54, 106-118.

[5] Bhatta, D. D. Wave diffraction by circular and elliptical cylinders in water of finite depth. *International Journal of Pure and Applied Mathematics.* **2005**, 19(1), 67-85.

[6] Bhatti, M. M.; Lu, D. Q. Head-on Collision Between Two Hydroelastic Solitary Waves in Shallow Water. *Qual. Theory Dyn. Syst.* **2018**, 17(1), 103-122.

[7] Bhatta, D. D.; Rahman, M. On scattering and radiation problem for a cylinder in water of finite depth. *International Journal of Engineering Science.* **2003**, 41(9), 931-967.

[8] Bhattacharjee, J.; Soares, C. G. Oblique wave interaction with a floating structure near a wall with stepped bottom. *Ocean Eng.* **2011**, 38(13), 1528-1544.

[9] Bora, S. N.; Martha, S. C. Scattering of surface waves over an uneven sea-bed. *Applied Mathematics Letters.* **2008**, 21(10), 1082-1089.

[10] Borah, P.; Hassan, M. Wave loads by an oscillating water column in presence of bottom-mounted obstacle in the channel of finite depth. *SN Appl. Sci.* **2019**, 1(10), 1-8.

[11] Chakrabarti, A. Solution of two singular integral equations arising in water wave problems. *ZAMM-Journal of Applied Mathematics and Mechanics/Zeitschrift für Angewandte Mathematik und Mechanik.* **1989**, 69(12), 457-459.

[12] Chakrabarti, A.; Ahluwalia, D. S.; Manam, S. R. Surface water waves involving a vertical barrier in the presence of an ice-cover. *International journal of engineering science.* **2003**, 41(10), 1145-1162.

[13] Chakrabarti, A.; Manam, S. R.; Banerjea, S. Scattering of surface water waves involving a vertical barrier with a gap. *Journal of Engineering Mathematics.* **2003**, 45(2), 183-194.

[14] Chakrabarti, A.; Mandal, B. N.; Gayen R. The dock problem revisited. *International Journal of Mathematics and Mathematical Sciences.* **2005**, 21, 3459-3470.

[15] Chakrabarti, A.; Martha, S. C. A note on energy-balance relations in surface water wave problems involving floating elastic plates. *J. Adv. Res. Appl. Math.* **2009**, 1, 27-34.

[16] Chakraborty, R.; Mandal, B. N. Water wave scattering by a rectangular submarine trench. *J. Eng. Math.* **2014**, 89(1), 101-112.

[17] Chakraborty, R.; Mandal, B. N. Oblique wave scattering by a rectangular submarine trench. *ANZIAM J.* **2015**, 56, 286-298.

[18] Chanda, A.; Bora, S. N. Effect of a porous sea-bed on water wave scattering by two thin vertical submerged porous plates. *European Journal of Mechanics-B/Fluids.* **2020**, 84, 250-261.

[19] Chanda, A.; Bora, S. N., Different approaches in scattering of water waves by two submerged porous plates over an elastic sea-floor. *Geophys. Astrophys. Fluid Dyn.* **2022**, 116, 1-28.

[20] Cho, Y. S.; Jeong, W. C.; Woo S. B. Finite element method for strong reflection of water waves, *Ocean Eng.* **2004**, 31, 653-667.

[21] Choudhary, A.; Martha, S. C. Diffraction of surface water waves by an undulating bed topography in the presence of vertical barrier. *Ocean Eng.* **2016**, 122, 32-43.

[22] Choudhary, A.; Koley, S.; Martha, S. C. Coupled eigenfunction expansion-boundary element method for wave scattering by thick vertical barrier over an arbitrary seabed. *Geophys. Astrophys. Fluid Dyn.* **2020**, 115, 44-60.

[23] Choudhary, A.; Kumar, N.; Martha, S. C. Interaction of surface water waves with a finite dock over two-stepped bottom profile. *Mar. Syst. Ocean Technol.* **2022**, 17(1), 39-52.

[24] Choudhary, A.; Trivedi, K.; Koley, S.; Martha, S. C. On the scattering and radiation of water waves by a finite dock floating over a rectangular trench. *Wave Motion.* **2022**, 110, 102869.

[25] Choudhary, S.; Martha, S. C. Dissipation of incident wave energy by two floating horizontal porous plates over a trench type bottom. *Ships and Offsore Structures.* **2023**, 18(5), 1-23.

[26] Dalrymple, R. A.; Martin, P. A. Wave diffraction through offshore breakwaters, *J. Waterway, Port, Coastal, Ocean Eng.* **1990**, 116(6), 727-741.

[27] Das, P.; Dolai, D. P.; Mandal, B. N.; Oblique wave diffraction by parallel thin vertical barriers with gaps. *J. Waterway, Port, Coastal, Ocean Eng.* **1997**, 123, 163-171.

[28] Das, D.; Mandal B.; Chakrabarti A. Energy identities in water wave theory for free-surface boundary condition with higher-order derivatives. *Fluid dynamics research.* **2008**, 40(4), 253-272.

[29] Das, S.; Bora, S. N. Reflection of oblique ocean water waves by a vertical porous structure placed on a multi-step impermeable bottom. *Appl. Ocean Res.* **2014**, 47, 373-385.

[30] Das, A.; De, S.; Mandal, B. N. Wave interaction with an elliptic disc submerged in a two-layer fluid. *Applied Mathematical Modelling.* **2023**, 117, 786-801.

[31] Davies, A. G. On the interaction between surface-waves and undulations on the seabed. *Journal of Marine Research.* **1982**, 40(2), 331-368.

[32] Davies, A. G. The reflection of wave energy by undulations on the seabed. *Dynamics of Atmospheres and Oceans.* **1982**, 6, 207-232.

[33] Davies, A. G.; Heathershaw, A. Surface wave propagation over sinusoidally varying topography. *J. Fluid Mech.* **1984**, 144, 419-443.

[34] Dean, W. On the reflexion of surface waves by a submerged plane barrier. *Mathematical Proceedings of the Cambridge Philosophical Society*, Cambridge Univ Press. **1945**, 41, 231-238.

[35] Dean, R. G.; Dalrymple, R. A. *Water wave mechanics for engineers and scientists.* volume 2. World Scientific, 1991.

[36] Dhillon, H.; Banerjea, S.; Mandal, B. Water wave scattering by a finite dock over a step-type bottom topography. *Ocean Eng.* **2016**, 113, 1-10.

[37] Evans, D. The influence of surface tension on the reflection of water waves by a plane vertical barrier. *Mathematical Proceedings of the Cambridge Philosophical Society*, Cambridge Univ Press. **1968**, 64, 795–810.

[38] Evans, D. Diffraction of water waves by a submerged vertical plate. *J. Fluid Mech.* **1970**, 40(3), 433-451.

[39] Evans D. V.; Morris, C. A. N. Complementary approximations to the solution of a problem in water waves. *J. Inst. Math. Applis.* **1972**, 10, 1-9.

[40] Evans, D. A note on the waves produced by the small oscillations of a partially immersed vertical plate. *IMA Journal of Applied Mathematics.* **1976**, 17(2), 135-140.

[41] Faulkner, T. R. The diffraction of an obliquely incident surface wave by a submerged plane barrier. *Z. Angew. Math. Phys.* **1966**, 17, 699-707.

[42] Fitz-Gerald, G. The reflexion of plane gravity waves travelling in water of variable depth. *Philosophical Transactions of the Royal Society of London A: Mathematical, Physical and Engineering Sciences.* **1976**, 284(1317), 49–89.

[43] Friedrichs, K.; Lewy, H. The dock problem. *Communications on Pure and Applied Mathematics.* **1948**, 1(2), 135-148.

[44] Gayen, R.; Mondal, A. A hypersingular integral equation approach to the porous plate problem. *Appl. Ocean Res.* **2019**, 346, 436-451.

[45] Guha, S.; Singh, A. K. Plane wave reflection/transmission in imperfectly bonded initially stressed rotating piezothermoelastic fiber-reinforced composite half-spaces. *European Journal of Mechanics-A/Solids.* **2021**, 88, 104242.

[46] Gupta, S.; Gayen, R. Water wave interaction with dual asymmetric non-uniform permeable plates using integral equations, *Appl. Math. Comput.* **2019**, 346, 436-451.

[47] Guo Y.; Liu Y.; Meng X. Oblique wave scattering by a semi-infinite elastic plate with finite draft floating on a step topography. *Acta. Oceanol. Sin.* **2016**, 35(7), 113-121.

[48] Haskind, M. Plane oscillations problem for a plate on the free surface of heavy fluid. *Izvestia Akademii Nauk SSSR, Otdelenie Technicheskich Nauk.* **1942**, 7(8).

[49] Hassan, M.; Bora S. N.; Biswakarma, M. Water wave interaction with a pair of floating and submerged coaxial cylinders in uniform water depth. *Mar. Syst. Ocean Technol.* **2020**, 15, 188-198.

[50] Havelock, T. H. LIX. Forced surface-waves on water. *Philos. Mag.* **1929**, 8, 569-576.

[51] Heathershaw, A. Seabed-wave resonance and sand bar growth. *Nature.* **1982**, 296(5855), 343-345.

[52] Heins, A. E. Water waves over a channel of finite depth with a dock. *American Journal of Mathematics.* **1948**, 70(4), 730-748.

[53] Hermans, A. J. Interaction of free-surface waves with a floating dock. *Journal of engineering mathematics.* **2003**, 45(1), 39-53.

[54] Holford, R. L. Short surface waves in the presence of a finite dock. i. *Mathematical Proceedings of the Cambridge Philosophical Society*, Cambridge Univ Press. **1964**, 60, 957-983.

[55] Holford, R. L. Short surface waves in the presence of a finite dock. ii. *Mathematical Proceedings of the Cambridge Philosophical Society*, Cambridge Univ Press. **1964**, 60, 985-1012.

[56] Isaacson, M.; Baldwin, J.; Premasiri, S.; Yang, G. Wave interactions with double slotted barriers. *Appl. Ocean Res.* **1999**, 21, 81-91.

[57] Jain, S.; Bora, S. N. Oblique water wave scattering by a floating bridge fitted with a rectangular porous structure and the resulting waveload mitigation. *Ocean Eng.* **2023**, 275, 114132.

[58] Kaligatla, R. B.; Prasad, N. M.; Tabssum, S. Oblique interaction between water waves and a partially submerged rectangular breakwater. *J. Eng. Mar. Environ.* **2020**, 234, 154-169.

[59] Kanoria, M.; Dolai, D. P.; Mandal, B. N. Water-wave scattering by thick vertical barriers. *Journal of Engineering Mathematics.* **1999**, 35, 361-384.

[60] Karmakar, D.; Sahoo, T. Gravity wave interaction with floating membrane due to abrupt change in water depth. *Ocean Eng.* **2008**, 35(7), 598-615.

[61] Kaur, A.; Martha, S. C.; Chakrabarti, A. Solution of the problem of propagation of water waves over a pair of asymmetrical rectangular trenches. *Appl. Ocean Res.* **2019**, 93, 101946.

[62] Kirby, J. T.; Dalrymple, R. A. Propagation of obliquely incident water waves over a trench. *J. Fluid Mech.* **1983**, 133, 47-63.

[63] Koley, S.; Behera, H.; Sahoo, T. Oblique wave trapping by porous structures near a wall. *J. Eng. Mech.* **2015**, 141(3),04014122.

[64] Koley, S.; Sahoo, T. An integro-differential equation approach to study the scattering of water waves by a floating flexible porous plate. *Geophys. Astrophys. Fluid Dyn.* **2018**, 112, 345-356.

[65] Kreisel, G. Surface waves. *Quarterly of Applied Mathematics.* **1949**, 7(1), 21–44.

[66] Kumar, N.; Goyal, D.; Martha, S. C. Algebraic Method for Approximate Solution of Scattering of Surface Waves by Thin Vertical Barrier Over a Stepped Bottom Topography. *Contemporary Mathematics.* **2022**, 3(4), 473-486.

[67] Kumar, N.; Martha, S. C. An integro-differential equation approach to study the scattering of water waves by a floating flexible porous plate. *Geophys. Astrophys. Fluid Dyn.* **2023**, 117(1), 1-25.

[68] Lamb, H. *Hydrodynamics.* Cambridge university press, 1932.

[69] Lassiter III, J. B. *The propagation of water waves over sediment pockets*; Technical report, 1972.

[70] Lee, J. J.; Ayer, R. M. Wave propagation over a rectangular trench. *J. fluid mech.* **1981**, 110, 335-347.

[71] Leonard, J. W.; Huang, M. C. Hydrodynamic interference between floating cylinders in oblique seas. *Appl. Ocean Res.* **1983**, 5(3), 158-166.

[72] Leppington, F. On the scattering of short surface waves by a finite dock. *Mathematical Proceedings of the Cambridge Philosophical Society*, Cambridge Univ Press. **1968**, 64, 1109-1129. .

[73] Leppington, F. On the radiation of short surface waves by a finite dock. *IMA Journal of Applied Mathematics.* **1970**, 6(4), 319-340.

[74] Levine, H.; Rodemich, E. *Scattering of surface waves on an ideal fluid*; Technical report, DTIC Document, 1958.

[75] Lewin, M. The effect of vertical barriers on progressing waves, New York University 1963, pp 287-300.

[76] Linton C. The finite dock problem. *Zeitschrift für angewandte Mathematik und Physik ZAMP.* **2001**, 52(4), 640-656.

[77] Liu, Huan-Wen; Zeng, Hui-Dan; Huang, Hui-Dong. Bragg resonant reflection of surface waves from deep water to shallow water by a finite array of trapezoidal bars. *Appl. Ocean Res.* **2020**, 94, 101976.

[78] Losada, I. J.; Losada, M. A.; Roldán, A. J. Propagation of oblique incident waves past rigid vertical thin barriers. *Appl. Ocean Res.* **1992**, 14(3), 191-199.

[79] Lu, D. Q. Interaction of viscous wakes with a free surface. *Applied Mathematics and Mechanics (English Edition).* **2004**, 25(6), 647-655.

[80] Maiti, P.; Mandal, B. N. Water wave scattering by an elastic plate floating in an ocean with a porous bed. *Appl. Ocean Res.* **2014**, 47, 73-84.

[81] Manam, S.; Bhattacharjee, J.; Sahoo, T. Expansion formulae in wave structure interaction problems. *Proceedings of the Royal Society of London A: Mathematical, Physical and Engineering Sciences*, **2006**, 462, 263-287.

[82] Mandal, B.; Basu, U. A note on oblique water-wave diffraction by a cylindrical deformation of the bottom in the presence of surface tension. *Archives of Mechanics.* **1990**, 42(6), 723-727.

[83] Mandal, B.; Basu, U. Free surface flow over a small geometric disturbance the bottom. *Bulletin of calcutta mathematical society.* **1996**, 88, 355-362.

[84] Mandal, B.; Chakrabarti, A. On galerkin's method applicable to the problems of water wage scattering by barriers. *In Proc. Indian Nat. Sci. Acad.* PINSA, 1999; Vol. 65(6), pp 61-71.

[85] Mandal, B. N.; De, Soumen. Surface wave propagation over small undulations at the bottom of an ocean with surface discontinuity. *Geophys. Astrophys. Fluid Dyn.* **2009**, 103(1), 19-30.

[86] Mandal, B.; Dolai, D. Oblique water wave diffraction by thin vertical barriers in water of uniform finite depth. *Appl. Ocean Res.* **1994**, 16(4), 195-203.

[87] Mandal, B.; Gayen, R. Water wave scattering by bottom undulations in the presence of a thin partially immersed barrier. *Appl. Ocean Res.* **2006**, 28(2), 113-119.

[88] Mandal, B.; Kundu, P. Scattering of water waves by a vertical barrier and associated mathematical methods. *In Proc. Indian Nat. Sci. Acad.* Part A, 1987; Vol. 53, pp 514-530.

[89] Manisha; Kaligatla, R.B.; Sahoo, T. Effect of bottom undulation for mitigating wave-induced forces on a floating bridge. *Wave Motion.* **2019**, 89, 166-184.

[90] Martha, S. C.; Bora, S. N. Oblique surface wave propagation over a small undulation on the bottom of an ocean. *Geophys. Astrophys. Fluid Dyn.* **2007** 101, 65-80.

[91] Mciver, P. Scattering of water waves by two surface-piercing vertical barriers. *IMA J. Appl. Math.* **1985**, 35, 339-355.

[92] Mei, C. C.; Le Méhauté, B. Note on the equations of long waves over an uneven bottom. *Journal of Geophysical Research.* **1966a**, 71(2), 393-400.

[93] Mei, C. C. Radiation and scattering of transient gravity waves by vertical plates. *The Quarterly Journal of Mechanics and Applied Mathematics.* **1966b**, 19(4), 417–440.

[94] Mei, C. C.; Black, J. L. Scattering of surface waves by rectangular obstacles in waters of finite depth. *J. Fluid Mech.* **1969**, 38(03), 499-511.

[95] Meng, Q. R.; Lu, D. Q. Scattering of gravity waves by a porous rectangular barrier on a seabed. *J. Hydro.* **2016**, 28(3), 519-522.

[96] Miles, J. W. Oblique surface-wave diffraction by a cylindrical obstacle. *Dynamics of Atmospheres and Oceans.* **1981**, 6(2), 121-123.

[97] Miles, J. W. On surface-wave diffraction by a trench. *J. Fluid Mech.*, **1982** 115, 315-325.

[98] Mondal, D; Banerjea, S. Scattering of water waves by an inclined porous plate submerged in ocean with ice cover. *Q. J. Mech. Appl. Math.* **2016**, 69(2), 195-213.

[99] Neelamani, S.; Vedagiri, M. Wave interaction with partially immersed twin vertical barriers. *Ocean Eng.* **2002**, 29, 215-238.

[100] Newman, J. N. Propagation of water waves over an infinite step. *J. Fluid Mech.* **1965**, 23(2), 399-415.

[101] Newman, J. N. Interaction of water waves with two closely spaced vertical obstacles. *J. Fluid Mech.* **1974**, 66, 97-106.

[102] Ni, Yun-lin; Teng, Bin. Bragg resonant reflection of water waves by a Bragg breakwater with porous trapezoidal bars on a sloping permeable seabed. *Appl. Ocean Res.* **2021**, 114, 102770.

[103] Panduranga, K.; Koley, S.; Sahoo, T. Surface gravity wave scattering by multiple slatted screens placed near a caisson porous breakwater in the presence of seabed undulations. *Appl. Ocean Res.* **2021**, 111, 102675.

[104] Parsons, N.; Martin, P. Scattering of water waves by submerged curved plates and by surface-piercing flat plates. *Appl. Ocean Res.* **1994**, 16(3), 129-139.

[105] Porter, D. The transmission of surface waves through a gap in a vertical barrier. *Mathematical Proceedings of the Cambridge Philosophical Society*, Cambridge Univ Press. **1972**, 71, 411-421.

[106] Porter, R.; Evans, D. Complementary approximations to wave scattering by vertical barriers. *J. Fluid Mech.* **1995**, 294, 155–180.

[107] Porter, R.; Porter, D. Interaction of water waves with three-dimensional periodic topography. *J. Fluid Mech.* **2001** 434, 301-335.

[108] Praveen, K. M.; Venkateswalru, V.; Karmakar, D. Wave transformation due to finite elastic plate with abrupt change in bottom topography. *Ships and Offshore Structures.* **2021**, 17(8), 1-19.

[109] Rahman, M. *Water waves: relating modern theory to advanced engineering applications*, Vol. 3, Clarendon Press, 1995.

[110] Ray, S.; De Soumen; Mandal B. N. Galerkin technique for water wave scattering by thin vertical barriers in deep water. *Bull. Cal. Math. Soc.* **2021**, 113(1), 1-14.

[111] Ray, S.; De Soumen; Mandal B. N. Wave propagation over a rectangular trench in the presence of a partially immersed barrier. *Fluid Dyn. Res.* **2021**, 53, 035509.

[112] Reddy, M. S.; Neelamani, S. Wave transmission and reflection characteristics of a partially immersed rigid vertical barrier. *Ocean Eng.* **1992**, 19(3), 313-325.

[113] Rezanejad, K.; Bhattacharjee, J.; Soares, C. G. Stepped sea bottom effects on the efficiency of nearshore oscillating water column device. *Ocean Eng.* **2013**, 70, 25-38.

[114] Rezanejad, K.; Bhattacharjee, J.; Soares, C. G. Analytical and numerical study of dual-chamber oscillating water columns on stepped bottom. *Renewable Energy* **2015**, 75, 272-282.

[115] Rhee, J. P. On the transmission of water waves over a shelf. *Appl. Ocean Res.* **1997**, 19, 161-167.

[116] Roy, R.; Basu, U.; Mandal, B. N. Oblique water wave scattering by two unequal vertical barriers. *J. Eng. Math.* **2016**, 97(1),119-133.

[117] Roy, R.; De, Soumen; Mandal, B. N. Water wave scattering by multiple thin vertical barriers, *Appl. Math. Comput.* **2019**, 355, 458-481.

[118] Rubin, H. The dock of finite extent. *Communications on Pure and Applied Mathematics.* **1954**, 7(2), 317-344.

[119] Sannasiraj, S. A.; Sundar, V.; Sundaravadivelu, R. Mooring forces and motion responses of pontoon-type floating breakwaters. *Ocean Eng.* **1998**, 25(1), 27-48.

[120] Sannasiraj, S. A.; Sundaravadivelu, R.; Sundar, V. Diffraction–radiation of multiple floating structures in directional waves. *Ocean Eng.* **2000**, 28, 201-234.

[121] Sarkar, A.; Bora, S. N. Hydrodynamic coefficients for a floating semi-porous compound cylinder in finite ocean depth. *Mar. Syst. Ocean Technol.* **2020**, 15, 270-285.

[122] Sarkar, B.; De S. Oblique Wave Diffraction by a Bottom-Standing Thick Barrier and a Pair of Partially Immersed Barriers. *J. Offshore Mech. Arct. Eng.* **2023**, 145(1), 010905.

[123] Selvan, S. A.; Behera, H.; Sahoo, T. Reduction of hydroelastic response of a flexible floating structure by an annular flexible permeable membrane. emphJ. Eng. Math. **2019**, 118, 73–99.

[124] Singh, A. K.; Mahto, S.; Guha, S. Analysis of plane wave reflection phenomenon from the surface of a micro-mechanically modeled piezomagnetic fiber-reinforced composite half-space. *Waves in Random and Complex Media.* **2021**, 31, 1-22.

[125] Singh, S.; Singh, A. K.; Guha, S. Reflection of plane waves at the stress-free/rigid surface of a micro-mechanically modeled Piezo-electro-magnetic fiber-reinforced half-space. *Waves in Random and Complex Media.* **2022**, 32, 1-30.

[126] Singla, S.; Behera, H.; Martha, S. C.; Sahoo, T. Scattering of obliquely incident water waves by a surface-piercing porous box. *Ocean Eng.* **2019**, 193, 106577.

[127] Singla, S.; Behera, H.; Martha, S. C.; Sahoo, T. Scattering of Water Waves by Very Large Floating Structure in the Presence of a Porous Box. *J. Offshore Mech. Arct. Eng.* **2022**, 144, 041904.

[128] Sneddon, I. N. Mixed boundary value problems in potential theory. NorthHolland, Amsterdam, 1966.

[129] Staziker, D.; Porter D.; Stirling, D. The scattering of surface waves by local bed elevations. *Appl. Ocean Res.* **1996**, 18(5), 283-291.

[130] Stoker, J. J. *Water waves: The mathematical theory with applications*, vol. 36, John Wiley Sons, 2011.

[131] Thorne, R. Multipole expansions in the theory of surface waves. *Mathematical Proceedings of the Cambridge Philosophical Society*, Cambridge Univ Press. **1953**, 49, 707-716.

[132] Tran, C. T.; Chang, J. Y.; Tsai, C. C. Step approximation for water wave scattering by multiple thin barriers over undulated bottoms. *J. Mar. Sci. Eng.* **2021**, 9, 629.

[133] Tsai, C. C.; Hsu, T. W.; Lin, Y. T. On step approximation for roseau's analytical solution of water waves. *Mathematical Problems in Engineering* **2011**, 607196, 1-20.

[134] Tsai, C. C.; Tai, W.; Hsu, T. W.; Hsiao, S.C. Step approximation of water wave scattering caused by tension-leg structures over even bottoms. *Ocean Eng.* **2018**, 166, 208-225.

[135] Tsai, C. C.; Chang, Y. H.; Hsu, T. W. Step approximation on oblique water wave scattering and breaking by variable porous breakwaters over uneven bottoms. *Ocean Eng.* **2022**, 253, 111325.

[136] Tseng, I. F.; You, C. S.; Tsai, C. C. Bragg reflection of oblique water waves by periodic surface-piercing and submerged breakwaters. *J. Mar. Sci. Eng.* **2020**, 8, 522.

[137] Ursell, F. The effect of a fixed vertical barrier on surface waves in deep water. *Mathematical Proceedings of the Cambridge Philosophical Society*, Cambridge Univ Press, **1947**, 43, 374-382.

[138] Venkateswarlu, V.; Karmakar, D. Wave scattering by vertical porous block placed over flat and elevated seabed. *Mar. Syst. Ocean Technol.* **2019**, 14, 85-109.

[139] Vijay, K. G.; Venkateswalru, V.; Sahoo, T. Bragg scattering of surface gravity waves by an array of submerged breakwaters and a floating dock. *Wave Motion.* **2021**, 106, 1-20.

[140] Wang, P.; Lu, D. Q. Nonlinear hydroelastic waves traveling in a thin elastic plate floating on a two-layer fluid. *Appl. Math. Comput.* **2016**, 274, 700-710.

[141] Wang, L.; Deng, Z.; Wang, C.; Wang, P. Scattering of oblique water waves by two unequal surface-piercing vertical thin plates with stepped bottom topography. *China Ocean Eng.* **2018**, 32(5), 524-535.

Curriculum Vitae

Personal Details:

- Name: Naveen Kumar

- Date of Birth: February 10, 1991

- Sex: Male

- Marital Status: Married

- Nationality: Indian

Educational Qualification:

- **Master of Science** in Mathematics: Hindu College, University of Delhi, Delhi, India, 2015 (1st Division)

- **Bachelor of Science**: Govt. College Narnaul, Maharshi Dayanand University, Rohtak, Haryana, India, 2013 (1st Division)

- **Higher Secondary**: Haryana Board of School Education, Bhiwani, Haryana, India, 2008 (1st Division)

- **Matric**: Haryana Board of School Education, Bhiwani, Haryana, India, 2006 (1st Division)

Professional Experience:

- Assistant Professor in Mathematics, Government College Krishan Nagar, Mahendergarh, Haryana (From July 2018 - till date)

- Part Time PhD Scholar, Department of Mathematics, IIT Ropar, Rupnagar, India (From July 2018 - June 2023)

- Regular PhD Scholar, Department of Mathematics, IIT Ropar, Rupnagar, India (From January 2017 - July 2018)

- Assistant Professor (Guest) in Department of Mathematics, National Institute of Technologoly, Kurukshetra, Haryana, India (From August 2016 to January 2017)

- Assistant Professor (Guest) in Department of Mathematics, University Institute of Engg. & Tech., Kurukshetra University, Kurukshetra, Haryana, India (From September 2015 to August 2016)

Awards & Honours:

- Qualified **CSIR-UGC NET (JRF)**, December 2014

- Qualified **GATE**, 2015

Home Address:

VPO: Mandhana, Tehsil: Narnaul,

District: Mahendergarh, Haryana, 123001